In compliance with the
Canadian Privacy Legislation
some supporting forms
may have been removed from
this dissertation.

While these forms may be included
in the document page count,
their removal does not represent
any loss of content from the dissertation.

University of Alberta

Fluid Properties At Coking Process Conditions

by

Moruf Olalekan Aminu ©

A thesis submitted to the Faculty of Graduate Studies and Research in partial
fulfillment of the requirements for the degree of Master of Science

in

Chemical Engineering

Department of Chemical and Materials Engineering

Edmonton, Alberta
Fall, 2003

National Library
of Canada

Acquisitions and
Bibliographic Services

395 Wellington Street
Ottawa ON K1A 0N4
Canada

Bibliothèque nationale
du Canada

Acquisisitons et
services bibliographiques

395, rue Wellington
Ottawa ON K1A 0N4
Canada

Your file Votre référence
ISBN: 0-612-87710-8
Our file Notre référence
ISBN: 0-612-87710-8

The author has granted a non-exclusive licence allowing the National Library of Canada to reproduce, loan, distribute or sell copies of this thesis in microform, paper or electronic formats.

The author retains ownership of the copyright in this thesis. Neither the thesis nor substantial extracts from it may be printed or otherwise reproduced without the author's permission.

L'auteur a accordé une licence non exclusive permettant à la Bibliothèque nationale du Canada de reproduire, prêter, distribuer ou vendre des copies de cette thèse sous la forme de microfiche/film, de reproduction sur papier ou sur format électronique.

L'auteur conserve la propriété du droit d'auteur qui protège cette thèse. Ni la thèse ni des extraits substantiels de celle-ci ne doivent être imprimés ou aturement reproduits sans son autorisation.

Canada

University of Alberta

Library Release Form

Name of Author: Moruf Olalekan Aminu

Title of Thesis: Fluid Properties At Coking Process Conditions

Degree: Master of Science

Year this Degree Granted: 2003

Permission is hereby granted to the University of Alberta Library to reproduce single copies of this thesis and to lend or sell such copies for private, scholarly or scientific research purposes only.

The author reserves all other publication and other rights in association with the copyright in the thesis, and except as herein before provided, neither the thesis nor any substantial portion thereof may be printed or otherwise reproduced in any material form whatever without the author's prior written permission.

Dated: 28/April/2003

University of Alberta

Faculty of Graduate Studies and Research

The undersigned certify that they have read, and recommend to the Faculty of Graduate Studies and Research for acceptance, a thesis entitled *Fluid Properties at Coking Process Conditions* by *Moruf Olalekan Aminu* in partial fulfillment of the requirements for the degree of Master of Science in Chemical Engineering.

Dated: 27/April/2003

ABSTRACT

The liquid bridge method was developed to measure fluid properties during the cracking of Athabasca bitumen vacuum residue (ABVR) at elevated temperatures. None of the existing methods for measuring surface tension or viscosity was suitable for ABVR at 300 °C – 530 °C. Surface tension was measured at 312 °C – 530 °C. Adhesive forces and viscosity were measured with increasing reaction time at 400 °C – 530 °C. The results showed that adhesive force remained constant, until the dry-out point, where it fell to zero. Surface tension was found to remain constant with increasing reaction time. Viscosity increased to order of 10^4 mPa.s before dry-out, for all the temperatures above 400 °C. Correlations were found to estimate surface tension at any temperature between 150 °C and 530 °C and viscosity at any reaction time and temperature between 400 °C and 530 °C for any film thickness.

ACKNOWLEDGEMENT

My very sincere gratitude goes to Dr. Murray Gray, Dr. Janet Elliott and Dr. William McCaffrey for their encouragement, invaluable guidance and unflinching resolve to make this project a success. I am also very grateful to Dr. I. Huq for his contributions

I would like to thank Dr. M. Williams, Dr. A. Yeung and Dr. K. Nandakumar for their advice. So would I like to thank Dr. A. Tangirala for guiding me through the development of a suitable filter for the sensor data while I am very grateful to Lisa Boddez for her help on the basics of the equipment and for collecting some of the data used in this study. Also appreciated is the help of P. Gonzalez in taking Pendant drop measurements. Thanks to Tuyet, Jeff, Samina, Oswaldo, Janeth and all members of the Upgrading team for their advice and for making my time here a painless experience.

The very reliable help of the instrument shop, the machine shop and the computer team was greatly appreciated. I would like to thank Olumide, Segun, Tunde, Amika, Pat, Gary, Martin, David, Sade, Sammie, Jason, Wa'el, Amar and Misha for their support. My heartfelt gratitude goes to the Dragers for their immeasurable kindness. I am grateful to my parents for their prayers; and to Lucia for her prayers and remarkable patience throughout my program.

Finally, I like to thank Natural Sciences and Engineering Research Council of Canada and Syncrude Canada for providing the funding for this research.

TABLE OF CONTENTS

1. INTRODUCTION 1

1.1 RESEARCH BACKGROUND 1
1.2 RESEARCH OBJECTIVES 3

2. LITERATURE REVIEW 5

2.1 PROPERTIES OF ATHABASCA BITUMEN VACUUM RESIDUE (ABVR) 5
2.1.1 VISCOSITY OF BITUMEN AND RHEOLOGY 6
2.1.2 SURFACE TENSION OF BITUMEN AND ABVR 9
2.2 MEASUREMENT OF FLUID PROPERTIES 11
2.2.1 VISCOSITY MEASUREMENT 12
2.2.2 TEMPERATURE DEPENDENCE OF VISCOSITY 15
2.2.3 SURFACE TENSION MEASUREMENT 17
2.2.4 DEPENDENCE OF SURFACE TENSION ON TEMPERATURE 20
2.3 SURFACE TENSION IN EVAPORATING SYSTEMS 24
2.4 FORCES DUE TO LIQUID BRIDGES 26
2.4.1 LIQUID BRIDGE BETWEEN TWO MOVING SPHERES 27
2.4.2 LIQUID BRIDGE BETWEEN TWO CROSSED CYLINDERS 31

3. THEORY 34

3.1 FORCES IN A LIQUID BRIDGE BETWEEN SPHERE AND PLATE 34

3.1.1 SURFACE COMPONENT OF THE FORCE 35

3.1.2 VISCOUS COMPONENT OF THE FORCE 36

3.2 FORCES IN A VARIABLE VOLUME LIQUID BRIDGE BETWEEN SPHERE AND PLATE 37

3.2.1 VISCOUS COMPONENT OF THE FORCE 37

3.2.2 MODEL DEVELOPMENT OF THE VISCOUS COMPONENT 38

3.3 CHANGE IN ABVR FILM THICKNESS WITH REACTION 40

4. MATERIALS AND METHODS 42

4.1 FEED AND CHEMICALS 42

4.2 THE CURIE-POINT ALLOYS FOR FILM HEATING 42

4.3 STANDARD CALIBRATION OILS 43

4.4 EXPERIMENTAL METHOD FOR MEASURING PROPERTIES OF A LIQUID BRIDGE 46

4.4.1 EQUIPMENT DESCRIPTION 46

4.4.2 IMAGE ANALYSIS OF THE LIQUID BRIDGE 49

4.5 EXPERIMENTAL PROCEDURES 50

4.5.1 FABRICATION OF RODS 50

4.5.2 COATING OF RODS 51

4.5.3 VISCOSITY AND SURFACE TENSION MEASUREMENT 52

5. CALIBRATION AND VALIDATION OF EQUIPMENT 55

5.1 Calibration of Position Sensors 55
5.1.1 Absolute Position Profile 56
5.1.2 Determination of Adhesive Forces 61
5.1.3 Determination of Point of Commencement of Bridge Elongation 64
5.2 Room Temperature Calibration with Standard Oils 65
5.2.1 Check on Derivation of Governing Equation 67
5.2.2 Determination of Constants in Governing Equation 68
5.2.3 Predicted and Actual Properties of Calibration Oil 72
5.3 High Temperature Equipment Calibration 76
5.3.1 Data Filtration 80
5.3.2 Magnetic Effects of The Induction Field 82
5.3.3 Film Thickness of Reacting ABVR at High Temperature 84

6. FLUID PROPERTIES OF ABVR AND DISCUSSION 86

6.1 Adhesive Forces in Liquid Bridges of Reacting ABVR 86
6.1.1 Adhesive Forces 86
6.1.2 Characteristics of Liquid Bridges 94
6.2 Surface Tension of ABVR 96

6.2.1 SURFACE TENSION OF NON REACTING ABVR 96
6.2.2 SURFACE TENSION OF REACTING ABVR 97
6.2.3 DISCUSSION: VALIDATION OF RESULTS 101
6.3 VISCOSITY OF ABVR 106
6.3.1 VISCOSITY OF NON REACTING ABVR 106
6.3.2 VISCOSITY OF REACTING ABVR 108
6.3.3 INFLUENCE OF DRIPPING ON MEASURED VISCOSITY OF REACTING ABVR 114
6.3.4 ROLE OF KINETICS IN VISCOSITY OF REACTING ABVR 117
6.4 DISCUSSION 122
6.5 PROCESS IMPLICATIONS 125

7. CONCLUSIONS AND RECOMMENDATIONS 126
7.1 CONCLUSIONS 126
7.2 RECOMMENDATIONS 128

REFERENCES 130

APPENDICES 142
A EXPERIMENTAL DATA AND PROOFS
142
A1 PROOF OF CAPILLARY FORCE FORMULAE 143

A2 STATISTICAL METHOD OF FINDING POINT OF COMMENCEMENT OF BRIDGE ELONGATION 148

A3 PARAMETRIC ESTIMATION DATA 150

A4 VISCOSITY AND SURFACE TENSION OF STANDARD OILS 151

A5 PROPERTIES OF ABVR 152

B PROGRAM CODES 159

B1 FILTERATION DRIVER CODE IN MATLAB 160

B2 DIFFERENTIAL EQUATION SOLVER FOR HIGH TEMPERATURE LIQUID FILM MODEL 161

C DETAILED EXPERIMENTAL PROCEDURES 166

C1 FABRICATION OF RODS 167

C2 COATING OF RODS 167

C3 CONDUCTING A RUN 168

LIST OF TABLES

Table 2-1. Properties of Athabasca Bitumen Vacuum Residue 6
Table 4-1. Properties of Standard Oils for Calibration 44
Table 4-2. Constants in ASTM Viscosity Model for the Standard Oils 45
Table 5-1. Volume and Reynolds Number of the Liquid Bridge with N1000 Standard Oil 67
Table 5-2. Measured versus Actual Surface Tension of Standard Oils 74
Table 5-3. Correction for Magnetic Effect of the Induction Field 83
Table 5-4. Kinetic Parameters in Model for Film Thickness of Reacting ABVR 85
Table 6-1. Surface Tension of non-reacting ABVR 97
Table 6-2. Results from Statistical Analysis of Slopes 104
Table 6-3. Effect of Dripping on Measured Viscosity of Reacting ABVR 116

LIST OF FIGURES

Figure 1-1. Schematic diagram of liquid behavior in a fluid coker 2

Figure 2-1. Surface tension of ABVR by the pendant drop method reported by Li et al., 2003 11

Figure 2-2. Cross section of liquid bridge between two spheres 28

Figure 2-3. Cross section of a liquid bridge between sphere and flat plate 32

Figure 3-1. Close up of the liquid bridge between sphere and plate 35

Figure 4-1. Schematic of the equipment for measuring the properties of a liquid bridge 47

Figure 4-2. Desired shape of fabricated rod 49

Figure 5-1. Typical sensors data from displacement 56

Figure 5-2. Equipment calibration plot: voltage reading of sensors versus absolute distance (flexural pivot, Model 5010-800) 57

Figure 5-3. Displacement-time profile of rods before rod correction 59

Figure 5-4. Displacement-time profile of rods after rod correction 60

Figure 5-5. Voltage-force calibration plot (using flexural pivot, Model 5010-800) 62

Figure 5-6. Method for evaluating capillary and viscous forces 63

Figure 5-7. Temperature response of the rods to the lights at room temperature 66

Figure 5-8. Elongated liquid bridge of N1000 oil at room temperature 70

Figure 5-9. Predicted versus actual viscosity of standard oil 73

Figure 5-10. Dependence of measured surface tension on film thickness 75

Figure 5-11. Temperature profile of Curie-point alloys 76

Figure 5-12. Typical data for rod positions at 503 °C 79

Figure 5-13. Data for rod positions after filtering 81

Figure 5-14. Dry rod data showing effect of magnetic field on rods at 466 °C 82

Figure 6-1. Adhesive forces of reacting ABVR versus time to touch rods at 400 °C 86

Figure 6-2. Adhesive forces of reacting ABVR versus time to touch rods at 466 °C 87

Figure 6-3. Adhesive forces of reacting ABVR versus time to touch rods at 503 °C 87

Figure 6-4. Adhesive forces of reacting ABVR versus time to touch rods at 530 °C 89

Figure 6-5. Dry out time as a function of reaction temperature 91

Figure 6-6. Trend in adhesive forces with temperature 93

Figure 6-7. Video image of a typical liquid bridge of reacting ABVR 95

Figure 6-8. Surface tension of reacting ABVR versus heating time at 400 °C 98

Figure 6-9. Surface tension of reacting ABVR versus heating time at 466 °C 99

Figure 6-10. Surface tension of reacting ABVR versus heating time at 503 °C 99

Figure 6-11. Surface tension of reacting ABVR versus heating time at 530 °C 100

Figure 6-12. Surface tension of ABVR from pendant drop method and from liquid bridge method 102

Figure 6-13. Trend in surface tension with temperature 105

Figure 6-14. Logarithm of viscosity of non-reacting ABVR versus temperature (< 300 °C) using the RMS 107

Figure 6-15. Viscosity of reacting ABVR versus heating time at 400 °C 109

Figure 6-16. Viscosity of reacting ABVR versus heating time at 466 °C 109

Figure 6-17. Viscosity of reacting ABVR versus heating time at 503 °C 110

Figure 6-18. Viscosity of reacting ABVR versus heating time at 530 °C 112

Figure 6-19. Selected adhesive forces for measuring the viscosity of reacting ABVR at 530 °C 112

Figure 6-20. Predicted extent of cracking and volatilization of reacting ABVR at dry-out time 118

Figure 6-21. Trend in the viscosity of reacting ABVR with heating time 120

Figure 6-22. Semi-log plot showing viscosity versus normalized reaction time 121

Figure 6-23. Semi-log plot showing viscosity of ABVR with increasing temperature from two different techniques 123

LIST OF NOMENCLATURE

A	Constant (Equation 2-1)
a	Radius of the neck of the bridge, mm
B	Constant (Equation 2-1)
b	Radius of the base of the bridge, mm
Ca	Capillary number (Equation 2-8)
D	Distance of closest approach, mm
$\mathbf{d_1, d_2}$	Constants (Equation 2-5)
dD/dt	Rate of separation of the rods, mm/s
$\mathbf{e_1, e_2}$	Constants for the various temperatures of interest (Equation 3-11)
$\mathbf{f_1, f_2}$	Constants (Equation 4-1)
$\mathbf{F_{cap}}$	Total capillary force, mN
$\mathbf{f_s}$	Solvation force per unit area, Pa
$\mathbf{F_s}$	Surface force component, mN (Equation 2-12)
$\mathbf{F_{s,D}}$	Dimensionless surface force (Equation 3-5)
$\mathbf{F_{s,L}}$	Limiting capillary force at minimum **D**, mN (Equation 2-13)
$\mathbf{F_T}$	Total force in the liquid bridge, mN (Equation 3-1)
$\mathbf{F_{T,D}}$	Dimensionless total force in the liquid bridge (Equation 3-7)
$\mathbf{F_{u,i}}$	Adhesive force at commencement of elongation, mN (Equation 5-4)
$\mathbf{F_{u,i,D}}$	Dimensionless adhesive force at commencement of elongation
$\mathbf{F_{u,m}}$	Adhesive force at maximum elongation, mN (Equation 5-3)
$\mathbf{F_{u,m,D}}$	Dimensionless adhesive force at maximum elongation

F_v	Viscous force component, mN (Equation 2-10)
$F_{v,D}$	Dimensionless viscous force component (Equation 3-6)
g_1, g_2	Constants (Equation 2-2)
h_L	Absolute position of the controlled rod, cm (Equation 5-2)
h_t	Perpendicular distance separating the sphere and the plate at the liquid-vapor interface, mm (Equation 2-12)
h_u	Absolute position of the free rod, cm (Equation 5-1)
k_1, k_2, k_3	Constants
L	Length of the sprayed portion of the alloy rod, cm
m_{dry}	Mass of the assembly before spraying and taping, g
$m_{sprayed}$	Mass of the alloy-glass assembly after spraying, drying and the tapes removed, g
n_1, n_2	Constants (Equation 2-3)
N_{Re}	Reynolds number
P	Pressure generated in the liquid bridge as the two bodies are moved apart, Pa
P_c	Critical pressure of liquid or liquid mixture, 0.1MPa(Equation 2-7)
P^L	Pressure in liquid, Pa
P^V	Pressure in gas/air, Pa
q	Variable dependent on thermodynamic properties, mN/m (Equation 2-6)
R	Radius of the sphere, mm (Equation 4-2)
r_1	Radius of the meridian profile at the contact with the sphere, mm
r_2	Radius of the meridian profile at the neck of the bridge, mm
S^{*}	Entropy per unit area at the interface, mN/(m.K)

S_k^L	Entropy of component k in the liquid phase, J/K
T	Temperature of the liquid phase, °C
t	Reaction time (heating time less time to reach 400 °C), s
t_h	Heating time, s
T_R	Actual room temperature of the rod, °C
t_a	Time to touch rods (heating time from the when furnace was turned on till rods touched), s
T_{br}	Reduced boiling point of the compound or mixture
T_c	Critical temperature of the liquid/liquid mixture, K
$t_{dry\text{-}out}$	Experimental dry-out times (heating time till rods dry up less time to reach 400 °C), s (Equation 6-1)
T_r	Reduced temperature of liquid/liquid mixture (Equation 2-6)
t_s	Heating time at the point of commencement of bridge elongation, s
t_v	Heating time at the maximum elongation of the bridge, s
V_L	Voltage reading from the equipment for the controlled rod, V
V_u	Voltage reading from the equipment for the free rod, V
$V_{u,e}$	Voltage reading of the free rod at equilibrium point, V
$V_{u,i}$	Voltage reading of the free rod at the commencement of bridge elongation, V
$V_{u,m}$	Voltage reading of the free rod at maximum elongation of bridge, V
x	Constant (Equation 2-6)
y_k	Mole fraction of component k in the liquid phase

Greek Symbols

ζ_k	Concentration of component k at the interface, mol/m^2
θ	Contact angle of the bridge with the solids (Equation 2-12)
β	Half filling angle
γ	Surface tension, mN/m (Equation 6-2)
η	Viscosity of the liquid, mPas (Equation 6-4)
δ	Initial liquid coating of film thickness, µm (Equation 4-2)
δ_t	Film thickness of the material on the rod after reaction time **t**, mm (Equation 3-11)
$\delta_{t=0}$	The original film thickness before reaction begins, mm
ρ_{liquid}	Density of the liquid of interest, g/cm^3

1. INTRODUCTION

1.1 RESEARCH BACKGROUND

Meeting the ever-increasing global energy demand has required the conversion of the abundant, but largely untapped, heavy oil and bitumen reserves found in many parts of the globe, including Alberta. Exploitation of these vast reserves of heavy oil and bitumen will help to meet the unquenchable demand for fuel energy not fully met by the supply of conventional crude into the world market. However, bitumen is found to contain as much as 50 % residuum, which will require upgrading to be marketable like the conventional crude.

There are a variety of processes used in the upgrading of residuum and one of these is the fluidized bed coking process. Coking involves the thermal cracking of residue feed to produce light ends (gases), distillable liquid and solid coke (Gray, 1994). In the case of vacuum residue, coking involves three reaction stages, with rapid vaporization taking place in the first stage, formation of a viscous surface layer and slower evolution of volatiles in the second stage and solidification in the final stage (McCaffrey et al., 1998). A typical fluidized bed coking process involves spraying the residue feed into a fluid bed, made up of coke particles on which cracking of the feed takes place at temperatures of 510-550 °C (Figure 1-1).

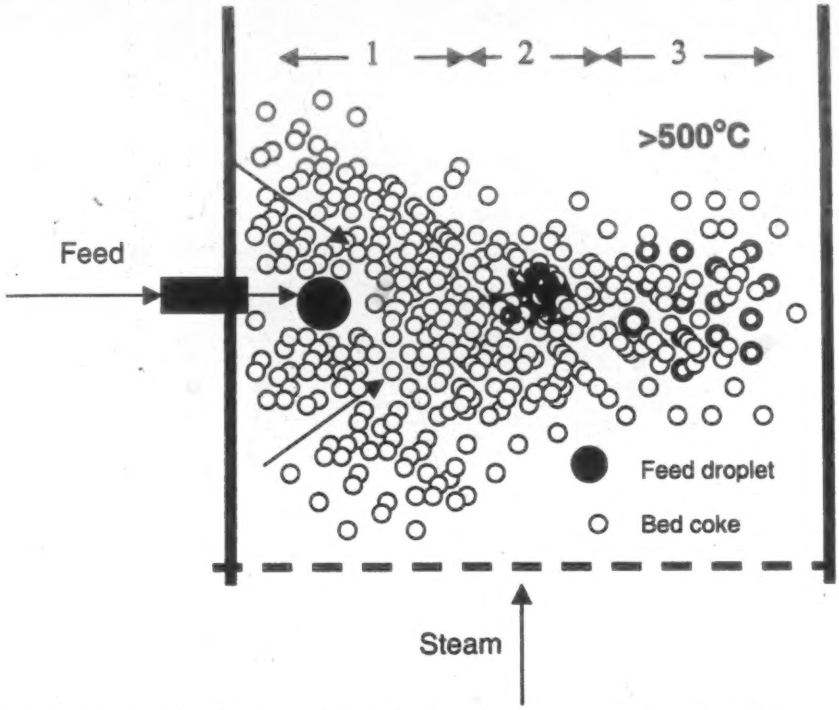

Figure 1-1. Schematic diagram of liquid behavior in a fluid coker (1 - Atomization of feed, 2 - Formation of granules, 3 – Breakup of granules)

The lower limit on temperature is normally operationally set by the ability to fluidize the coke particles. At lower reaction temperatures, the conversion to coke and light ends is too slow, causing the coke particles to become sticky. The stickiness is a result of the drastically increased viscosity that occurs in stage two of the coking reaction of the vacuum residue. Stickiness and the subsequent agglomeration have been found to be largely responsible for the fouling of reactor internals (Gray et al., 2002). Attention is also drawn to the fact that the feed material undergoes tremendous changes in its fluid properties, such as viscosity, throughout its reactions in the fluid coker. These changes in properties are largely believed to be responsible for the stickiness and subsequent agglomeration of coke particles in the reactor.

Since agglomeration of coke particles is undesirable, the changes in the forces responsible for the stickiness with reaction are important. Residue reaction involves bubbling and vaporization, making the use of any existing methods in measuring these fluid properties extremely difficult. To obtain a consistent and reliable measure of properties in a reacting system, a device for measuring adhesive forces in liquid bridges has been fabricated and its performance evaluated in the Chemical and Materials Engineering department of the University of Alberta. Gray et al. (2002) used this device to evaluate the adhesive forces in liquid bridges of Athabasca bitumen vacuum residue (hereafter ABVR) between crossed cylinders. The dependence of pull-off force on reaction time was revealed, and they determined the time required to convert liquid feed of ABVR to a non-adhesive fluid or solid at 503 °C.

1.2 RESEARCH OBJECTIVES

The main objective of this research is the determination of important fluid properties, namely viscosity and surface tension, of reacting ABVR at coking process conditions (temperatures of 510-550 °C). These fluid properties have a relationship with the forces in a liquid bridge (Mazzone et al., 1987), and would allow prediction of the adhesive forces causing stickiness and agglomeration of coke particles in a fluid coker. This study has the following major research objectives:

1. To measure forces in liquid bridges formed between two crossed cylinders, and to develop a method for estimating the viscosity and surface tension of liquid substances from these forces
2. To apply the method developed to evaluate the surface tension and viscosity of ABVR at the process temperatures found in the fluid coker.

2. LITERATURE REVIEW

2.1 PROPERTIES OF ATHABASCA BITUMEN VACUUM RESIDUE (ABVR)

Vacuum residue is a fraction obtained from vacuum distillation of bitumen with an atmospheric equivalent boiling point above 524 °C (Sanford and Chung, 1991). Bitumen is the word used to describe all petroleum-based liquids or semi-solids with a gas-free viscosity greater than 10,000 mPa.s at original reservoir temperature, or an API of less than 10 at 15.6 °C. Athabasca bitumen has an average molecular weight of 620 and consists of 80 % maltene and 20 % wt. asphaltenes (Khan et al., 1984). It contains 52 % 525 °C+ vacuum residue by volume, has a density of between 1002 kg/m^3 and 1027 kg/m^3 at 25 °C (Ward and Clark, 1950), and a viscosity of 500 mPa.s at 80 °C (Schramm et al., 1988). Athabasca bitumen is rich in sulfur, nitrogen, nickel and vanadium, and readily forms coke after thermal reaction (Khan et al., 1984; Dolbear et al., 1987). ABVR, derived from the vacuum thermal reaction of Athabasca bitumen, has the properties shown in Table 2-1 reported.

Table 2-1. Properties of Athabasca Bitumen Vacuum Residue (524 °C+)
McCaffrey et al., 1998

Properties	Values
Density, g/cm^3 at 20 °C	1.0868
Carbon, wt%	81.6
Hydrogen, wt%	9.1
H/C Ratio	1.34
Sulfur, wt%	5.72
Nitrogen, wt%	0.72
Molecular Weight (VPO)	1190
Aromatic Carbon, %	38.7
Micro-carbon Residue, wt%	27.8

2.1.1 VISCOSITY OF BITUMEN AND RHEOLOGY

Viscosity is the resistance of a fluid to flow, defined as the rate of change of shear stress with shear rate. A Newtonian fluid is one that has a constant ratio of shear stress to shear rate over a large range of shear rate. Whenever the ratio is not constant, the fluid is non-Newtonian (Evans and Wennerstrom, 1994; Bird et al., 2002).

Numerous studies have been carried out to classify Athabasca bitumen. Ward and Clark (1950) determined the viscosities and specific gravities of oils in Athabasca bituminous sand. Athabasca bitumen has a frictional force that is directly proportional to the rate of shear; therefore, Athabasca bitumen is a Newtonian fluid. The specific gravity and viscosity of the bitumen vary depending on the mineral content, for example, mineral-free bitumen was found to have a viscosity of 23,600 mPa.s at 29 °C and this increases linearly with mineral content. The viscosity of bitumen was found to depend on the method used for bitumen preparation and the site from which the oil sand was taken. Dealy (1979) found that the viscosity of bitumen increased with the concentration of asphaltenes and dispersed water, while it decreased with the addition of solvents. The rheological properties of bitumen were significantly altered by exposure to air and/or elevated temperatures.

Jacobs et al. (1980) found that the viscosity of Athabasca bitumen was reduced with increasing pressure below 100 °C due to gas saturation. The presence of dissolved carbon dioxide and methane caused a significant reduction in the viscosity of bitumen. On the other hand, Svrcek et al. (1982) found that the viscosity of gas-saturated bitumen decreased significantly with temperature and remained unchanged with pressure. Khan et al. (1984) showed that the slight associative effects that exist between asphaltene molecules caused Athabasca bitumen to have an extremely high viscosity at temperatures below 60 °C, which explained the slight non-Newtonian behavior observed by Dealy (1979) at 27.5 °C, 42.5 °C and 57.5 °C. Chistensen et al. (1984) found that bitumen has non-Newtonian (Bingham) behavior below 100 °C in the low shear rate regime of 0.1 s^{-1} and Newtonian behavior above 100 °C. Shu (1984) observed that the viscosity of Cold Lake bitumen dropped from 1.706 x 10^6 mPa.s to 1.59 x 10^3 mPa.s as temperature increased from 25 °C to 82.2 °C. Schramm and Kwak (1988) found Athabasca bitumen to be Newtonian with a viscosity of 500 mPa.s at 80 °C. From these results, we can conclude that Athabasca bitumen will be a Newtonian fluid at process temperatures >100 °C, and that viscosity will depend on composition and temperature.

The viscosity and rheology of ABVR have not been studied. However, the many studies already done on the rheology of bitumen have indicated that ABVR will exhibit Newtonian behavior at the temperatures characteristic of distillation (200-350 °C) and coking (>450 °C).

Viscosity of crude oil could also be estimated using two-parameter correlations. These correlations have viscosity expressed as a function of temperature and would require taking measurements at two temperatures to apply. Examples of such correlations are the ASTM method and the two-parameter model developed by Khan et al. (1984) for viscosity of Athabasca bitumen. Svrcek and Mehrotra (1988) proposed a one-parameter correlation that matched the data with an average deviation of 6 % compared to 7.1 % - 8.2 % obtained from the model of Khan et al. (1984) at the same applicability temperature range of 20 °C – 130 °C. In their model, Puttagunta et al. (1993) separated the effects of temperature and pressure in viscosity. They proposed another one-parameter model that expressed viscosity as a function of temperature and pressure. Their model gave an average deviation of 4.79 % over the temperature range of 20 °C – 120 °C when used with Athabasca bitumen. One-parameter correlations require only one measurement and to use the correlation proposed by Puttagunta et al. (1993), measurement will have to be taken at 30 °C and 101.3 kPa. These correlations are particularly not suitable for ABVR at temperatures over 350 °C for two reasons. The first reason is that they will not extrapolate well to 500 °C considering that the upper range of their temperature applicability is 130 °C. Secondly, since the ABVR starts reacting at about 350 °C, there will be significant changes in liquid composition as temperature increases.

2.1.2 SURFACE TENSION OF BITUMEN AND ABVR

Surface tension is the force that acts on the surface of a liquid tending to reduce the area of the surface. It is the force that acts across a line of unit length on the surface of a liquid. Surface tension is also defined as the free energy of a surface per unit area of the surface (Evans and Wennerstrom, 1994).

Bowman (1967) found that the surface tension of Athabasca bitumen decreased with increase in temperature. Surface tension decreased from 35 mN/m to less than 20 mN/m as the temperature rose from 20 °C to 100 °C. Using the spinning drop method, Isaacs and Smolek (1983) found the surface tension of Athabasca bitumen to decrease from 30 mN/m at 60 °C to 25 mN/m at 110 °C.

Mehrotra et al. (1985) predicted the surface tension of Athabasca bitumen using models that are based on the principle of corresponding states and the Rice-Teja correlations. Their models predicted the effect of temperature on surface from 60 °C to 112 °C.

Drelich and Miller (1994) measured the surface tension of Whiterock bitumen using the Wilhelmy plate technique. They found that surface tension decreased from 23.6 mN/m at 20 °C to 20.5 mN/m at 60 °C, which is consistent with the observations on Athabasca bitumen. All these studies showed that surface tension is a weak function of temperature. The only work on surface tension of ABVR was done by Li et al. (2003). Surface tension was measured using the pendant drop method and values were reported for ABVR saturated with nitrogen. Both the initial surface tension (after 46 seconds) and the equilibrium surface tensions were measured for various temperatures in the range 150 °C - 280 °C. The results obtained from that study are shown in Figure 2-1. This technique has not been applied at higher temperatures, which are characteristic of vacuum distillation and primary upgrading processes.

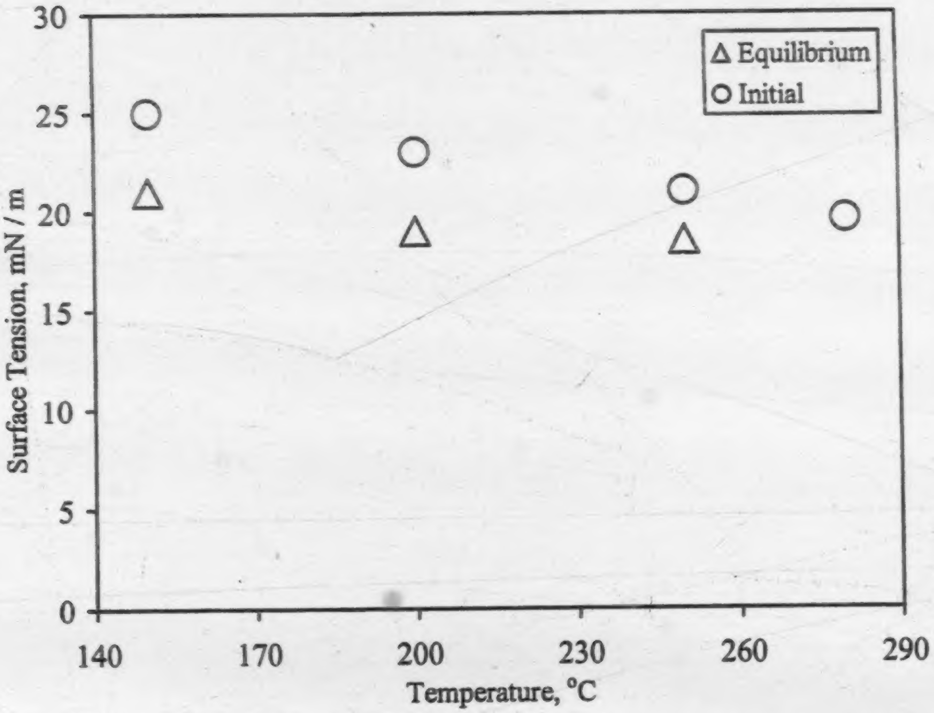

Figure 2-1. Surface tension of ABVR by the pendant drop method reported by Li et al., 2003

2.2 MEASUREMENT OF FLUID PROPERTIES

Viscosity and surface tension of fluids are important properties that determine the behavior of fluids in both reactors and transport systems. For this reason, numerous studies have been done to measure viscosity and surface tension for aqueous solutions, hydrocarbons, polymers and liquid metals. In particular, many authors have measured properties of water. A significant number of studies have developed techniques for measuring the viscosity and surface tension of polymers and liquid metals. The purpose of this section is to discuss some of the methods found in literature and to consider their suitability for measuring viscosity and surface tension of ABVR over 300 °C.

At temperatures over 350 °C, ABVR will begin to react to form vapor products. The rate of cracking to form vapors increases with temperature, until very high rates of reaction are observed above 500 °C. At these conditions, bubbling will occur even in thin films of order 50 µm (Gray et al., 2001; McCaffrey et al., 1998). Eventually, the liquid phase is completely converted to vapors and coke residue. The liquid phase must be heated rapidly to a constant temperature, in order to obtain measurements under controlled kinetic conditions. Reaction times of as little as 30 seconds are observed at 530 °C (Gray et al., 2001), therefore, heating times of much less than 30 seconds are needed. Methods for measuring high temperature properties must control the kinetics of reaction and allow for evolution of vapor.

2.2.1 VISCOSITY MEASUREMENT

Several methods exist for measuring the viscosity of liquids with the most widely used being the rotational viscometer. Couette developed the first practical rotational viscometer in 1890. The viscometer by Couette consisted of concentric cylinders with the outer being a rotating cup and the inner cylinder supported by a torsion wire and rested on a point bearing in the bottom of the cup. Various other forms of rotational viscometers have been developed with the most common being the coaxial cylinder viscometer. Others include cone-and-plate viscometers and the coni-cylindrical viscometer. Some commercial versions can measure viscosity up to 4 x 10^7 Pas (Hatschek, E., 1928; Van Wazer, et al., 1963). Schramm and Kwak (1988) used the concentric cylinder rotational viscometer to measure the viscosity of Athabasca bitumen. The cone and plate viscometer is another type of rotational viscometer that has enjoyed commercial application. It has been developed into the mechanical spectrometer used by Dealy (1979) to study the rheology of Athabasca oil sand bitumen. Rotational viscometers have been developed commercially to measure viscosities at high temperature. However, because the system of interest is a reacting system with bubbling and vaporization, the use of the equipment for this system will give flawed estimates of viscosity, as already noted by Jacobs et al. (1980).

Another prominent viscometer is the capillary viscometer, based on the work of Poiseuille on capillary-flow problems with water. Until 1890, when Couette developed the two concentric cylinders, capillary flow was the only method for estimating properties of fluid. The commercially available versions are the cylinder-piston viscometers, glass capillary viscometers and the orifice viscometers. These viscometers are particularly useful for both Newtonian and non-Newtonian fluids. While these viscometers allow for measurement at high pressure, results become temperature sensitive at temperatures above 300 °C (Van Wazer, et al., 1963). Additionally, Ward and Clark (1950) as well as Schramm and Kwak (1988) used this rheometer to measure the viscosity of Athabasca bitumen and found it to have accuracy within ± 3.5 % of the highest viscosity measured.

Like the rotational viscometers, the capillary viscometers will also give erroneous results with bubbles of gas or vapors in the fluid being measured. The results are highly dependent on the density of the fluid, which will also vary with temperature and time for reacting ABVR.

The vacuum viscometer was used by Christensen et al. (1984) to measure the viscosity of Utah tar sand. This viscometer was particularly useful as it could measure viscosities lower than 0.01 Pas and higher than 50,000 Pas with accuracy of < 0.1 % up to a temperature of 200 °C. This method is not as accurate at temperatures above 500 °C needed for this study, as bubbling will significantly increase the variability that this method has been known to exhibit above 200 °C.

Other viscometers include the falling-ball, rolling-ball, rising-bubble, telescopic-shear, transverse flow, sliding parallel-plate and band viscometer methods. None of these methods are useful for the system of interest, for either or both of the reasons of extreme temperature and vapor presence in the reacting system.

Additional novel techniques have been developed to allow for the measurement of viscosity where the viscometers mentioned above were found deficient. One of these methods is the oscillating drop method used by Matsumoto et al. (2002) to measure the viscosity of water at 23.5 °C, which was found to be 0.92 mPa.s. Reaction leading to volatilization will alter the results from this method, as it is very sensitive to the presence of any external force. Another novel technique is the contactless viscosity measurement by the gas-film levitation used for high temperature measurements. Haumesser et al. (2002) used it to measure the viscosity of oxides and metallic glasses. They found this method to measure viscosity with an accuracy of ±10 % at temperatures as high as 1700 °C. The constant mass and density of the drop, on which this method relies, makes it unsuitable for the reactive system of interest with changing density and mass of material. In addition, the gas stream will be enriched with the volatile products of reaction thus introducing errors into the viscosity estimation.

Based on this review, none of the existing measurement methods are suitable for measuring the viscosity of ABVR under reaction conditions.

2.2.2 TEMPERATURE DEPENDENCE OF VISCOSITY

Liquids become less viscous as their temperature increases (Poling et al., 2000). Several authors have studied this decrease in viscosity with temperature. Based on the theory of liquid viscosity, Andrade (1930) proposed a correlation to show the dependence of viscosity on temperature. The correlation developed by Andrade (1930) showed an Arrhenius relationship between temperature and viscosity as shown below:

$$\eta = Ae^{B/T} \tag{2-1}$$

where **A** and **B** are constants. Two viscosity-temperature data points are needed to fix the values of the two constants, which vary for different liquids. Equation 2-1 forms the basis for most of the other correlations of liquid viscosities. However, because of the failure of this correlation at low temperatures and for liquid mixtures, other correlations had to be developed for other systems (Poling et al., 2000). Temperature dependence of viscosity in hydrocarbon mixtures is widely estimated with the ASTM D341 correlation (Svrcek and Mehrotra, 1988) given in Equation 2-2.

$$\log(\log(\eta)) = g_1 + g_2 \log(T) \tag{2-2}$$

Where $\mathbf{g_1}$ and $\mathbf{g_2}$ are constants. Another correlation widely used for hydrocarbon is the Walther equation (Gray, 1994) given below:

$$\ln(\ln(\eta)) = n_1 + n_2 \ln(T) \tag{2-3}$$

where $\mathbf{n_1}$ and $\mathbf{n_2}$ are constants.

Svrcek and Mehrotra (1988) proposed a one-parameter correlation for bitumen viscosity over a temperature range of 10 °C to 130 °C. The correlation is based on the ASTM D341 correlation. Khan et al. (1984) empirically modified the model theories of Eyring and Hilderbrand to correlate and predict viscosity of Athabasca bitumen in the temperature range of 20 °C to 130 °C. The average deviations were 13 % and 7.5 % respectively for Eyring and Hilderbrand models. The two-parameter models in Equation 2-1 to Equation 2-3 predicted bitumen viscosity with an average deviation of 4 % - 10 %. Puttagunta et al. (1993) isolated the effects of temperature and pressure on viscosity of bitumen to develop a one-parameter correlation relating viscosity to temperature and pressure. The correlation required taking a viscosity measurement at 30 °C and 101.3 kPa pressure to evaluate the constant. The correlation is useful in the range 20 °C to 120 °C with an average deviation of 4.79 %.

These equations gave a good correlation of viscosity with increasing temperature. However, all these equations only accounted for the effect of T at constant composition and they cannot be used for ABVR above 350 °C, where reaction causes compositional changes. Furthermore, the parameters in these equations were obtained below 130 °C and they cannot be used for ABVR above 350 °C. Extrapolating to such a high temperature will give flawed estimates of viscosity.

2.2.3 SURFACE TENSION MEASUREMENT

One of the most reliable methods for measuring surface tension is the capillary rise method. The surface tension of a liquid is estimated by the relationship between the curvature of a meniscus formed by the liquid in a capillary tube and the pressure head of the liquid in the tube. A more precise estimate can be obtained if a correction is made for the difference in densities of the liquid and the other gas present (Burdon, 1949). For example, Okada et al. (1989) used this method to measure the surface tension of n-hexane and n-octane with an accuracy of ± 0.20 mN/m. However, for ABVR at elevated temperatures, vaporization and bubbling of volatiles will render the method inaccurate.

The drop-weight or drop-number is another method used for measuring the surface tension of liquid, but its accuracy was found to be doubtful as the estimate from this method is completely dependent on the weight or number of drops from a standard capillary tip (Burdon, 1949). The weight or number of these drops will be completely unreliable in a system with a significant vaporization, as mass loss will occur.

In the maximum bubble pressure method, a pure neutral gas is used to blow bubbles through two tubes of different diameters dipped into a liquid of unknown surface tension. The surface tension is related to the pressure required to release the bubbles from each tube. This method has been used to rapidly determine the surface tension of liquid metals. A limitation of this method is that it is difficult to differentiate bubbles that originated from the neutral gas from those that originated from vaporization or from reaction products. In addition, Horozov et al. (1996) found a strong effect of wettability of the capillary on the bubble growth, which introduced some errors in the surface tension measured.

Surface tension can also be found from the shape of a pendant or a sessile drop, based on the Laplace relation between curvature, surface tension and pressure difference. The main advantage of this approach is that data can be collected in either vacuum or under elevated pressures. A flaw in this method is that significant error can be introduced by variable density (Sangiorgi et al., 1982). Once again, volatilization and bubbling will render the drop unstable, thus making the method unusable for reacting ABVR. Li. et al. (2003) measured the surface tension of ABVR at < 280 °C, as discussed in Section 2.1.2. A related approach is the quasi-containerless pendant drop method used by Man (2000) to measure surface tension of liquid metal. In this case, surface tensions of greater than 2000 mN/m were measured. However, like the other methods already discussed, this method will be inapplicable at the required temperature of up to 500 °C, due to volatilization and bubbling.

Surface tension can also be calculated from measurements of the rate of oscillation of falling drops and jets from non-circular orifices. This method was found to have a reasonable margin of error for the surface tension of water, with values between 72.98 mN/m and 73.41 mN/m at 23.5 °C. Matsumoto et al. (2002) improved this method by using a needle sharpened like a circular cone. The improved version was used to measure the surface tension of water, which was found to be 68.9 mN/m and 71.8 mN/m at the same temperature of 23.5 °C. This method is not applicable to reacting systems because the jets or drops will be rendered unstable by the volatiles produced by the generation of reaction products.

Kelvin derived a relationship for the dependence of the velocity of waves on deep water, on the surface tension, wavelength and either the velocity or the frequency of the waves (Burdon, 1949). His work formed the basis for the capillary ripples method for surface tension measurement. The patterns formed at a gas/liquid interface of a system that agitates are capillary ripples or waves with structures dominated by the surface tension of the liquid. With this method, the surface tension of water was found to range from 71 mN/m to 76 mN/m. A major limitation when this method is applied to reacting system is that the surface cannot be disturbed by the formation of bubbles.

The most common method used to measure surface tension is the adhesion rings and plate method. This technique is based on measuring the force needed to lift a narrow glass slide or a horizontal ring of wire from a liquid surface. An improved version is the Wilhelmy plate method, used by Anilkumar et al. (1987) to measure the values of the surface tension of water, which they found to be 72.93 ± 0.03 mN/m at 20 °C and 72.13 ± 0.04 at 25 °C. Rolo et al. (2002) used this method to estimate the surface tension of alkanes and found that the method gave results with an average deviation of 1.6 % between 25 °C and 70 °C. This Wilhelmy method has been used extensively to develop digital tensiometers. However, it is not suitable for reacting system because the system must be very stable without bubbles.

Several of the techniques mentioned can be used at high temperature but none of them is suitable for a reacting material that generates bubbles of vapor, and has mass that changes.

2.2.4 DEPENDENCE OF SURFACE TENSION ON TEMPERATURE

Tester and Modell (1996) developed an expression for the changes in surface tension with temperature in terms of entropy and surface concentration on the liquid-gas interface with a view to giving a thermodynamic explanation to the changes in surface tension at high temperature. They proved that, regardless of curvature, temperature and chemical potentials were equal in all phases of any equilibrium multiphase system. This observation was used to arrive at Equation 2-4 for an ideal solution of a multi-component system, assuming constant composition and constant pressure in the liquid phase.

$$-\left(\frac{\partial \gamma}{\partial T}\right)_{y_k} = S^{*} - \sum_{k=1}^{n} \zeta_k S_k^L \qquad (2\text{-}4)$$

Where S^* is the entropy per unit area at the interface, S_k^L is the entropy of component **k** in the liquid phase, y_k is the mole fraction of component **k** in the liquid phase, ζ_k is the concentration of component **k** at the interface and **T** is the temperature of the liquid phase.

The right hand side of Equation 2-4 is approximately constant due to compensating changes in the three variables with temperature, in systems with reduced temperature (T/T_c) of 0.4 – 0.7 (Poling et al., 2000). The degree of disorderliness is greater at the interface than in the bulk liquid phase, therefore, S^* is greater than the summation term on the right hand side of Equation 2-4 and surface tension will decrease with increasing temperature. However, estimating surface tension from Equation 2-4 is difficult because of the indefinite nature of S^*

and its dependence on the thickness of the interface. Instead, other correlations were developed to estimate surface tension as a function of temperature.

Following Equation 2-4, one useful correlation relating surface tension and temperature linearly (Poling et al., 2000).

$$\gamma = d_1 + d_2 * T \tag{2-5}$$

where **d_1** and **d_2** are constants. This correlation clearly showed that change in surface tension with temperature is a constant. Equation 2-5 gave a satisfactory approximation of surface tension, notably for pure organic compounds, and the values of **d_1** and **d_2** have been obtained for many materials. Most authors used a correlation of the form given below (Poling et al., 2000):

$$\gamma = q*(1-T_r)^{4x} \tag{2-6}$$

where **x** is a constant, **T_r** is the reduced temperature and **q** is dependent on thermodynamic properties. Equation 2-6 suggests that surface tension has a weak non-zero order dependence on T. For example, the principle of corresponding states for any non-polar liquid gave a value of 0.305 for **x** and an expression for **q** given by Equation 2-7 (Darwish et al., 1995).

$$q = P_c^{2/3} T_c^{1/3} \left[0.1196 \left(1 + \frac{T_{br} \ln(P_c / 1.01325)}{1 - T_{br}} \right) - 0.279 \right] \quad (2\text{-}7)$$

where P_c is the critical pressure of the compound or mixture, T_c is the critical temperature of the compound or mixture; and T_{br} is the reduced boiling point of the compound or mixture. Most organic liquids were found to have similar values of **x**, consequently, their surface tensions were found to be similar to within ± 5 mN/m at the same temperature (Poling et al., 2000).

Tripathi and Mathur (1977) modified the expression for **q** and the value of **x** in Equation 2-6 to develop another model, which they found to predict surface tension of hydrocarbon mixtures with an absolute average deviation of 5.54 % up to 170 °C. The principle of corresponding states was found to give good prediction of surface tension between 60 °C and 112 °C. It was used to estimate the surface tension of Athabasca bitumen by Mehrotra et al. (1985) and of naphtha reformate by Darwish et al. (1995). In the same temperature range, the Rice-Teja correlation was found to agree with experimental data of Isaacs and Smolek (1983) with 5 % to 12 % deviation (Mehrotra et al., 1985). The Rice-Teja correlation employed Equation 2-6 but used properties of two non-spherical reference fluids to predict the surface tension of liquid mixtures, instead of the mixing rule of pseudocritical properties used in the principle of corresponding states. Therefore, surface tension dependence on temperature will be similar for both the Rice-Teja correlation and the principle of corresponding states. The chosen reference fluids for the Rice-Teja correlation often have properties similar to those of the key components in the liquid mixture. An empirical correlation was proposed by Lielmezs and Herrick (1986) for predicting surface tension between the triple and critical points of pure liquids. Their correlation showed a weak non-zero dependence of surface tension on temperature. None of the surface tension correlations could be used with ABVR because they will not extrapolate well to temperatures above 350 °C, at which surface tension of ABVR is desired.

2.3 SURFACE TENSION IN EVAPORATING SYSTEMS

The peculiar nature of ABVR is that measurement of surface tension is required under conditions where vaporization and reaction are significant. The following section reviews the literature on surface tension in the presence of evaporation, to determine the dependence of surface tension on mass transfer.

Malyshenko and Dunikov (2002) considered the surface tension corrections in non-uniform and non-equilibrium liquid-gas systems and concluded that non-uniformities of temperature and pressure arising due to intense phase transitions or on curved interfaces lead to modification of the surface tension. Surface tension was also observed to decrease for bubbles with intense evaporation from their planar interface. Chen (2001) found that the process of migration and adsorption of volatile organic compounds to the liquid-air interface of evaporating systems before evaporation is not diffusion controlled but rather evaporation controlled. At shorter time range, diffusion was found to play minor roles but not at later times.

So, an evaporation-diffusion model was developed to explain the dynamic surface tension. The model failed at longer times because of its diffusion portion that has short time applicability. In their study of the interfacial conditions during evaporation or condensation of water, Ward and Stanga (2001) found that a temperature discontinuity exists at the liquid-vapor interface, which is independent of the direction of phase change with the temperature always greater in the vapor. They concluded that the difference in temperature between the vapor and the liquid phases determines how well the liquid is compressed by the interface and how well the vapor is superheated.

Effects of compositional changes on surface tension were studied by Eres et al. (1999), who found that surface tension gradients were created due to compositional changes in a layer of liquid. They concluded that surface tension gradients, arising from compositional changes across a film, have an extreme effect on the flow pattern of thin liquid coatings. Ricci and Passerone (1993) showed that thermodynamic equilibrium considerations alone are not sufficient to explain surface tension measurements at high temperatures, but rather diffusion and interactions in the vapor phase are equally vital. Therefore, to have a complete understanding of surface tension values at high temperatures, variation of surface tension with temperature as well as with composition effects should be known.

2.4 FORCES DUE TO LIQUID BRIDGES

At coking conditions of 500 °C and above, the ABVR undergoes significant cracking that leads to the volatilization of lower molecular weight products, which makes it difficult to use standard methods to measure fluid properties. One possible technique that may apply to reacting systems is to measure the forces in a liquid bridge between two solid objects. These forces are related to the viscosity and surface tension of the liquid forming the bridge.

Plateau (1863-1866) was the first to note that the geometry and properties of a liquid placed between two plates is related to the force in the fluid when the two plates are pulled apart. Since then, a variety of work has been done on the forces in liquids in contact with solid surfaces. Moriarty and Schwartz, (1991) found that the motion of a droplet, detaching from a thin liquid film on the surface of a vertical wall, is governed by a force balance between viscosity, gravity and surface tension at the free surface while inertia is negligible for the viscous flow. Eggers and Dupont (1994) studied necking in drop formation, and found singularities at the break point of the drop from the body of the fluid. Gillette and Dyson (1971) predicted the minimum volume needed to form a bridge between a pair of flat plates and the maximum possible volume for a stable bridge to exist between circular plates. The studies of Meseguer (1983) and Slobozhanin et al. (2002) considered the stability margins for stable liquid bridges and found the domain of the stability region and the finite height of the potential energy barriers that must be exceeded for a bridge to lose stability. In other studies, Peregrine et al. (1990) presented an exploratory study of the fluid motion associated with breaking of liquid bridges and identified the three stages involved as necking, bifurcation and recoil. Wilson (1988) found the mass of a pendant droplet that drips out of a vertical tube, and defined its dependence on surface tension.

In the context of fluid bed of particles, Huang and Kono (1988) established that the existence of a liquid at the contact area of colliding surfaces necessitates the formation of liquid bridges, which causes adhesive force, and coalescence between the colliding granules. This mechanism lead to the growth of the granules in batch fluidized bed granulation. This result was very similar to the findings of Ennis et al. (1991), who also confirmed that the strength of a dynamic pendular bridge could exceed that of the static bridge by at least an order of magnitude. Viscosity makes an additional and often dominant contribution to the strength of the dynamic pendular liquid bridge, which is in agreement with the findings of Mazzone et al. (1987).

The published work on liquid bridges discussed gave the origin and importance of the liquid bridge between solid bodies and its inter-relationship with properties of the liquid. Information was also presented on the need to consider both static and dynamic components in a liquid bridge.

2.4.1 LIQUID BRIDGES BETWEEN TWO MOVING SPHERES

The coke particles used in the fluid coker are approximately spherical; therefore, a liquid bridge between two moving spheres is an important geometry.

A cross section of a liquid bridge between two spheres is shown below in Figure 2-2.

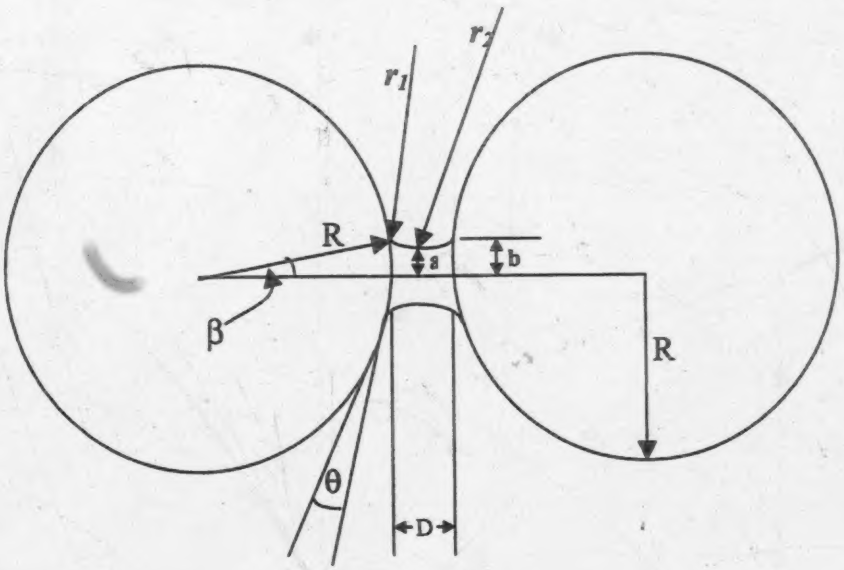

Figure 2-2. Cross section of liquid bridge between two spheres

Where **R** is the radius of the sphere, r_1 is the radius of the meridian profile at the contact with the sphere, r_2 is the radius of the meridian profile at the neck of the bridge, **D** is the distance of closest approach, **a** is the radius of the neck of the bridge, **b** is the radius of the base of the bridge, θ is the contact angle of the bridge and β is the half filling angle.

Mazzone et al. (1987) found that the force in a liquid bridge comprises the viscous force and the surface force due to the bridge. Ennis et al. (1990) agreed with this assertion and went further to estimate the viscous force based on lubrication theory and the surface force based on a circular approximation. By analyzing two spheres in relative motion with each other, both studies confirmed that only full understanding of the properties of liquid bridges can allow for the development of models for agglomeration. Ennis et al. (1990) also went further to infer that capillary number, **Ca**, a function of viscosity, surface tension and relative velocity of the spheres, largely governs the strength of a dynamic pendular liquid bridge. **Ca** is defined below in Equation 2-8.

$$\mathrm{Ca} = \frac{\eta}{\gamma} * \frac{dD}{dt} \qquad (2\text{-}8)$$

Where η is viscosity, **t** is time and γ is surface tension. They also confirmed that the bridge strength is a function of only viscosity at high **Ca** (>1). While studying the rupture in liquid bridges between two spheres in relative motion, Willet et al. (2000) and Fairbrother et al. (1998) found that the contribution of capillary force due to surface interactions is small in systems involving bodies where the neck radius is small relative to the sphere radius (**a** << **R**). This situation is normally observed when there is considerable elongation of the bridge.

As suggested by Ennis et al. (1990), the viscous force component of the force in a liquid bridge, was determined by several authors using the Reynolds lubrication theory of fluid flow through a very small clearance bounded by two solid surfaces. Lubrication theory assumes that flow between nonparallel surfaces can be considered locally as flow between parallel surfaces (Bird, et al., 2002). This assumption is referred to as the lubrication approximation. Pitois et al. (2000 and 2001) adopted the same approach for viscous force in a constant volume liquid bridge between two spheres with relative motion. This allowed them to develop an expression for Reynolds equation given in Equation 2-9, which relates the pressure **P** generated in the liquid bridge as the two bodies were moved apart.

$$\frac{d}{dr}\left[r h_t^3(r)\frac{dP(r)}{dr}\right] = 12\eta r\frac{dD}{dt} \tag{2-9}$$

After assuming an infinite liquid and cylindrical bridge, double integration yielded an expression for the viscous forces acting on the two spheres. This expression is given in Equation 2-10.

$$F_v = \frac{3}{2}\pi\eta\frac{R^2}{D}\frac{dD}{dt} \tag{2-10}$$

The expression given for $\mathbf{F_v}$ represents only a portion of the force in dynamic liquid bridges. The second part is the surface component not shown. It is the addition of these two portions that make up the total force in a liquid bridge (Pitois et al., 2001). Also, dynamic rupture distance was observed to increase compared to the static and this increase could be related to **Ca** when both the surface and viscous components are summed up to obtain the total force in a liquid bridge.

2.4.2 LIQUID BRIDGES BETWEEN TWO CROSSED CYLINDERS

Though, the coke particles in a fluid coker are approximately spherical, for simplicity of design, the simplest experimental method is to employ crossed cylinders to simulate the bridge contact between two spherical particles. For this reason, it is important to understand liquid bridges between crossed cylinders.

Fisher and Israelachvili (1981) found that the geometry of a liquid bridge between non contacting crossed cylinders of radius **R** with separation distance **D** will have a geometry that is almost equivalent to that of a sphere of radius **R** near a flat plate. This approximation allows for the use of a sphere and plate geometry for the analysis of the force in liquid bridges between crossed cylinders. Figure 2-3 shows the cross section of a liquid bridge between a sphere and a flat plate. As will be shown later in Section 3.1, the use of proper geometry will have a pronounced effect on the estimation of capillary force.

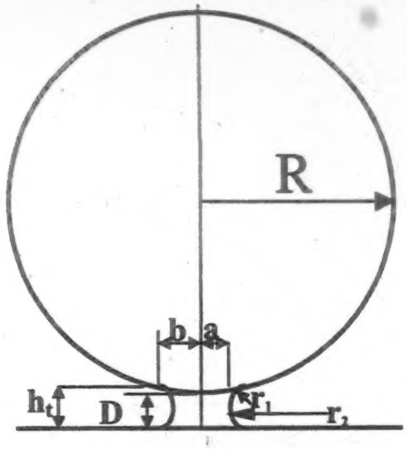

Figure 2-3. Cross section of a liquid bridge between sphere and plate

All the variables in Figure 2-3, except **h_t**, are defined as in Figure 2-2. **h_t** is the separation distance at the liquid solid contact lines. Equation 2-11 gives the definition for **h_t** (Evans and Wennerstrom, 1994).

$$h_t = D + \frac{b^2}{2R} \qquad (2\text{-}11)$$

Frink and Swol (1997) found an expression for the capillary force in the sphere and plate geometry, which is dependent on surface tension, separation distance, radius of the sphere and the contact angle. The expression is given in Equation 2-12.

$$F_s = 4\pi R\gamma\cos\theta\left(1-\frac{D}{h_t}\right); \qquad D \le h_t \tag{2-12}$$

Where $\mathbf{F_s}$ is the surface force and γ is the surface tension. From this expression, the limiting capillary force was obtained for a minimum value of **D** to be $\mathbf{F_{s,L}}$ given in Equation 2-13.

$$F_{s,L} = 4\pi R\gamma; \quad \text{when} \quad D \ll b \quad \text{or} \quad D \sim 0 \tag{2-13}$$

Which is in agreement with the expression found by Tabor (1977) to be the force at instantaneous separation when the sphere and the plate were pulled apart.

This, like other studies mentioned here, gave expressions for capillary force in a relevant geometry, which means that one component of the force in liquid bridge, is obtained. The viscous component, yet to be determined for the useful geometry, will have to be developed separately.

3. THEORY

In the preceding chapter, it was established that the liquid bridge between two coke particles is a microcosm of one mechanism for agglomeration found in a fluid coker. From fundamental work, the bridge between two spheres in relative motion may also be used to analyze liquid properties. However, for simplicity of fabrication, the liquid bridge between two crossed cylinders was used in this study to simulate the bridge between two spheres. For this reason, the liquid bridge between sphere and plate, which represents the best approximation for crossed cylinders, was employed in the derivations in this study.

3.1 FORCES IN A LIQUID BRIDGE BETWEEN SPHERE AND PLATE

As mentioned in Section 2.4.1, Mazzone et al. (1987), Ennis et al. (1990) and Pitois et al. (2000 and 2001) all asserted that force in a liquid bridge is the sum of the viscous force and the surface force, with inertia being negligible. Consequently, a simple expression shown in Equation 3-1 can be written for the total force in a liquid bridge.

$$F_T = F_s + F_v \qquad (3\text{-}1)$$

F_T is the total force in the liquid bridge, which is measured experimentally, **F_s** is the surface force component and **F_v** is the viscous force component. In this section, these forces will be discussed as they apply to the sphere and plate geometry. To aid in this analysis is Figure 3-1, which is the close up of a liquid bridge between sphere and plate (based on Figure 2-3 from Section 2.4.2).

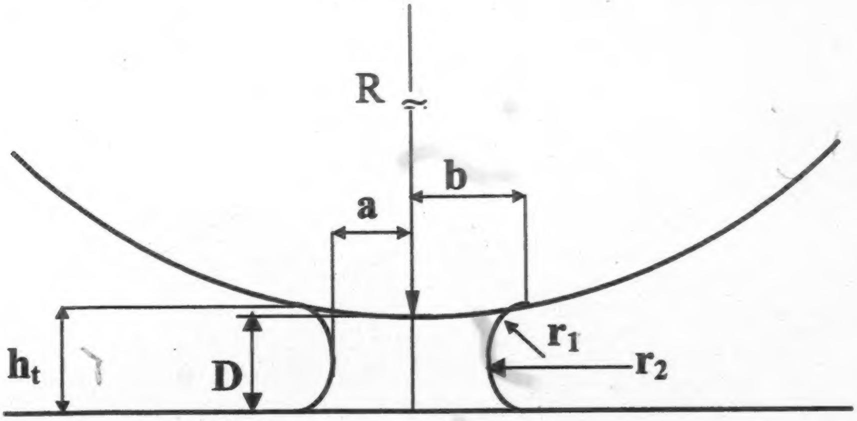

Figure 3-1. Close up of the liquid bridge between sphere and plate

3.1.1 SURFACE COMPONENT OF THE FORCE

Surface force in the liquid bridge is equivalent to the capillary force because the distance of closest approach of the sphere and the plate is very small compared to the radius of the sphere (Frink and Swol, 1997). For the equipment used in this study, the crossed cylinders were coated with a continuous film of liquid material, so the contact angle is zero. Two regimes are expected in the course of the formation, elongation and final rupture of the liquid bridge. The first is the regime where **D** is extremely small compared to the radius of the base of the bridge, **b**, and the second regime is when the bridge is visibly elongated (**D** ≥ **b**). In the first regime, the surface force expression in Equation 2-13 is applicable. In the second regime with elongated bridge, Equation 2-11 can be written for h_t (Evans and Wennerstrom, 1994) and the surface force reduced to Equation 3-2:

$$F_s = \pi \gamma b \left(1 + \frac{b}{r_1}\right); \quad \text{when} \quad D \geq b \tag{3-2}$$

A complete proof is given in Appendix A1. It is particularly noteworthy that Equation 3-2 is similar to the equation obtained by Fairbrother et al. (1998) and Pitois et al. (2000 and 2001) using the Gorge method, for a liquid bridge between two spheres with relative motion.

3.1.2 VISCOUS COMPONENT OF THE FORCE

Variable h_t given in Equation 2-11 as obtained by Evans and Wennerstrom (1994) for sphere and plate geometry was used to solve Equation 2-9. The assumptions of an infinite liquid and a cylindrical bridge were employed as used by Pitois et al. (2000 and 2001) and an expression similar to Equation 2-10 was written for the viscous force acting on the sphere in the sphere and plate system. This expression is given in Equation 3-3.

$$F_v = \pi \eta \frac{3R^2}{D} \frac{dD}{dt} \tag{3-3}$$

Equation 3-3 is valid only for a constant-volume liquid bridge. When the crossed cylinders, or the sphere and the plate, are coated with a thin liquid film of thickness, δ, the volume of the bridge will change due to the drainage of the liquid into and out of the bridge. This drainage will have a pronounced effect on the viscous force; the equations for a constant volume bridge will serve as a useful guide for the analysis of the film geometry.

3.2 FORCES IN A VARIABLE VOLUME LIQUID BRIDGE BETWEEN SPHERE AND PLATE

Equation 3-1 is valid for describing the total forces in a variable volume liquid bridge. However, the component forces will be expected to behave differently in a variable volume liquid bridge as compared to a constant volume bridge. The surface force is relatively unaffected by the change in volume, because the geometry is unaffected in the limit of **D** << **b**. The main challenge, therefore, is the analysis of the viscous component.

3.2.1 VISCOUS COMPONENT OF THE FORCE

With an initial liquid coating of film thickness, δ, the effect of the variable volume on the viscous force has to be studied and a more accurate expression developed to take into account the drainage of liquid from the film into the bridge. A semi-empirical dimensional analysis was used to develop the appropriate expression for the viscous component of the force in a variable volume liquid bridge.

3.2.2 MODEL DEVELOPMENT OF THE VISCOUS COMPONENT

To allow for the analysis in dimensionless terms, the variable $\mathbf{F_T}$ was made dimensionless by multiplication with $\mathbf{D/(R^2.\gamma)}$ to obtain $\mathbf{F_{T,D}}$, dimensionless total force in the liquid bridge:

$$F_{T,D} = F_{s,D} + F_{v,D} \tag{3-4}$$

Where $\mathbf{F_{s,D}}$, the dimensionless surface force, obtained from rendering $\mathbf{F_s}$ dimensionless can be estimated from the expression given below.

$$F_{s,D} = \begin{cases} 4\pi\left(\dfrac{D}{R}\right); & D << b\,,\ D \neq 0 \\ \dfrac{\pi b D}{R^2}\left(1+\dfrac{b}{r_1}\right); & D \geq b \end{cases} \tag{3-5}$$

$\mathbf{F_{v,D}}$ is the dimensionless viscous force, which will have to be determined by a semi-empirical method. All the dimensionless groups that could contribute to this variable were considered critically. Capillary number, **Ca**, was found to be natural to this system because it is the ratio of viscous to capillary forces. In this case, the capillary number is defined as in Equation 2-8. Reynolds number, N_{Re}, was assumed to be less than 2, due to the low velocity and creeping flow. The other relevant dimensionless groups are **(δ/R)** and **(D/R)**, the ratios that include the initial film thickness of liquid **(δ)**, causing the drainage into the liquid bridge, and the separation between the sphere and plate **(D)** on which the drainage also has a pronounced effect. The dimensionless viscous force is given in Equation 3-6.

$$F_{v,D} = k_1 \, Ca \left(\frac{\delta}{R}\right)^{k_2} \left(\frac{D}{R}\right)^{k_3} \tag{3-6}$$

This expression was substituted into Equation 3-4 to obtain Equation 3-7.

$$F_{T,D} = F_{s,D} + k_1 \, Ca \left(\frac{\delta}{R}\right)^{k_2} \left(\frac{D}{R}\right)^{k_3} \tag{3-7}$$

This equation can be used with liquids of known properties to determine the values of constants $\mathbf{k_1}$, $\mathbf{k_2}$ and $\mathbf{k_3}$ after obtaining values of other variables from either experiments or standard oil specifications.

It is important to note that the expression for $\mathbf{F_{T,D}}$ in Equation 3-7 can be simplified depending on the regime of the bridge being considered. For a bridge regime with **D << b**, and zero rate of separation (i.e. **Ca** = 0), then the measurable force will be:

$$F_{T,D} = 4\pi\left(\frac{D}{R}\right) \tag{3-8}$$

As the bridge elongates, the viscous term becomes non-zero and the surface force is based on Equation 3-5 where **D ≥ b**:

$$F_{T,D} = \frac{\pi b D}{R^2}\left(1+\frac{b}{r_1}\right) + k_1\,\mathrm{Ca}\left(\frac{\delta}{R}\right)^{k_2}\left(\frac{D}{R}\right)^{k_3} \tag{3-9}$$

3.3 CHANGE IN ABVR FILM THICKNESS WITH REACTION

For ABVR, the original film thickness, **δ**, depletes with time of reaction at cracking temperatures (> 350 °C). Consequently, in order to determine the correct film thickness that goes into Equation 3-9, a model was developed to describe the variation of film thickness of ABVR with reaction time.

$$\frac{d\delta}{dt} = -e_1\,\delta^{e_2} \tag{3-10}$$

Equation 3-10 has constants, e_1 and e_2, which are functions of temperature, and reflect the underlying cracking reactions. Equation 3-11 is obtained from the integration of Equation 3-10.

$$\delta_t = \left[\delta_{t=0}^{(1-e_2)} + e_1 t_h (e_2 - 1)\right]^{\frac{1}{(1-e_2)}} \qquad (3\text{-}11)$$

Where δ_t is the film thickness of the material on the rod after heating time, t_h, and $\delta_{t=0}$ is the original film thickness before reaction begins.

4. MATERIALS AND METHODS

4.1 FEED AND CHEMICALS

Syncrude Canada Limited supplied ABVR, the 524 °C+ boiling fraction of Athabasca bitumen, with a density of 1086.8 kg/m^3. The ABVR contains 5.8 % sulfur, 0.7 % nitrogen, 24.7 wt % pentane asphaltenes and 27.8 % microcarbon residue, 1.8 % toluene insolubles and 1.25 % ash. Methylene chloride, the solvent, was supplied by Fisher Scientific (Toronto, Ontario) while pre-purified nitrogen was supplied by PRAXAIR Canada (Mississauga, Ontario). Both methylene chloride and prepurified nitrogen were used as supplied.

4.2 CURIE POINT ALLOY FOR FILM HEATING

To allow for rapid heating of the ABVR to the reactor temperature of 510-550 °C in the laboratory, a safe, fast and effective means was by using Curie point alloys in an induction furnace. The Curie point is the temperature at which a material loses its magnetic properties. Nickel/iron alloys have Curie point temperatures that range from 160 °C to 1040 °C depending on composition (DyChrome, San Jose, California, U.S.A). The components of an induction furnace system are an alternating current power supply, an induction coil, and a work-piece (Curie point alloy to be heated or treated). The power supply sends alternating current through the coil to generate a magnetic field. When the alloy is placed in the coil and enters the magnetic field, eddy currents are induced within the alloy, rapidly generating precise amounts of localized heat without any physical contact between the coil and the alloy. The temperature of the alloy rises until the Curie point temperature is reached and magnetism is lost. Consequently, Curie point alloys were used for the crossed cylinders coated with very thin films (24 µm – 28 µm) of ABVR in order to heat the ABVR to the desired temperature in the shortest possible time.

The rods of Curie point alloy used in this study came from four different sources. Those for temperatures of 312 °C, 356 °C and 400 °C, of diameters 0.62 mm, 0.98 mm and 0.62 mm respectively, were supplied by DyChrom (San Jose, California, U.S.A.). The Curie point alloy for temperature of 466 °C, of diameter 1.47 mm, was supplied by National Specialty Alloys (Houston Texas, U.S.A). AMETEK Specialty Metal Products Division (Wallingford, Connecticut, U.S.A) supplied the Curie point alloy for temperature of 504 °C with a diameter of 1.9558 mm. For temperature of 530 °C, welding rod (UTP Econocast 55NiFe-Cl, AIR LIQUIDE) was scraped of its flux and the rod turned on a lathe machine to a 2.04 mm diameter rod.

4.3 STANDARD CALIBRATION OILS

Viscosity standards for viscometer calibration were supplied by Cannon Instrument Company (State College Pennsylvania, U.S.A.). The properties of the standard oils are presented in Table 4-1. N600 is a mineral oil, N1000 is a clear poly alpha olefin and N2000, N4000 and N8000 are clear poly-butenes. The supplier provided viscosity and density data. Surface tension of the oils was measure using the pendant drop method (1999 model, LIA Technologies, Woodridge, Ontario, Canada).

Table 4-1. Properties of Standard Oils for Calibration

Oil Code	Viscosity at 25 °C, mPa.s	Density at 25 °C, g/cm^3	Surface tension at 25 °C, mN/m
N600	1,405	0.8898	32.610 ± 0.073
N1000	2,003	0.8467	31.432 ± 0.018
N2000	5,995	0.8753	31.655 ± 0.632
N4000	10,410	0.8798	30.671 ± 0.057
N8000	21,250	0.8877	32.667 ± 0.138

The lighting used to enhance video images produced some heat, which raised the temperature of the oil some degrees above that of the room. During the experiments, the rods were coated with the oil, with which it was assumed to be at the same temperature because of the thinness film. The response of the Curie point rods to the lights was used to estimate the response of the oil to the heat of the lights. Since oil viscosity is sensitive to minor changes in temperature, the Walther correlation of viscosity (Gray, 1994), given by Equation 4-1, was used to estimate the actual viscosity of the oil at the temperature, T_R, when the measurements were taken. Depending on the length of exposure time, Figure 5-7 was used to obtain rise in oil temperature above room temperature. T_R is obtained by adding this rise in temperature to the real time room temperature.

$$\ln[\ln(\eta)] = f_1 + f_2 \ln(T_R) \qquad (4\text{-}1)$$

The values for the constants, f_1 and f_2 in the equation, were determined based on the viscosity data supplied with each of the oils and the values obtained are given in Table 4-2.

Table 4-2. Constants in ASTM Viscosity Model for the Standard Oils (Equation 4-1)

Oil Code	f_1	f_2	Temperature Range, °C
N600	4.1498	-0.6540	23 - 135
N1000	3.2951	-0.3909	20 - 100
N2000	4.2628	-0.6327	23 – 135
N4000	3.6804	-0.3577	20 - 100
N8000	3.6472	-0.3958	23 - 60

The viscosity estimate from Equation 4-1 was used as the actual viscosity at room temperature rather than those quoted in Table 4-1. Surface tension has a very weak sensitivity to temperature; therefore, the surface tension values in Table 4-1 were used as quoted, without correction.

4.4 EXPERIMENTAL METHOD FOR MEASURING PROPERTIES OF A LIQUID BRIDGE

Equipment was constructed for the purpose of measuring adhesive forces in dynamic liquid bridges between crossed cylinders. This equipment was also capable of recording video images of the bridge during each experiment. The use of video allowed image analysis to determine the geometric properties of the liquid bridges. In this section, both the equipment and the subsequent image analysis will be discussed in detail.

4.4.1 EQUIPMENT DESCRIPTION

The schematic of the equipment used in this study is given in Figure 4-1.

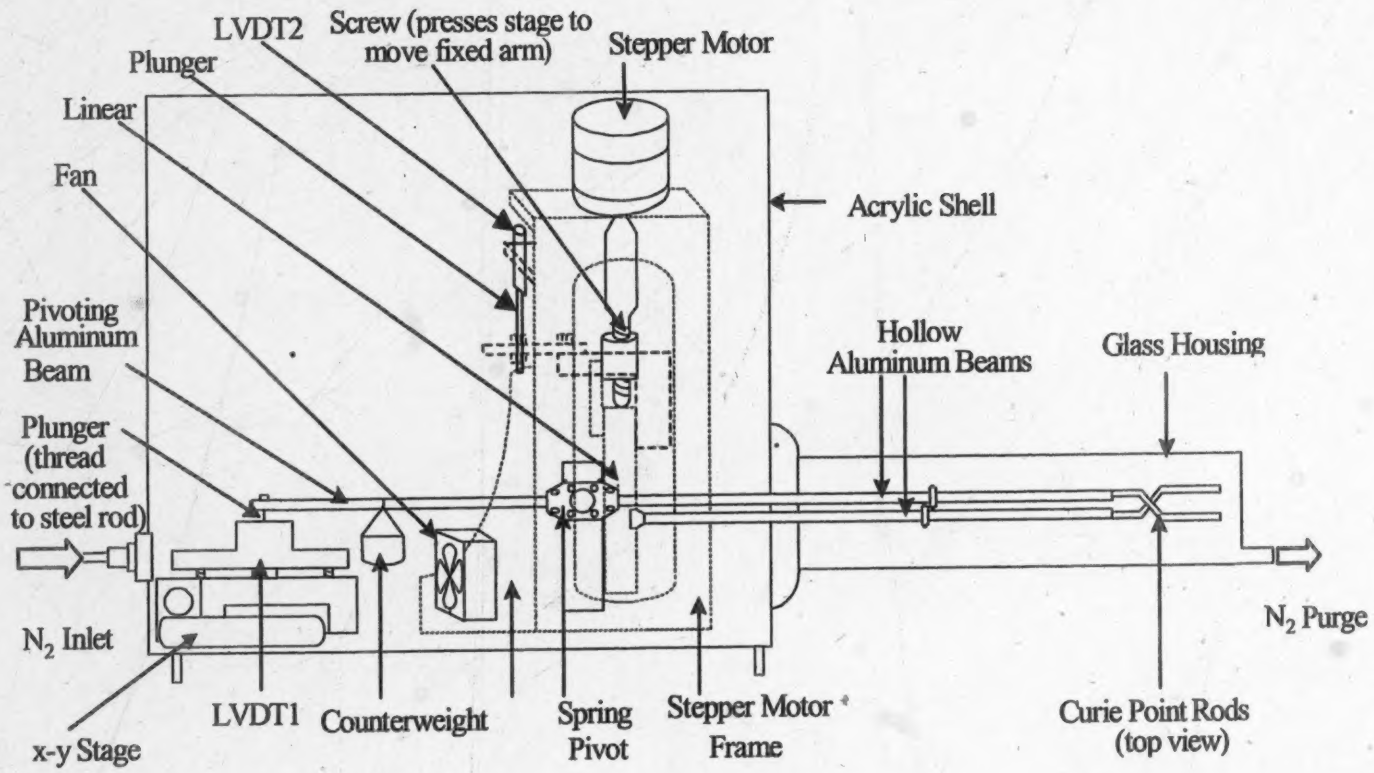
LVDT2
Screw (presses stage to move fixed arm)
Stepper Motor
Plunger
Linear
Fan
Acrylic Shell
Pivoting Aluminum Beam
Hollow Aluminum Beams
Glass Housing
Plunger (thread connected to steel rod)
N_2 Inlet
N_2 Purge
x-y Stage
LVDT1
Counterweight
Spring Pivot
Stepper Motor Frame
Curie Point Rods (top view)

Figure 4-1. Schematic of the equipment used for measuring the properties of a liquid bridge.

It is important for this experiment to have crossed Curie point rods that could easily couple with the induction furnace and get heated. Each of the Curie point rods was bent to a 45° shape such that the bent portion of the two rods crosses each other at 90°. Each of the rods was mounted in tubes of Pyrex glass (diameter 3.9 mm) to hold the rods for easy attachment to the hollow aluminum beams.

As shown in Figure 4-1, one of the aluminum beams was connected, through a flexural pivot (Model 5010-800, Goodrich, Rome, New York U.S.A.), to a linear variable differential transducer (LVDT1, Model D540050HH, Daytronic Corporation, Dayton Ohio U.S.A.). The other aluminum beam and the plunger of LVDT2 were attached to a vertical motion stage, driven by a stepper motor (Model 5704M-0202, The Motion Group Inc. Clovis CA U.S.A.). The two LVDT sensors were connected, through a signal conditioner (Model 3130, Daytronic Corporation, Dayton Ohio U.S.A.), to a personal computer. The computer recorded data from the two LVDTs and controlled the stepper motor with the aid of the LabVIEW program (version 6.0, National Instruments Austin Texas U.S.A).

The motion of the rods and the changes in the liquid bridge were recorded by video camera (Model TMC-7DSP, PULNiX America Inc. Sunnyvale CA U.S.A.), which was connected to a television monitor (Model 20AF14C, Toshiba, Ontario) via a video timer (Model VTG-33, FOR.A Corporation Limited Japan) and a time-lapse VCR (Model SVT-S480ES, Sony Corporation, Japan) that recorded the bridge dynamics on videotape. The video timer was also controlled through the PC computer. To collect high quality video images, the equipment was lit by filament lights (Models 3852582 and 4187531, Lowel-Light Manufacturing Inc. Brooklyn New York, U.S.A.).

The induction furnace (Model XP-30, Ameritherm Inc. Scottsville New York U.S.A.) provided the heating of the films of ABVR, by heating the Curie point alloys. The heating coil of the induction furnace was connected to an induction furnace controller, which in turn was controlled by a personal computer. Before being inserted into the induction coil, the alloy rods were mounted on the aluminum beams, and enclosed in a glass housing attached to the side of an acrylic box. The mounts for the aluminum beams, the LVDT sensors and the stepper motor were all enclosed in the gas-tight acrylic box, which served as an enclosure. The equipment was purged with nitrogen at a flow-rate controlled by a flow meter (model DTM-200A, American Meter Company, Burlingame, CA, U.S.A). An electric fan was mounted in the acrylic box to allow for mixing of gas and speedy purging of air from the apparatus. A Faraday shield was mounted around the induction coil to protect surrounding equipment from the field of the coil. The PC computer that controlled the operation of the induction furnace also controlled the operation of the valve on the nitrogen line with the aid of the GeniDAQ program (version 3.11, Advantech Cincinnati OH, U.S.A).

4.4.2 IMAGE ANALYSIS OF THE LIQUID BRIDGE

Recordings of the changes in the liquid bridge during pull apart of the rods were used in the image analysis of the liquid bridge. The time-lapse VCR was connected to a Marvel digitizing card (model G400-TV, Matrox, Dorval Quebec Canada). The Marvel video-digitizing software was used to convert the analog video into an AVI file. Selected frames of video of the liquid bridges could be saved in JPEG format.

The clips in JPEG format were opened with Sigma Scan Pro (Version 4.01, SPSS Science, Chicago IL U.S.A.), to measure the dimensions of the bridge after scaling with the known diameter of the rod. Consequently, all the geometrical variables in the surface force equation given in Section 3.1.1 were obtained by direct measurement.

4.5 EXPERIMENTAL PROCEDURES

4.5.1 FABRICATION OF RODS

The crossed rods of the device were constructed by bending Curie point wires into the desired shape (Figure 4-2).

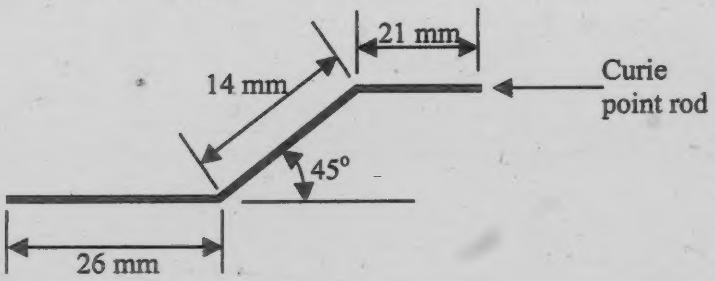

Figure 4-2. Desired shape of fabricated rod (not drawn to scale)

A jig was constructed for this purpose so that a large number of these pieces could be bent reproducibly. Each of the bent rods was then firmly mounted in glass rods of diameter 3.9 mm and length 100 mm. The glass portion of the rod was marked with an engraver for identification.

4.5.2 COATING OF RODS

Each Curie point rod, with the attached glass rod, was weighed on a balance. The unbent portions of the alloy were covered with tape exposing only the bent portion, for the purpose of coating with ABVR. A 2 % solution by weight of the liquid (standard oil during calibration or ABVR for high temperature) was prepared with methylene chloride. This 2 % solution was sprayed on the mid section of the Curie point rods. After spraying, the glass rod was cleaned with paper towel drained in methylene chloride to ensure that only the desired portion was coated. The coated rod was then left for two days to evaporate the solvent. At this point, the rod assembly was weighed to determine the mass of liquid film on the rod. The taping, weighing and spraying processes were repeated until the desired film thickness of 24 µm - 28 µm was attained (Gray et al., 2001, Gray et al., 2002). Film thickness on the rod was calculated based on Equation 4-2 given below:

$$\delta = \frac{m_{\text{sprayed}} - m_{\text{dry}}}{\rho_{\text{liquid}}\,(2\pi R L)} \times 10^4 \qquad (4\text{-}2)$$

where $\mathbf{m}_{\mathbf{sprayed}}$ is the mass in grams of the alloy-glass assembly after spraying, drying and the tapes removed, $\mathbf{m}_{\mathbf{dry}}$ is the mass in grams of the assembly before spraying and taping, $\rho_{\mathbf{liquid}}$ is the density in g/cm^3 of the liquid of interest and **L** is the length in cm of the sprayed portion of the alloy. δ and **R** are respectively the film thickness in μm and radius in cm of the Curie point rod.

4.5.3 VISCOSITY AND SURFACE TENSION MEASUREMENT

With two coated rods of the same Curie point temperature, the equipment was configured as shown in Figure 4-1. The controlled rod was moved with the stepper motor assembly until it just touched the free rod, while making sure the free rod stayed within the sensing range of both LVDT sensors. Depending on reaction time desired, the controlled rod was moved down by a predetermined number of steps such that the ABVR was heated for the desired time while moving towards the free rod. The length of time the rods were pressed together was also set by a known number of steps, referred to as nudge amount.

For reaction experiments with ABVR, the apparatus was flushed with nitrogen for 20 minutes at about 9 – 12 dm^3/min and 101.15 x 10^3 Pa to rid the system of oxygen. The flow of nitrogen was maintained, during cracking reactions at high temperature, at a lower rate of about 1 dm^3/min. At 3 minutes before the end of purging, LabVIEW was started for data acquisition and equipment control and the furnace power was switched on.

At the completion of purging, the Curie-point rods were moved until they touched, while the induction furnace heated the ABVR through the rods. After they touched, they were pressed together by the nudge amount and afterwards pulled apart by the motion of the controlled rod, which was moved down at a speed of 0.409 mm/s. This speed was used in all the experiments because it allowed for significant shear of the liquid bridge and the observation of bridge formation, elongation and rupture. The stepper motor controlled the motion of the controlled rod while the LVDT sensed the voltage and time, which was recorded in the personal computer. The motion of the free rod, sensed by the second LVDT, was also recorded by the personal computer. When there was a liquid between the rods, the free rod moved together with the controlled rod until a point when the liquid bridge formed between the rods was broken. Since the free rod worked on the principle of a microbalance, the adhesive force due to the liquid bridge would be sensed in terms of voltage by the LVDT on the other side of the pivot. The experiment was completed the moment the liquid bridge was broken at which point the furnace power was switched off. A detailed experimental procedure is provided in Appendix C.

In addition to the data recorded on the personal computer, video recordings of the liquid bridge as it was formed, elongated and ruptured were kept on videotape for further processing and image analysis to determine the geometric properties of the bridge. Data acquired from the experiment were then used to obtain values of adhesive force, viscosity and surface tension. The steps involved in obtaining these properties from the data collected by the equipment are explained in Section 5.2 and Section 5.3.

5. CALIBRATION AND VALIDATION OF EQUIPMENT

The description of the calibration of the equipment is presented in this chapter. Also presented here are the results obtained during the validation of the equipment.

5.1 CALIBRATION OF POSITION SENSORS

Data from the two sensors, each indicating the position of one rod, were collected and saved during the experiment. The raw data were the voltage-time response for each of the two rods. A plot of a typical data from the equipment at room temperature is shown in Figure 5-1.

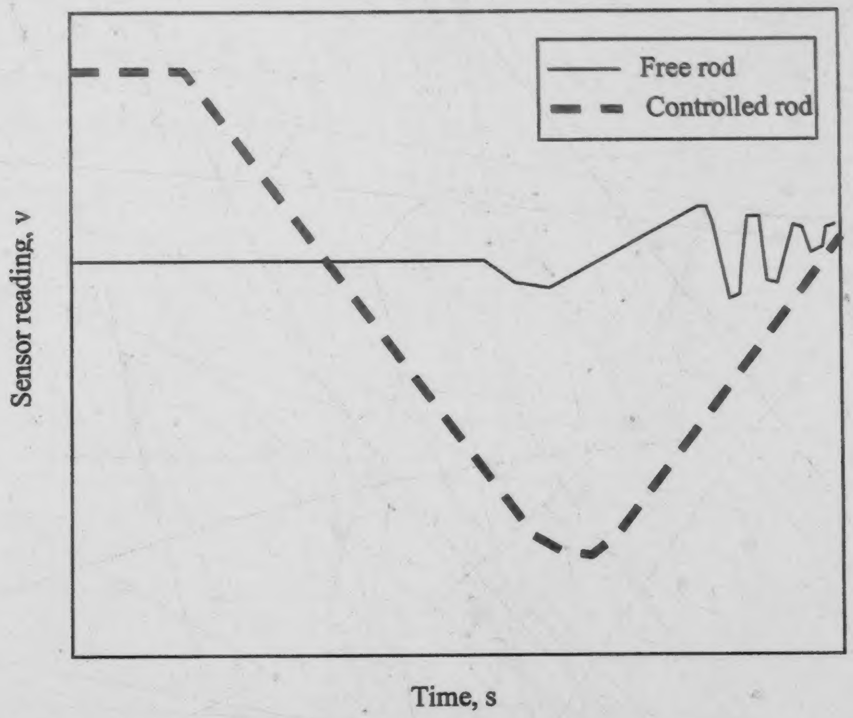

Figure 5-1. Typical sensors data from displacement of rods

A calibration was done to transform the voltage data from the equipment to a more representative absolute position data and to obtain a measure of the force in the liquid bridge.

5.1.1 ABSOLUTE POSITION PROFILE

To obtain the absolute position profile of the rods, the equipment was first calibrated to relate the absolute position to the voltage data from each of the sensors. The calibration plot is presented below in Figure 5-2. The calibration was done with both the free and controlled Curie-point rod tied firmly together, while stepped up and down by the stepper motor. A cathetometer (Precision Tool and Instrument, England) was used to measure the vertical displacement of each of the rods from a common datum, while recording the voltage from each of the sensors.

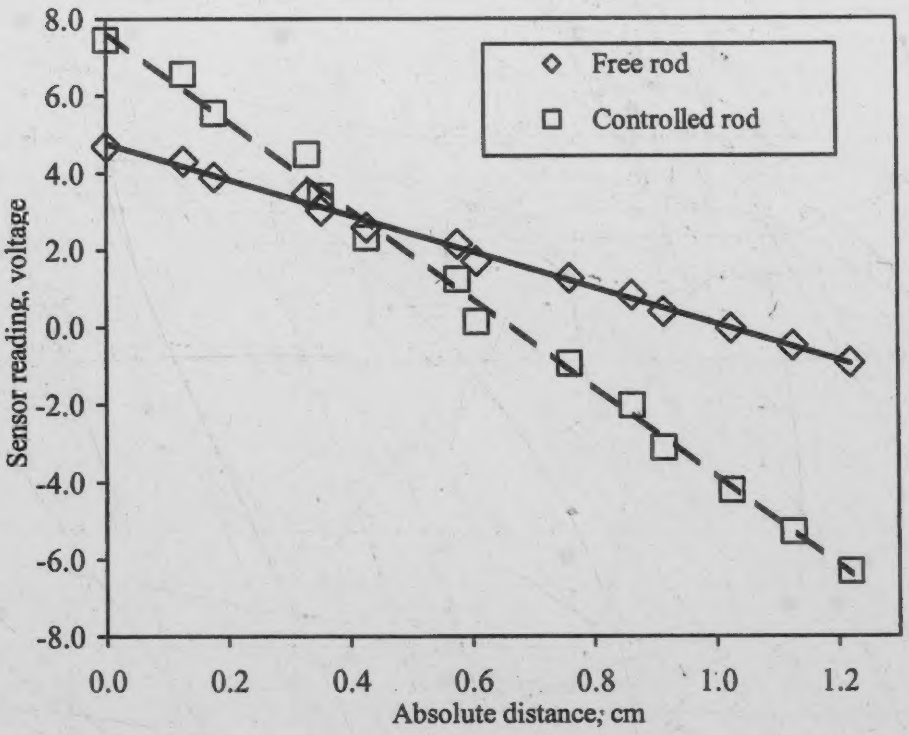

Figure 5-2. Equipment calibration plot: voltage reading of sensors versus absolute distance (flexural pivot, Model 5010-800)

From the calibration results in Figure 5-2, Equation 5-1 and Equation 5-2 were developed for converting the voltage data to absolute position of the rods.

$$h_u = \frac{4.7598 - V_u}{4.6813} \tag{5-1}$$

$$h_L = \frac{7.6673 - V_L}{11.53} \tag{5-2}$$

$\mathbf{h_u}$ and $\mathbf{h_L}$ are the absolute position of the free rod and the controlled rod respectively. $\mathbf{V_u}$ and $\mathbf{V_L}$ are the respective voltage readings from the sensors for the free rod and the controlled rod. When these calibration equations were applied to the data in Figure 5-1, the plot shown below as Figure 5-3 is obtained.

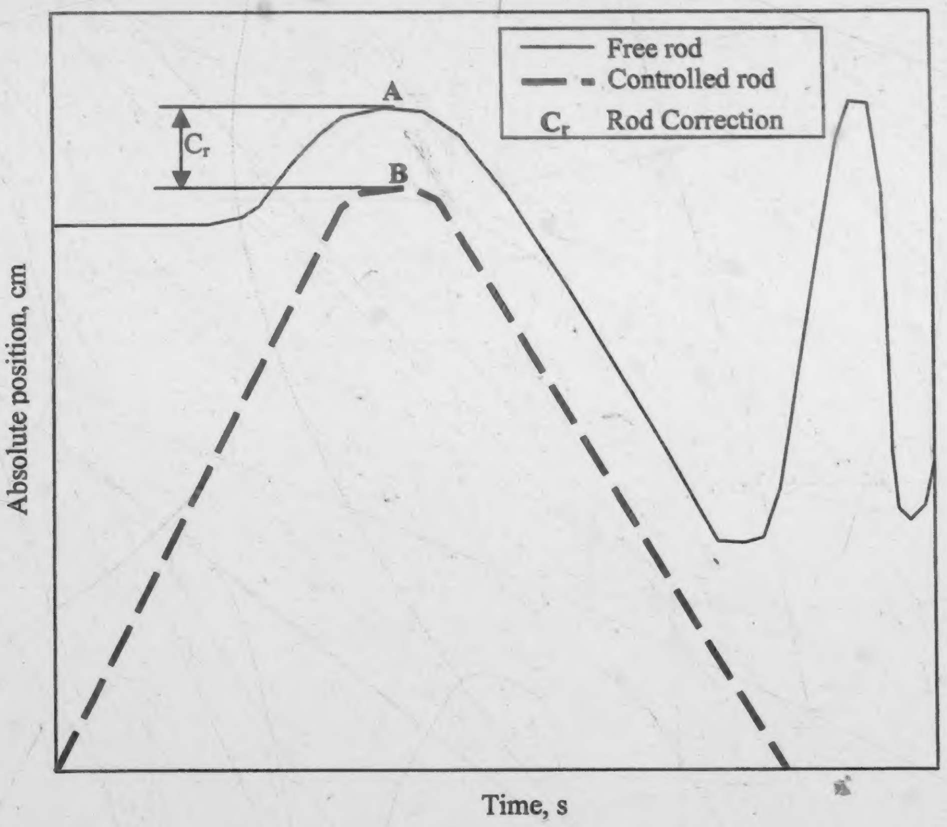

Figure 5-3. Displacement-time profile of rods before rod correction

Points A and B on Figure 5-3 should overlap because they represent the time period when the two rods were pressed together. The discrepancy was caused by the fact that each of the rods used in the experiments is unique in its dimensions. A rod correction factor, C_r, which is simply the difference in the absolute distance of A and B, was added to the data points of the controlled rod, giving the data of Figure 5-4.

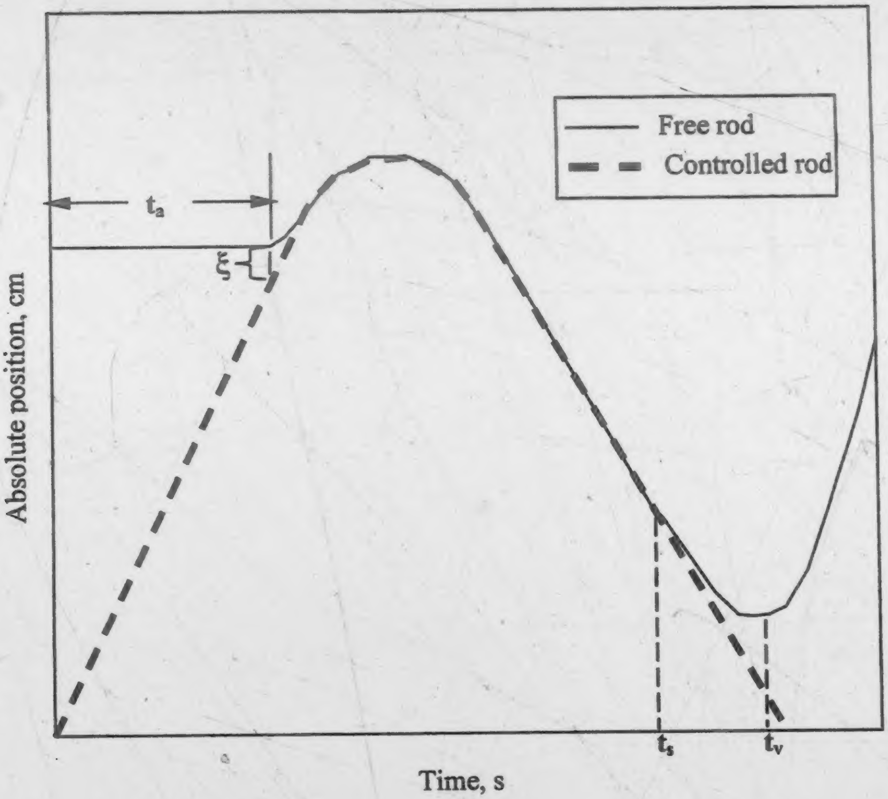

Figure 5-4. Displacement-time profile of rods after addition of rod correction factor (t_a is the heating time to touch rods , t_s is the heating time at point of commencement of bridge elongation, t_v is the heating time at the point of maximum elongation, and ξ is the approximate total film thickness of the two rods)

Clearly, Figure 5-4 gave a better representation of the phenomenon. It showed the approach of the rods, their being pressed together, their being pulled apart and rupture of the liquid bridge. It also showed the point of commencement of bridge elongation, described by Tabor (1977) as the point of instantaneous separation. The point of first contact of the rods gave ξ, an approximate measure of the total film thickness of the two rods before the rods made metal-to-metal contact. This two-stage calibration, of sensor voltage conversion and addition of rod correction factor, allowed for accurate calculation of the relative position of any of the pairs of Curie-point rods.

5.1.2 DETERMINATION OF ADHESIVE FORCES

The equipment was calibrated with a view to extracting force data from the normal voltage data collected from it. Several known weights were applied to one end of the rod on a flexural pivot. The reactions to the weights were obtained at the other end of the rod connected to the plunger of the LVDT sensor. The sensor recorded these reactions as changes in voltage. The calibration plot in Figure 5-5 shows the force applied against the change in voltage of the sensor.

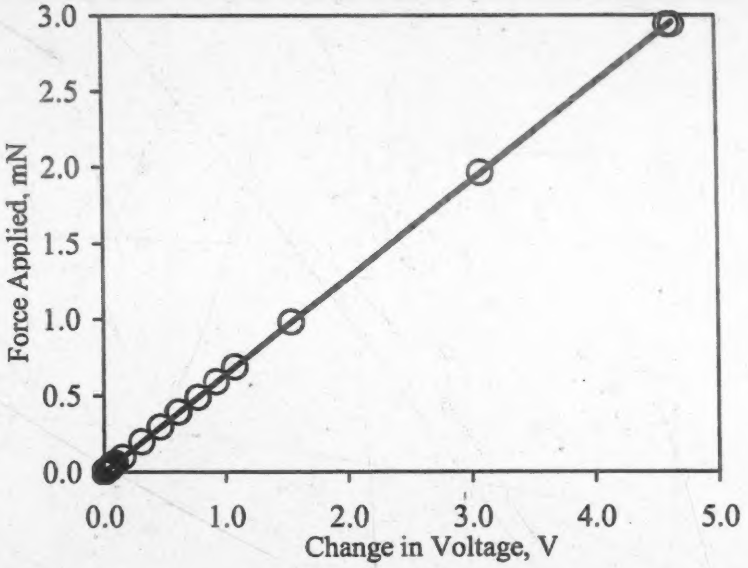

Figure 5-5. Voltage-force calibration plot (using flexural pivot, Model 5010-800)

In order to determine the fluid properties, the apparatus was used to measure two forces; the adhesive force at the commencement of bridge elongation, and the force at the maximum elongation of the liquid bridge. As illustrated in Figure 5-4, the points of commencement of bridge elongation and maximum elongation of the bridge were clearly indicated by the relative positions of the rods. Heating time, $\mathbf{t_s}$, for the commencement of bridge elongation was determined by both visual analysis of the video frames and by statistical analysis of the sensor displacement data. The method of statistical analysis, which was less subjective, is described in Appendix A2 and Section 5.1.3. Heating time, $\mathbf{t_v}$, for maximum elongation of the bridge was easily obtained from Figure 5-4 from the minimum in the position of the free rod. These times could then be used with the voltage readings and Figure 5-5 to determine the forces as shown in Figure 5-6. The time t_a represents the heating time during which the material was heated before the rods touched. In typical experiments, the time interval from t_s to t_v was significantly smaller than t_a.

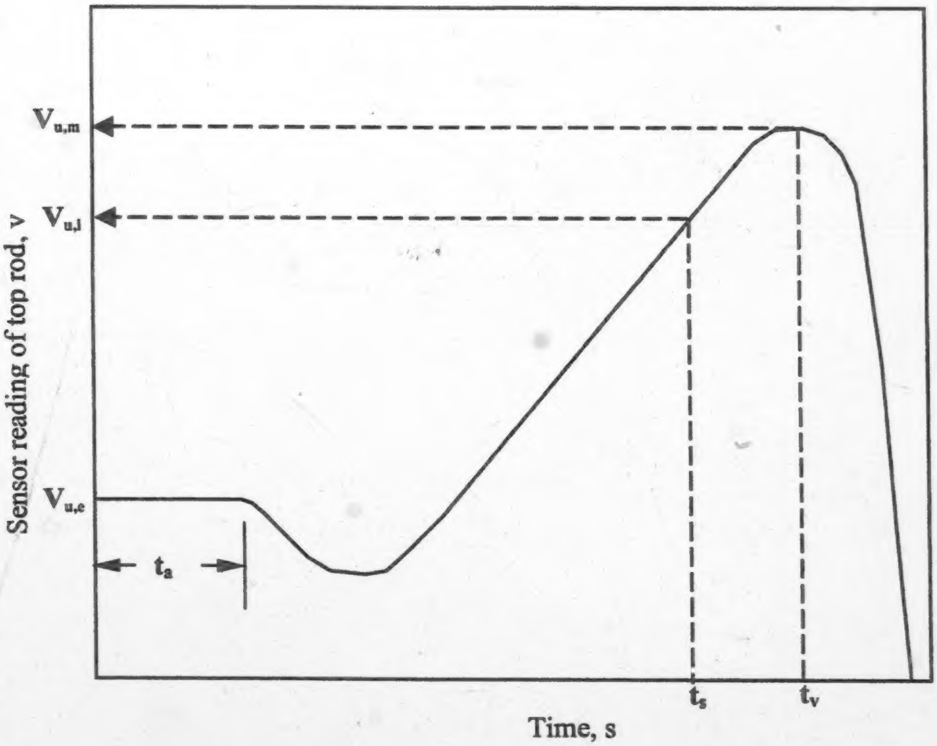

Figure 5-6. Method for evaluating capillary and viscous forces ($V_{u,m}$ is the voltage reading of free rod at the maximum elongation of bridge, $V_{u,e}$ is the voltage reading of the free rod at the equilibrium position, $V_{u,l}$ is the voltage of the free rod at the commencement of elongation)

With $V_{u,m}$ and $V_{u,e}$ determined, Equation 5-3 and Equation 5-4 can respectively be used to determine the force at maximum elongation of the liquid bridge and the force at commencement of bridge elongation.

$$F_{u,m} = 0.636 * (V_{u,m} - V_{u,e}) \tag{5-3}$$

$$F_{u,i} = 0.636 * (V_{u,i} - V_{u,e}) \tag{5-4}$$

Where $\mathbf{F_{u,m}}$ is the adhesive force in mN, at maximum elongation and $\mathbf{F_{u,i}}$ is the adhesive force in mN, at commencement of elongation. As illustrated in Figure 5-4, the accuracy with which $\mathbf{F_{u,i}}$ is determined will depend largely on the precision with which the point of commencement of bridge elongation ($\mathbf{t_s}$) is determined.

5.1.3 DETERMINATION OF POINT OF COMMENCEMENT OF BRIDGE ELONGATION

The point of commencement of bridge elongation was determined by both the video recordings and by statistical analysis of the displacement data. The video method used the frame-by-frame examination of the videotapes of bridges to determine the heating time when bridge elongation began. The point at which the first liquid bridge was observed was noted. The time obtained by moving two frames backward from this point was used as the approximate value of $\mathbf{t_s}$, having ascertained that the time between any two frames is 0.017 second.

The statistical method considered the difference in the absolute distance between the two rods (Figure 5-4) at each data point during pull-apart and compares this distance with absolute error (defined in Appendix A2) obtained from the T-test at 95% confidence level at those points when the rods are certainly together. When the separation distance between the two rods was greater than the absolute error, then the time of commencement of bridge elongation was defined.

5.2 ROOM TEMPERATURE CALIBRATION WITH STANDARD OILS

The relationship between the forces in liquid bridges was determined by calibration experiments with oils of known properties, at room temperature. Lighting was used to improve video quality, and this lighting was found to heat the rod and oil to a temperature higher than the room temperature. As explained in Section 4.3, the actual temperature of the rod and oil (**T_R**) was obtained by using the temperature response measured by type k thermocouple spot welded to the rod as shown in Figure 5-7 to estimate the rise in temperature of oil and rod above that of the room. The rise in temperature was added to the room temperature to obtain **T_R**. Equation 4-1 was then used to estimate the viscosity of the oil at **T_R** for any time of exposure to the lights.

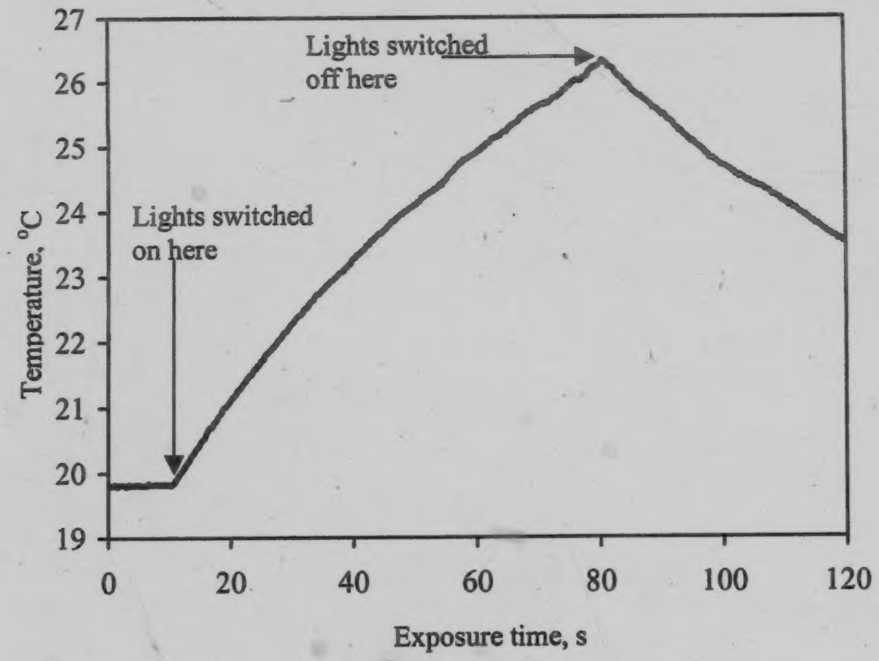

Figure 5-7. Temperature response of the rods to the lights at room temperature

The temperature sensitivity of surface tension is low; therefore, this property was not corrected. With the actual viscosities and surface tensions of the standard oils known, they could then be used to determine the adjustable constants in Equation 3-9.

5.2.1 CHECK ON DERIVATION OF GOVERNING EQUATION

The dimensionless analysis in Section 3.2.1 assumed that the Reynolds number for liquid bridges is low. Table 5-1 shows the values obtained for Reynolds number of oil flow into a bridge of N1000 standard oil as it elongated and ruptured. The length scale in the Reynolds number was assumed to be the diameter at the base of the bridge because the circular section at the base of the bridge represents the section through which oil flowed into the bridge. Using the known rod diameter for scaling, image analysis was used to obtain the necessary dimensions of the liquid bridge. Assuming an axially symmetric liquid bridge allowed for the use of the measured dimensions to estimate the volume of the liquid bridge by the method of cross sections (Edwards and Penney, 1982).

Table 5-1. Volume and Reynolds Number of Flow Into/Out of the Liquid Bridge with N1000 Standard Oil

Frames	Volume of liquid bridge, mm^3	Reynolds Number
1	0.021	0.540
2	0.018	0.137
3	0.027	0.850
4	0.028	0.132
5	0.028	0.025
6	0.029	0.258

These data confirmed that the volume of the liquid in the bridge was not constant. The Reynolds number was less than 1, which showed that the oil exhibited creeping flow in the course of formation, elongation and rupture of the liquid bridge. Therefore, Reynolds number was not significant for this type of flow.

5.2.2 DETERMINATION OF CONSTANTS IN GOVERNING EQUATIONS

As discussed in Section 3.2.1, the dimensional analysis indicated that capillary number and the two dimensionless distance ratios, **δ/R** amd **D/R**, should be sufficient to define the viscous forces in liquid bridges.

The resulting expression, Equation 3-9, was semi empirical with three adjustable constants. Calibration experiments were then conducted, at room temperature, using the five standard oils to determine the values of $\mathbf{k_1}$, $\mathbf{k_2}$ and $\mathbf{k_3}$. For these experiments, rod radius, **R** was 0.9779 mm with coating film thickness, δ, ranging from 7 μm to 13 μm. $\mathbf{F_{T,D}}$ was measured throughout the elongation of the bridge while **b, D, dD/dt** and $\mathbf{r_1}$ were obtained from image analysis for various video frames of bridge elongation as the controlled rod was pulled apart from the free rod at a speed of 0.4086 mm/s. The speed of pull apart should not be confused with **dD/dt,** which qualitatively represents the rate of increase of bridge elongation with time. The speed used for the experiment was not a concern because it was already established in Section 2.1.1 that Athabasca bitumen has a Newtonian behavior above 100 °C. ABVR, like its precursor, was considered Newtonian above 350 °C. Therefore, increased or reduced shear rate (pull apart speed) would not change the liquid properties measured above 350 °C. $\mathbf{k_1}$, $\mathbf{k_2}$ and $\mathbf{k_3}$ remained the unknowns in Equation 3-9. The best-fit values were obtained by minimizing the sum of squared residuals between the measured $\mathbf{F_{T,D}}$ and that calculated from Equation 3-8 and Equation 3-9 for five calibration oils at various times between bridge formation and rupture (Appendix A3). The best-fit values obtained are given as $\mathbf{k_1} = 400.0$; $\mathbf{k_2} = 0.752$; $\mathbf{k_3} = 0.677$ with sum of square residual of 1.281.

Further analysis of the experimental data showed that adhesive force increased during pull apart until reaching the point of commencement of elongation, where the adhesive force is equal to the capillary force. It continued to increase as the bridge was visibly elongating, when $\mathbf{D} \geq \mathbf{b}$, and the capillary component of the force was negligible. In other words, once the bridge became visible, as in Figure 5-8, then the viscous component was almost equal to the measured $\mathbf{F_{T,D}}$.

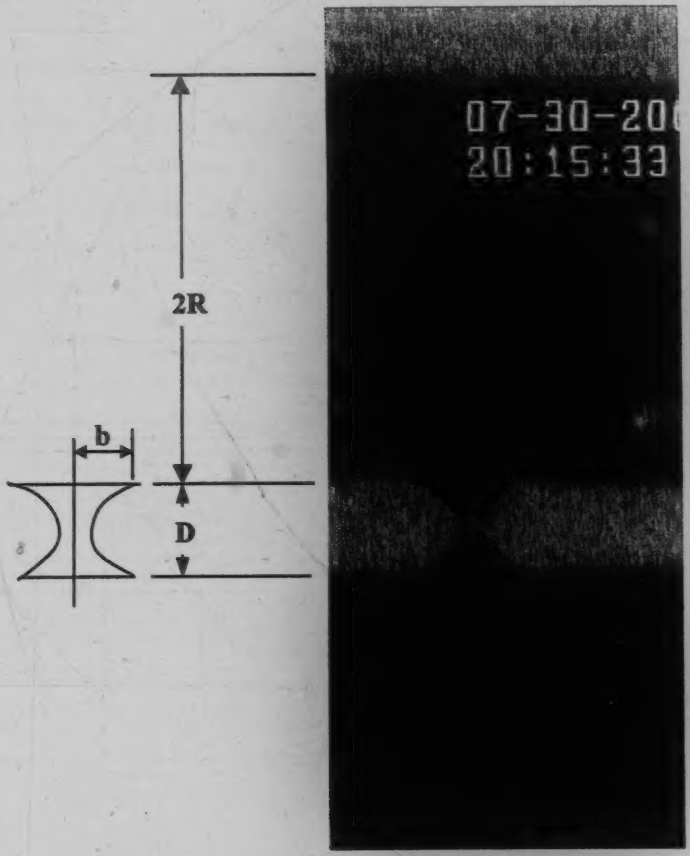

Figure 5-8. Elongated liquid bridge of N1000 oil at room temperature (**R** = 0.9779 mm, **D** = 0.483 mm, **b** = 0.17 mm)

This observation allowed for further simplification of Equation 3-8 and Equation 3-9 into Equation 5-5 and Equation 5-6, which could be used respectively at the points of commencement of bridge elongation and maximum elongation of bridge.

$$F_{T,D} = F_{u,i,D} = 4\pi\left(\frac{D}{R}\right); \quad D << b,\ D \neq 0 \qquad (5\text{-}5)$$

$$F_{T,D} = F_{u,m,D} = 400\ Ca \left(\frac{\delta}{R}\right)^{0.752} \left(\frac{D}{R}\right)^{0.677} ; \quad D \geq b \quad (5\text{-}6)$$

$F_{u,m,D}$ and **$F_{u,i,D}$** are the dimensionless adhesive forces at maximum elongation and point of commencement of bridge elongation respectively. From Equation 5-5 and Equation 5-6, dimensional equations can easily be written for **$F_{u,m}$** and **$F_{u,i}$**. The dimensional expressions are given in Equation 5-7 and Equation 5-8 in a format similar to that used in literature (Pitois et al. 2000; Pitois et al., 2001; Tabor, 1977; Frink et al., 1997) to allow for easy comparison.

$$F_T = F_{u,i} = 4\,\pi\,R\,\gamma\,; \quad D << b\,,\ D \neq 0 \qquad (5\text{-}7)$$

$$F_T = F_{u,m} = \pi\,\eta\,\frac{3R^2}{D} * \frac{dD}{dt}\left[42.44 \left(\frac{\delta}{R}\right)^{0.752} \left(\frac{D}{R}\right)^{0.677}\right]; \ D \geq b \quad (5\text{-}8)$$

Both **D** and **dD/dt** in Equation 5-8 were not controlled parameters in the liquid bridge experiments, but dependent on the properties of the liquid bridge and the uncontrolled movement of the free rod. **dD/dt** qualitatively represents the rate of change of bridge elongation with time and should not be confused with the speed with which the controlled rod was pulled apart from the free rod.

Equation 5-7 for **$F_{u,i}$** agreed well with the observations of Tabor (1977) and Frink et al. (1997) when **D** << **b** (Section 2.4.2). It could be seen that this approach produced Equation 5-8 that gave the expression in the square bracket as a correction to the expression suggested by Pitois et. al (2000 and 2001). Additionally, by decoupling **Ca** from the equations in dimensional format, it is possible to use Equation 5-7 to determine surface tension and Equation 5-8 to determine viscosity independently.

5.2.3 PREDICTED AND ACTUAL PROPERTIES OF CALIBRATION OILS

Equation 5-7 was used to measure surface tension when $\mathbf{D \ll b}$, using $\mathbf{F_{u,l}}$ from experimental data (Figure 5-6). The radius of the rod, R = 0.9779 mm. Viscosity can be determined using Equation 5-8 when $\mathbf{D \geq b}$; $\mathbf{F_{u,m}}$, **D**, **dD/dt** and δ were known. The values of **D** and **dD/dt** were determined from the absolute position data (Figure 5-4). This force analysis approach was then used to determine the surface tension and viscosity of the all the standard oils used for the calibration for comparison with their actual values. The comparison of viscosity measured by the liquid bridge method and actual viscosity is shown in Figure 5-9.

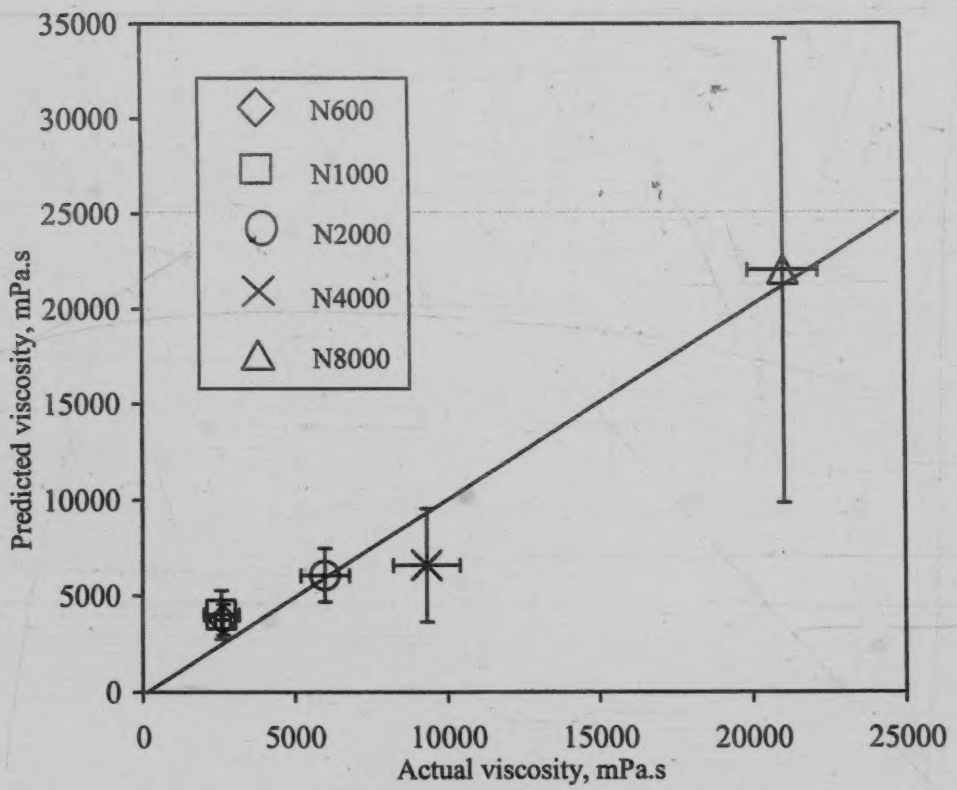

Figure 5-9. Predicted versus actual viscosity of standard oil with actual viscosity corrected for ambient temperature and heat from the lighting

From Figure 5-9, viscosity measurement of up to 10,000 mPa.s was found to agree with the actual viscosity. The long bridge formed in the experiments with the calibration oils caused slight difference between the temperature of the liquid bridge and that of the rods. Since the actual viscosity of oil is calculated based on the temperature response of the rods, actual viscosity values reported did not account for this slight difference in temperature. Therefore, the error in the actual viscosity is underestimated. However, the predicted viscosity captured the errors due to the difference between the temperature of the long liquid bridge and that of the rods. The N600, N1000, N2000 and N4000 oils are not as responsive as the N8000 oil to minor changes in temperature. Therefore, the N8000 oil showed the highest error in its predicted viscosity because of its high responsiveness to the minor difference in temperature.

The method was also used to measure surface tension of these oils for comparison with that measured by the pendant drop method. The results are shown in Table 5-2. The trend of surface tension with film thickness is shown in Figure 5-10, which showed that the surface tension measured with the liquid bridge method showed no trend with film thickness.

Table 5-2. Measured versus Actual Surface Tension of Standard Oil

Oil Code	Actual Surface Tension, mN/m	Measured Surface Tension, mN/m	
		Force Analysis Method	Video Method
N600	32.60 ± 0.07	32.30 ± 1.17	31.60 ± 1.80
N1000	31.40 ± 0.02	30.70 ± 1.22	31.20 ± 2.12
N2000	31.70 ± 0.63	30.10 ± 1.89	33.60 ± 1.50
N4000	30.70 ± 0.06	27.70 ± 2.83	32.50 ± 1.73
N8000	32.70 ± 0.14	31.10 ± 1.80	33.50 ± 2.66

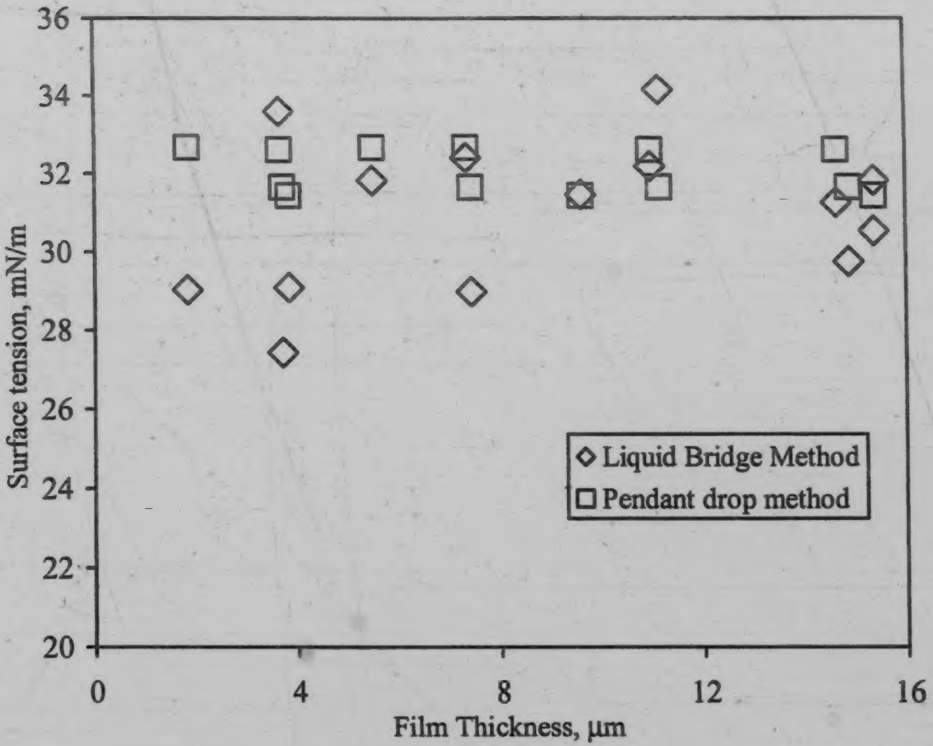

Figure 5-10. Dependence of measured surface tension on film thickness

Apparently, Figure 5-9 and Table 5-2 validated the liquid bridge technique for measuring fluid viscosity and surface tension. Figure 5-9 showed that viscosity could be measured with an error of < 40 % in spite of the additional error introduced by the sensitivity of oil viscosity to heat of the lighting. Table 5-2 indicated that surface tension could be estimated, by the liquid bridge method, with an error of < 10 % and a maximum error of 2.83 mN/m. Figure 5-10 showed that the surface tension measured with the liquid bridge method showed no trend with film thickness. These findings allowed for the use of the liquid bridge method for measuring surface tension and viscosity of reacting ABVR at temperatures found in fluid cokers.

5.3 HIGH TEMPERATURE EQUIPMENT CALIBRATION

The experimental apparatus was designed to take measurements at temperatures of up to 550 °C. Therefore, it was necessary to have crossed Curie-point rods that could easily couple with the induction furnace and rapidly rise to the desired temperature. To achieve this, each of the rods is bent such that each is at 45° to the field of the induction coil (Figure 4-2). Experiments showed that a rod parallel to the field of the induction coil was heated while a rod perpendicular to it was not. The rod is parallel to the field of the induction coil when the direction of the rod is parallel to the coil and it is perpendicular to the field when its direction is perpendicular to the coil. An angle of 45° was chosen to ensure that the induction furnace heated both rods. Figure 5-11 shows the response time of the alloy rods to heating by the induction furnace. The measurements were taken with the aid of thermocouples spot welded to the bent portion of the rods and connected to a HP Bench-link data logger. For example, rods of radius 0.735 mm and Curie-point temperature of 466 °C were found to have a response time of 6 seconds.

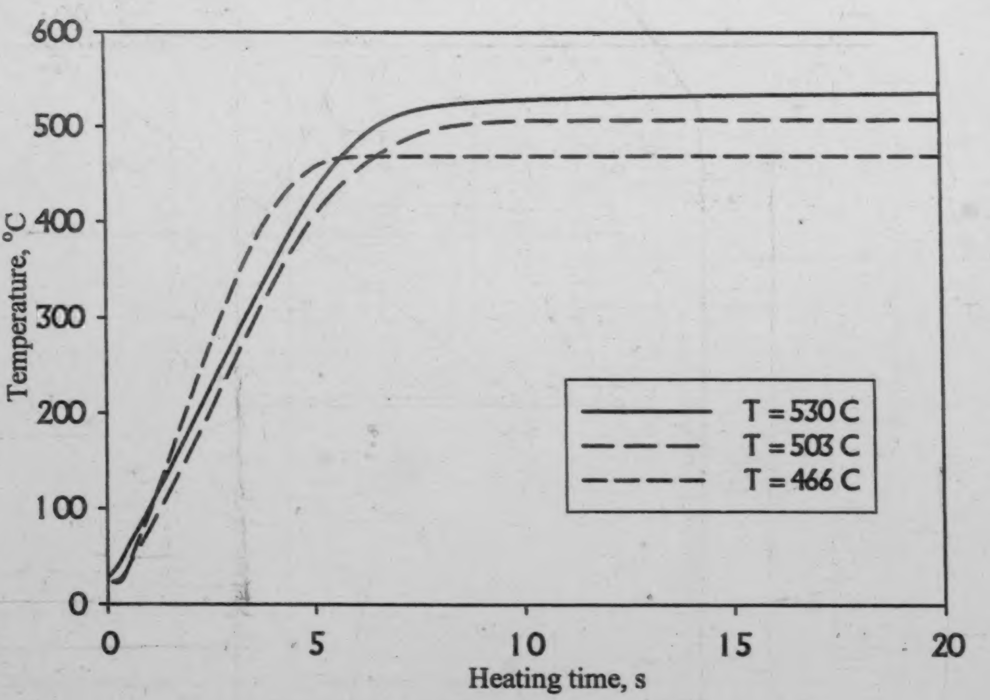

Figure 5-11. Temperature profile of Curie-point alloys

Figure 5-11 showed that 97 % of the Curie-point temperature was attained in 5.32 seconds at 466 °C, while it was attained in 7.06 seconds at 504 °C and 530 °C. The temperature of the rod remained steady at the Curie point temperature as expected. Since significant reaction of the ABVR started at 400 °C, heating times required to reach 400 °C were also noted. The time to reach 400 °C is important because it enables the estimation of the reaction time needed for kinetic analysis at 466 °C, 503 °C and 530 °C. Therefore, reaction time was defined as the heating time less the time to reach 400 °C. This correction was done at 466 °C, 503 °C and

530 °C but not at 400 °C because the time at dry out of 240 seconds at 400 °C will make the effect of the correction insignificant. The rod with a Curie-point temperature of 466 °C attained 400 °C in 3.83 seconds while the rod with a Curie-point temperature of 503 °C reached 400 °C in 4.92 seconds. The rod with a Curie-point temperature of 530 °C attained 400 °C in 4.58 seconds. These response times are slower than that obtained with strips of Curie-point alloy (Sourdararajan, 2001). The slower response time was due to the 45° angle between the center portion of the rods and the field of the induction coil.

Having established that the Curie point rods could attain the temperatures desired, experiments could then be conducted to measure the adhesive forces at high temperature. The equipment was setup as shown in Figure 4-1 in Section 4.4.1 and experiments conducted as described in Section 4.5.3 with the furnace switched on during experiments. Typical data from the experiment, after being processed as described in Section 5.1.1 produced the results shown below in Figure 5-12.

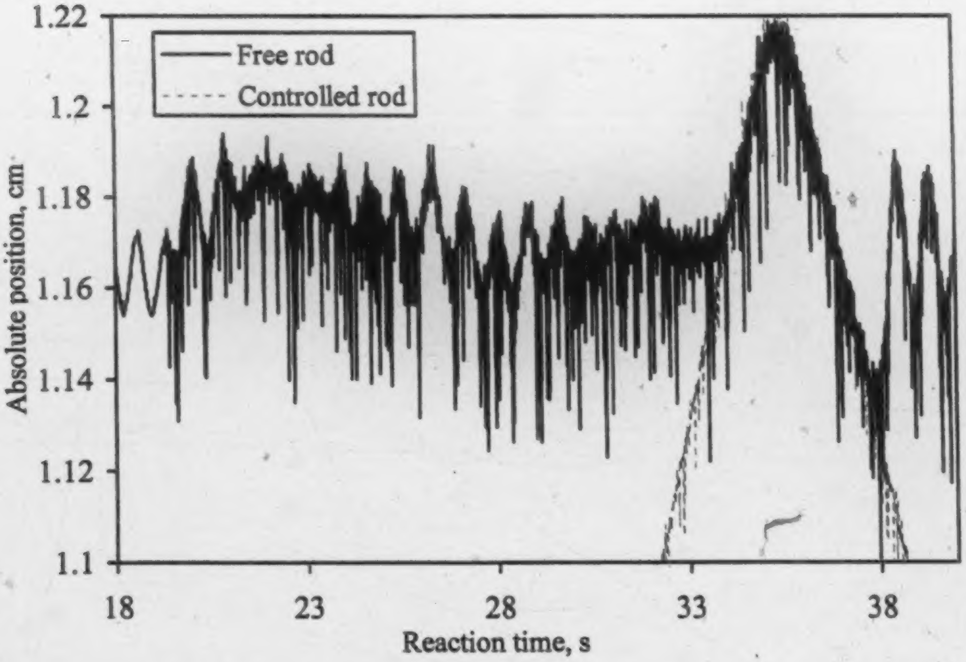

Figure 5-12. Typical data for rod positions at 503 °C

With Figure 5-12, it is impossible to decipher the point of commencement of bridge elongation, which is critical to the determination of surface tension of the liquid forming the liquid bridge. Figure 5-12 showed both low frequency and high frequency peaks on the free rod. The low frequency peaks were real, due to the oscillation of the free rod as a result of the magnetic effect of the induction field on the Curie-point material. The low frequency noise disappeared the moment the rods touched. The high frequency noise came from the effect of the field of the induction furnace on the sensors of the equipment, and this noise continued to persist even after the rods touched. Consequently, successful application of this technique at high temperature requires filtering of the data to remove most of the high frequency noise introduced by the induction furnace.

5.3.1 DATA FILTERING

A frequency filter was developed to remove the noise from the sensor data. A special filtration toolbox (Wavelab 8.02, developed in the Stanford University Department of Statistics) was utilized as the main engine behind the filtration. The toolbox employ low pass filters that decompose data into portions of high and low frequencies with the low frequency portion passed through the filter as many times as necessary to achieve the desired level of noise removal without altering the important features of the data. A general code (wavetimefreq, authored by Dr. A. Tangirala) was used in conjunction with a data-specific code named "FILTER_CODE" to achieve the filtering of the data in Matlab 6.5. The files for Matlab 6.5 are listed in Appendix B1.

The data from the high temperature experiment was extracted in Microsoft Excel and then saved in a Matlab working file. The data for both absolute position and voltage were filtered and the resulting noise-free data saved into a separate file. Figure 5-13 shows the result after filtration of the data shown in Figure 5-12.

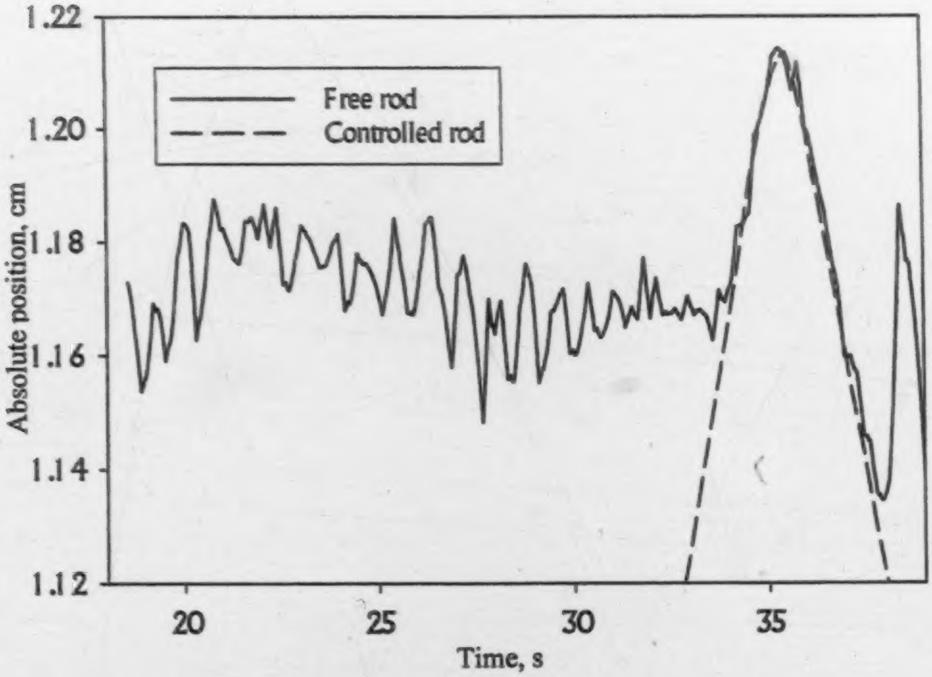

Figure 5-13. Data for rod positions after filtering

Clearly, Figure 5-13 can now be used for the analyses described in Section 5.1.2, Section 5.1.3 and Section 5.2. Figure 5-13 also showed that the magnetic effect of the induction furnace altered the equilibrium point mentioned in Figure 5-6. Since the accurate estimation of forces depends on the equilibrium point (Equation 5-3 and Equation 5-4), it is important to quantify the effect of the magnetic field on the forces.

5.3.2 MAGNETIC EFFECTS OF THE INDUCTION FIELD

To estimate the effect of the field on measured forces at high temperature, experiments were conducted with dry rods at both room temperature and high temperature for each of the temperatures studied (312 °C – 530 °C). Sensor data of the free rod in both the cold and the hot experiments were compared as shown in Figure 5-14.

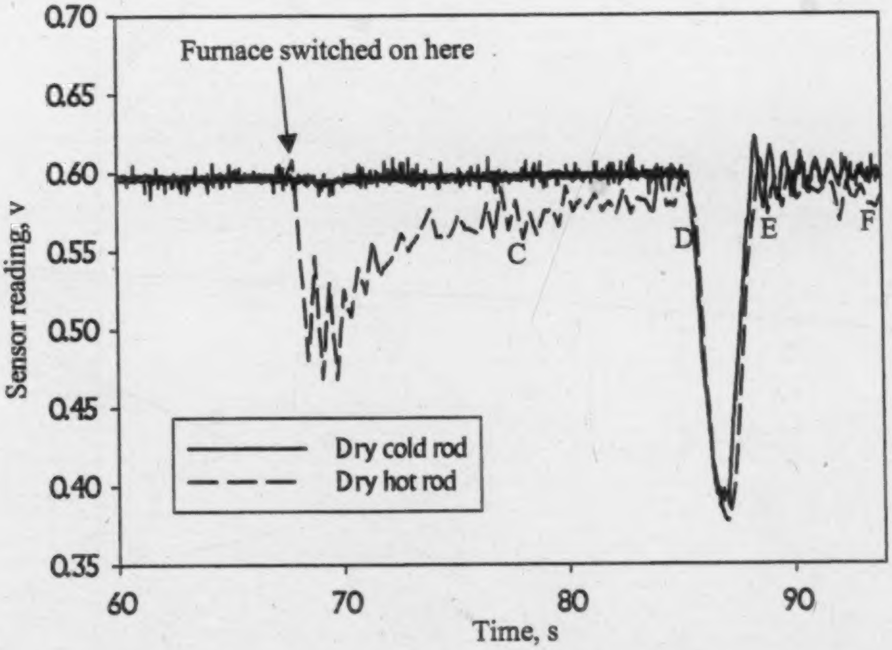

Figure 5-14. Dry rod data showing effect of magnetic field on rods at 466 °C

Figure 5-14 showed a lowering of the equilibrium point as soon as the furnace comes on. The equilibrium point remained reduced due to the magnetic effects. Since the equilibrium position before turning on the furnace was used for the initial estimate of the forces as described in Equation 5-3 and Equation 5-4, the forces were under estimated. To correct for the magnetic effects, the time-averaged voltage was calculated for period CD and for period EF of the hot data. The average of these two gave a more representative equilibrium position at high temperature. The force equivalent to the difference between the old equilibrium position and the calculated equilibrium position was added to the force estimates as a correction due to magnetic effects. Table 5-3 gives the result obtained from the correction due to magnetic field for all the temperatures of interest.

Table 5-3. Correction for Magnetic Effect of the Induction Field

Curie-point Temperature, °C.	Average voltage, v				Force Correction, mN
	Furnace off	Period CD	Period EF	Correction	
312	1.0330	1.0238	1.0255	0.0083	0.0053
358	0.6835	0.6793	0.6781	0.0049	0.0031
400	1.7996	1.7869	1.7920	0.0102	0.0065
466	0.5977	0.5766	0.5864	0.0162	0.0103
503	0.3500	0.3213	0.3336	0.0226	0.0144
530	0.5412	0.5227	0.5410	0.0094	0.0060

The only uncertainty left unresolved at high temperature is the depletion of film thickness due to reaction. It is necessary to determine the changes in the film thickness of ABVR in order to apply Equation 5-8 at high temperature (400 °C – 530 °C).

5.3.3 FILM THICKNESS OF REACTING ABVR AT HIGH TEMPERATURE

As explained in Section 3.3, the reacting ABVR gives volatile components and so gets depleted as the reaction progresses. Consequently, unlike the constant initial film used in the calibration of the method, a depleting initial film was evident during reactions at high temperature. In the application of the liquid bridge technique for measuring viscosity and surface tension at high temperature, a model was developed as shown by Equation 3-11 to determine the changes in the film thickness of ABVR as reaction progresses. This way, the appropriate film thickness would be used in Equation 5-8 at high temperatures. The parameters, e_1 and e_2, in Equation 3-11 were determined for the temperatures of interest from the kinetic data of Soundararajan, S (2001). Those data points were used to solve Equation 3-10 for these parameters by minimizing the sum of squared residuals between experimental and predicted film thickness to obtain values of e_1 and e_2 at all the temperatures of interest as given in Table 5-4. The density of the residual material, comprising coke of density 1500 kg/m^3 and ABVR of density 1087 kg/m^3 (McCaffrey et al., 1998), was obtained by assuming that volume and mass are additive.

Table 5-4. Kinetic Parameters in Model for Film Thickness of Reacting ABVR (Equation 3-11)

Temperature, °C	e_1	e_2
400	1.518E-07	5.9841
466	1.945E-04	3.2128
504	2.444E-03	2.6618
530	3.770E-03	2.7340

To apply Equation 5-8 at high temperature, δ is replaced with δ_t given by Equation 3-11. This allows for the determination of surface tension and viscosity as was done for the standard oils at room temperature.

6. FLUID PROPERTIES OF ABVR

6.1 ADHESIVE FORCES IN LIQUID BRIDGES OF REACTING ABVR

Adhesive forces in liquid bridges were measured, as described in Section 5.1.2, at the point of maximum elongation for varying time to touch rods, $\mathbf{t_a}$. These forces were measured for all the temperatures of interest: 400 °C, 466 °C, 503 °C and 530 °C.

6.1.1 ADHESIVE FORCES

The adhesive forces measured at 400 °C, 466 °C and 503 °C are presented below in Figure 6-1, Figure 6-2 and Figure 6-3 respectively.

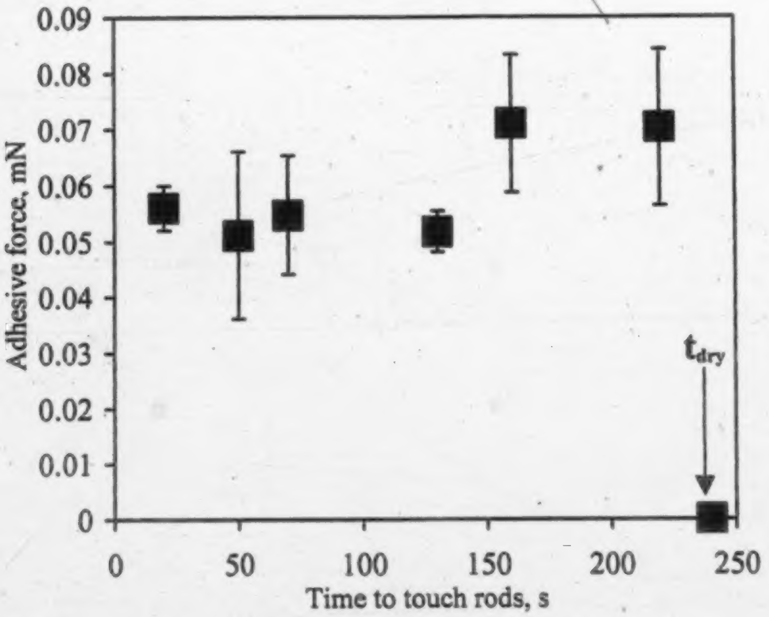

Figure 6-1. Adhesive forces of reacting ABVR versus time to touch rods at 400 °C

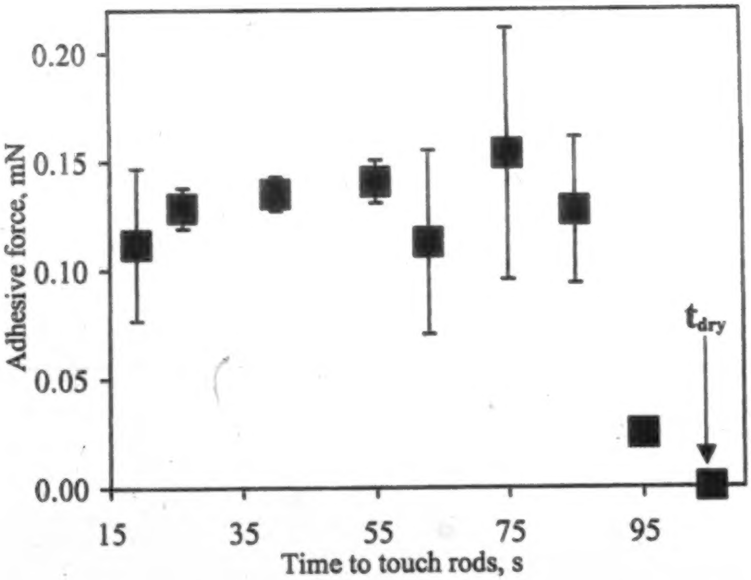

Figure 6-2. Adhesive forces of reacting ABVR versus time to touch rods at 466 °C

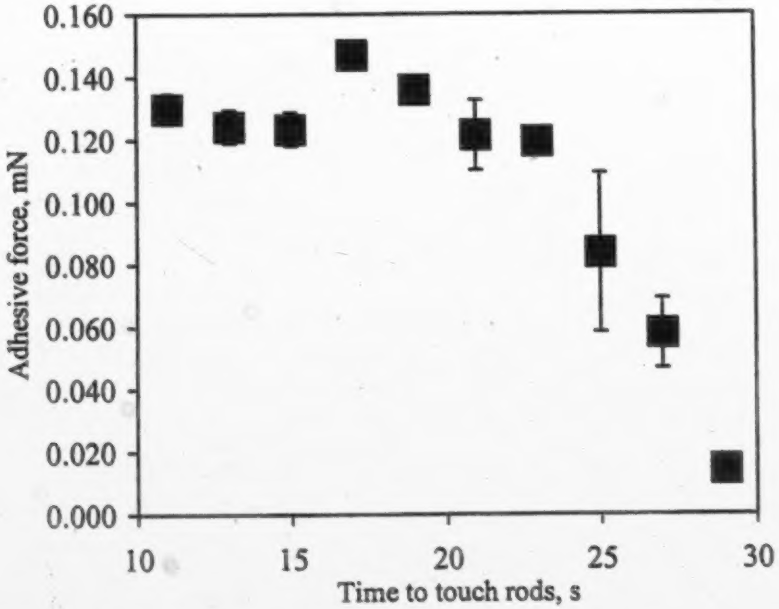

Figure 6-3. Adhesive forces of reacting ABVR versus time to touch rods at 503 °C

Figure 6-1 showed that adhesive forces at 400 °C remained constant at approximately 0.05 ± 0.01 mN (95 % confidence interval) for about 220 seconds, after which there was rapid decrease to zero indicating a dry film. The implication of this observation is that the adhesive forces in liquid bridges at this temperature will be constant until dry-out. It took 240 seconds for the liquid bridge to dry out at 400 °C. The fact that the ABVR did not react so vigorously at this temperature accounted for the long touch time it took for the material to dry out. Very little vapor of volatiles was seen at 400 °C, which implied that less cracking took place at this temperature. The long time required to dry out could be a result of cross-linking and polymerization, with little cracking.

At 466 °C, Figure 6-2[∇] showed a similar trend in adhesive forces with increasing time to touch rods, $\mathbf{t_a}$. Adhesive forces were found to be constant at 0.13 ± 0.03 mN (95 % confidence interval) till about 75 seconds. Afterwards, the adhesive force gradually decreased to zero at a touch time of 105 seconds at dry out. The shorter touch time for dry-out compared to that at 400 °C implied that there was more cracking and volatilization at this temperature than at 400 °C. Another noticeable fact in this figure is the higher adhesive forces measured at 466 °C compared to those at 400 °C, by a factor of 2 – 3 times.

Adhesive forces at 503 °C, like those at 466 °C, were approximately constant at 0.13 ± 0.01 mN (95 % confidence interval) for 23 seconds (Figure 6-

---

[∇] Figure 6-2 is from data collected by L. Boddez

3[®]). Adhesive forces slowly decreased to zero at dry out with touch time of 29 seconds. The short touch time of 29 seconds at dry out and the rigorous evaporation of volatiles showed that cracking was dominant at this temperature. Therefore, cross-linking and polymerization would be very limited.

Considerable cracking and evaporation of volatiles was found at 530 °C, which is characteristic of the reaction temperature of ABVR in fluid cokers. The trend in the adhesive force with time to touch rods was different at this temperature. Figure 6-4 gives the results of the measurement of adhesive forces with increasing time to touch rods at 530 °C.

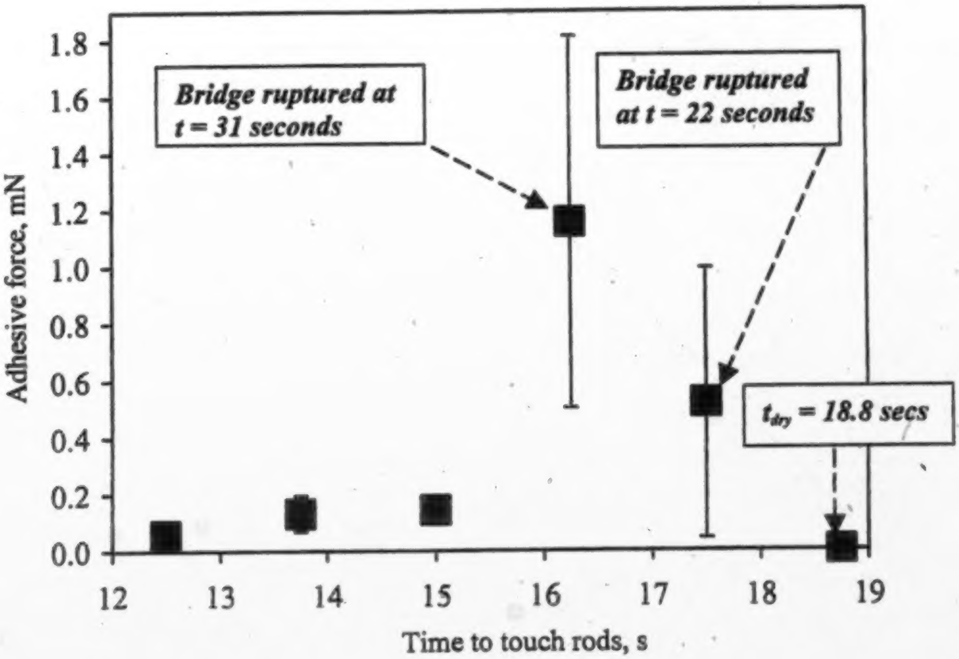

Figure 6-4. Adhesive forces of reacting ABVR versus time to touch rods at 530 °C

[®] Figure 6-3 was reported by Gray, et al. (2002)

Figure 6-4 showed a pronounced maximum compared to the results of Figure 6-1, Figure 6-2 and Figure 6-3. For the first 15 seconds, the force was constant at 0.12 ± 0.06 mN (95 % confidence interval), then attained a maximum of 1.16 mN at 16.25 seconds and gradual decreased to zero at dry out. Dry out was attained at time to touch rods of 19 seconds. As shown in Figure 6-4, for times to touch rods of 16.25 seconds and 17.5 seconds, the bridge ruptured at 31 seconds and 22 seconds respectively. These ruptures occurred long after dry-out touch time at this temperature. Consequently, the bridge remained, in the region of **D** << **b**, and was sticky enough to keep the two rods together until a point when the bridge hardened and fractured. This hardness caused the bridge to have an unusually high force that is equivalent to the force required to fracture the solid between the rods. This result showed that the reaction at 530 °C was so rapid and drastic that viscosity increased much more rapidly than at any other temperature studied. The forces measured after touch time at dry out were not representative of liquid properties.

Adhesive forces measured for liquid bridges at 503 °C and 530 °C model the adhesive forces that would be experienced by coke particles due to liquid bridging in fluid cokers. Therefore, adhesive forces determined here will help to ascertain the residence time required in the reactor to inhibit fouling (Gray et al., 2002). Additionally, the results on adhesive forces also gave an indication of the reaction times beyond which adhesive forces cannot be measured for each of the temperatures.

The data of Figures 6-1 to Figure 6-4 showed a decrease in touch time for dry out with increasing temperature. To better understand the effect of temperature on touch time for dry out, Figure 6-5 shows the Arrhenius relationship between dry out time data and temperature. Since appreciable reaction only started at 400 °C, dry-out time is corrected for heat-up time to attain 400 °C. Therefore, dry-out time is the touch time at dry out of the rods less the time taken to heat rods up to 400 °C.

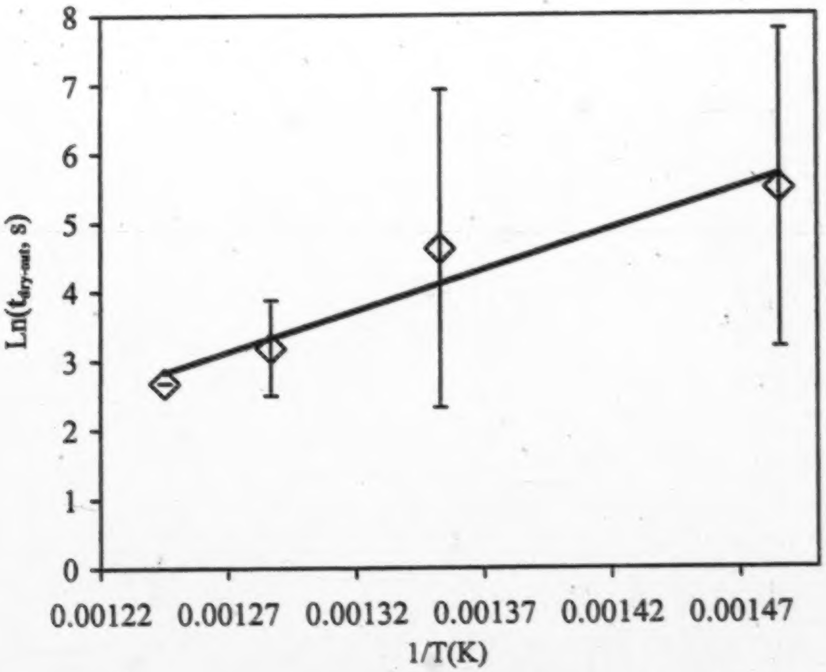

Figure 6-5. Dry out time (touch time at dry out less time to reach 400 °C) as a function of reaction temperature[∇]

[∇] Data at 466 °C and 503 °C obtained by L. Boddez

Figure 6-5 showed that dry out times fit the Arrhenius form as expected of a reacting system. From the fit shown above, an Arrhenius relationship could be written relating dry out time to reaction temperature.

$$\ln(t_{\text{dry-out}}) = \frac{11865}{(T + 273.15)} - 11.943; \quad 400\,^{\circ}\text{C} \leq T\ 530\,^{\circ}\text{C} \qquad (6\text{-}1)$$

Equation 6-1 could be used to estimate the dry out time at any reaction temperature between 400 °C and 530 °C.

The trend in initial and maximum adhesive forces with temperature is shown in Figure 6-6. Initial value represents a value that agreed with all the data before the maximum was attained with at least 90 % statistical probability while the maximum was obtained experimentally.

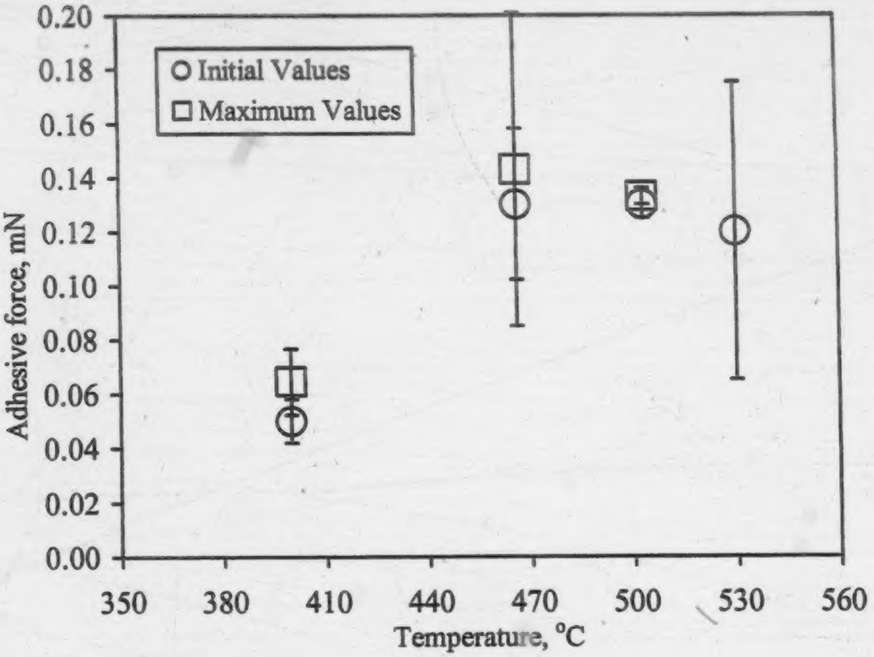

Figure 6-6. Trend in adhesive forces with temperature

The plot showed an increase in both the initial and maximum adhesive force till 466 °C. Examination of all data points at 466 °C and 503 °C revealed that both the initial and maximum values remained statistically constant till 503 °C within 95 % confidence interval. The initial value maintained the same value till 530 °C. With very similar initial forces, some similarities are expected in some properties of ABVR at 466 °C, 503 °C and 530 °C. However, a significant difference is expected in the properties of ABVR at 400 °C because of the lower forces.

6.1.2 CHARACTERISTICS OF LIQUID BRIDGES

At temperatures above 350 °C, ABVR undergoes cracking reactions, which leads to the release of volatiles. The remaining liquid continually gets depleted as discussed in Section 5.3.3. Consequently, the volume of liquid in the coating film of ABVR at high temperature will be smaller than the initial volume. The small volume in the coating film caused the liquid bridge formed at high temperature to be different from that observed at room temperature in both its length and lifespan. The liquid bridge was observed to be as long as 0.5 mm at room temperature (Figure 5-8) compared to the short bridge (up to 0.15 mm) found at high temperature (Figure 6-7). Liquid bridges at high temperature persisted for only 0.07 second compared to bridges at room temperature that persisted for as long as 0.25 second.

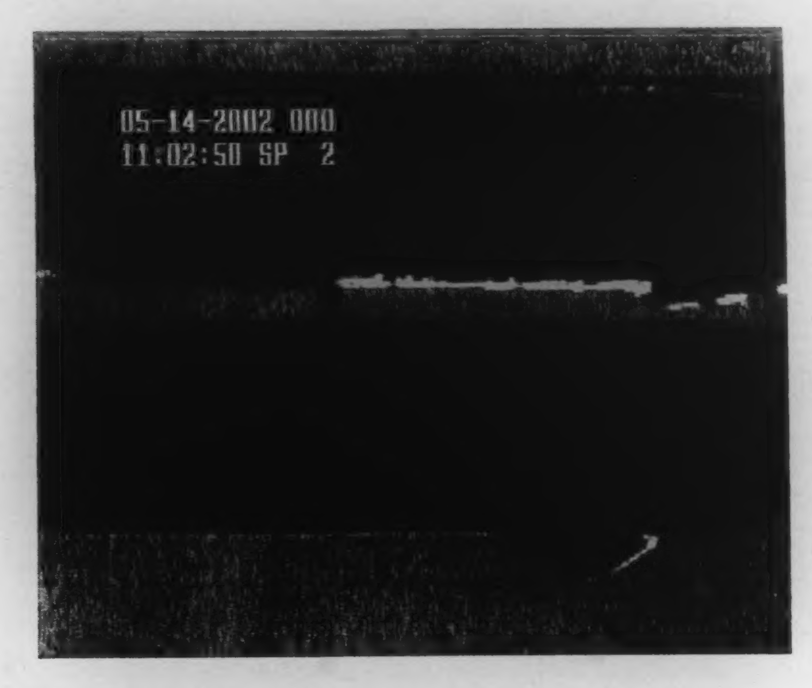

Figure 6-7. Video image a typical liquid bridge of reacting ABVR
(Length of bridge is of circa 0.1 mm)

The liquid bridge of reacting ABVR at 530 °C for time to touch rods of ≤ 15 seconds was similar to that shown in Figure 6-7 and to those found at 400 °C, 466 °C and 503 °C. For all these cases, adhesive forces were found to be lower than those measured at room temperature with the calibration oils. This change in the order of magnitude of the forces could be explained by the difference between liquid bridges formed at room temperature and those formed at high temperature. Consequently, the measurements of forces by the liquid bridge method were most useful for determining properties.

Adhesive forces in liquid bridges measured by this method were used to evaluate viscosity and surface tension of reacting ABVR (Equation 5-7 and

Equation 5-8). While the viscosity was obtained from the force measured at the point of maximum elongation (Equation 5-8), surface tension was measured from the force measured at the point of commencement of bridge elongation (Equation 5-7). Surface tension of standard oil (Table 5-2) calculated by the force and displacement analyses showed that the statistical method determined the point of commencement of liquid bridge with better accuracy than did the video method.

6.2 SURFACE TENSION OF ABVR

This section will present the surface tension determined using the liquid bridge method for all the temperatures of interest. Results will be presented for surface tension at temperatures when the ABVR was not reacting and also for temperatures when the ABVR was reacting. For reacting ABVR, results will show the trends in surface tension of ABVR with heating time at point of commencement of bridge elongation, $\mathbf{t_s}$, already described in Section 5.1.1.

6.2.1 SURFACE TENSION OF NON REACTING ABVR

ABVR was considered to be non-reacting when there was no noticeable evaporation of volatiles at which point polymerization was assumed to be predominant. This was noticed at temperatures of 312 °C and 358 °C. Surface tension was estimated from the measured forces at 20 seconds heating time at these two temperatures and the results are shown in Table 6-1.

Table 6-1. Surface Tension of non-reacting ABVR

Temperature, oC	Surface tension, mN/m	
	Liquid bridge method	Extrapolation from Li et al. (2003)
312	14.0 ± 1.5	16.71
358	14.7 ± 2.1	15.57

Error in the liquid bridge method corresponds to one standard deviation. Table 6-1 showed that the surface tension of reacting ABVR at 312 °C and 358 °C are the same (95 % confidence interval). Surface tension at 312 °C was found to be 14.0 mN/m, while that at 358 °C was found to be about 14.7 mN/m. This result is in agreement (95 % confidence interval) with the value predicted by Li et al. (2003).

6.2.2 SURFACE TENSION OF REACTING ABVR

Above 350 °C, the ABVR reacted because evaporation of volatiles became noticeable. The surface tension of ABVR was measured at 400 °C using the liquid bridge method and the results are shown below in Figure 6-8.

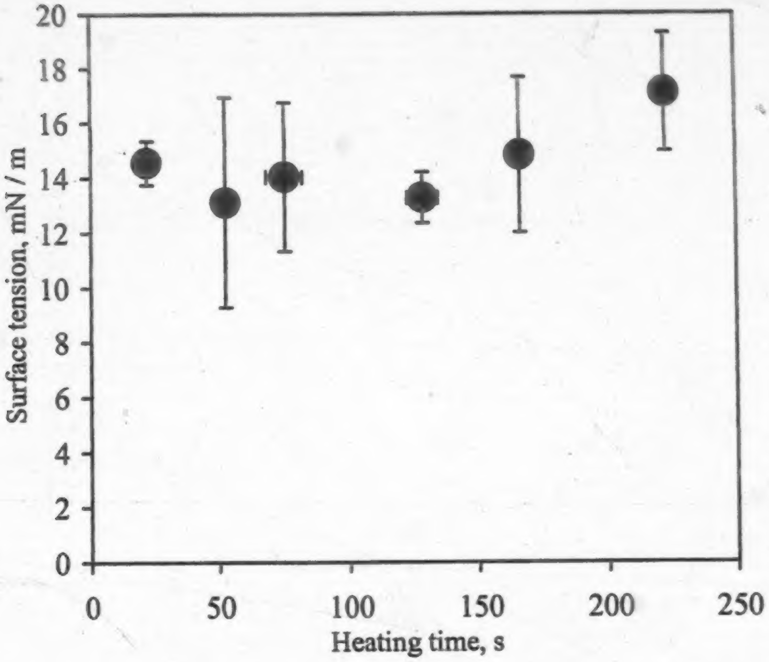

Figure 6-8. Surface tension of reacting ABVR versus heating time at 400 °C

The figure showed that the surface tension was constant with heating time for reacting ABVR at 400 °C. Though surface tension ranged from 13.0 mN/m to 17.0 mN/m, it was approximately constant with time at a mean value of 13.5 ± 2.2 mN/m (95 % confidence interval). This result is also within the order of magnitude predicted by Li et al. (2003), which was 14.5 mN/m. Surface tension results obtained at 466 °C, 503 °C and 530 °C are shown respectively in Figure 6-9, Figure 6-10 and Figure 6-11.

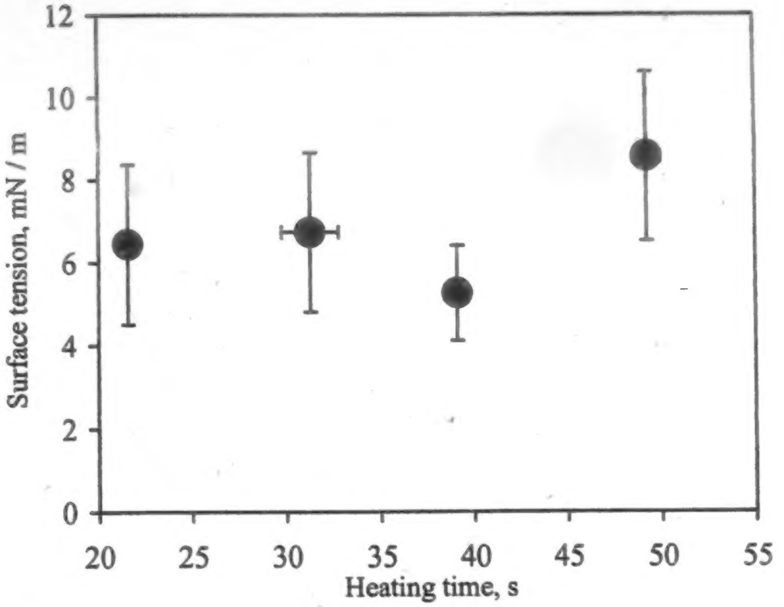

Figure 6-9. Surface tension of reacting ABVR versus heating time at 466 °C

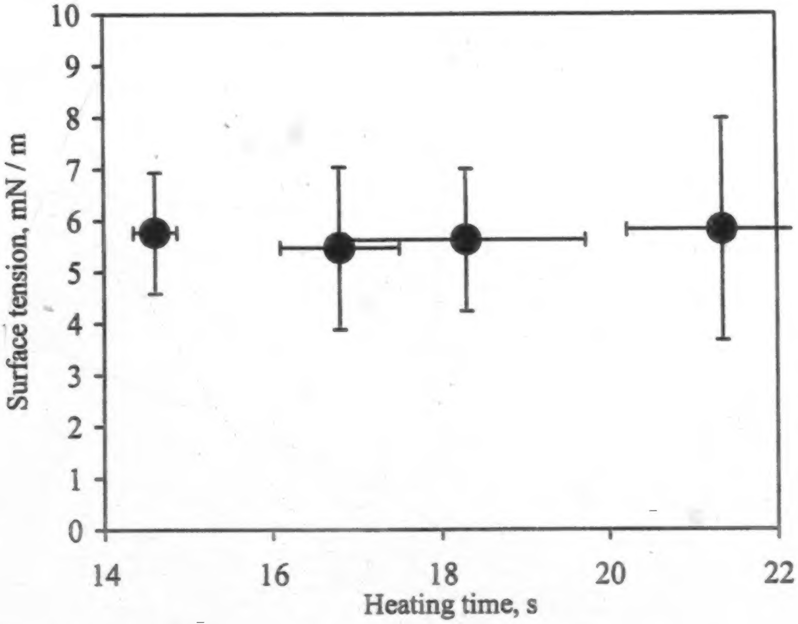

Figure 6-10. Surface tension of reacting ABVR versus heating time at 503 °C

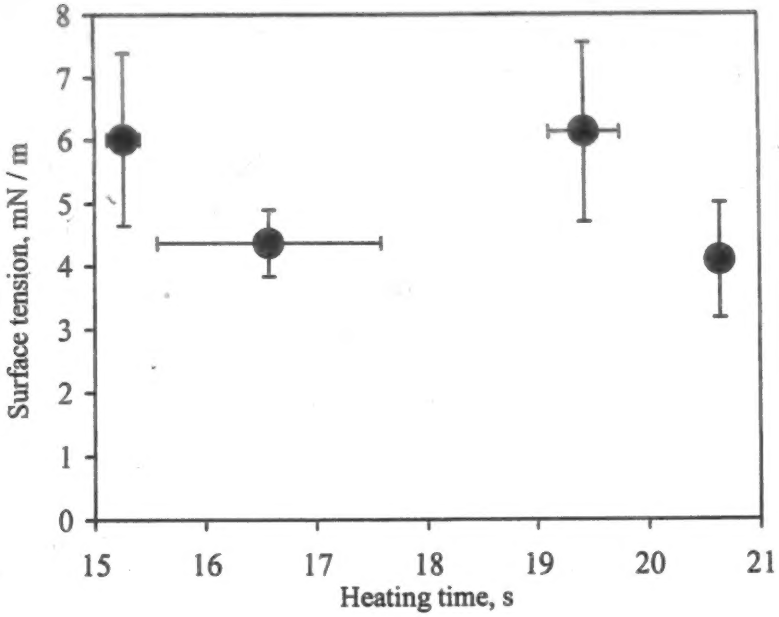

Figure 6-11. Surface tension of reacting ABVR versus heating time at 530 °C

At 466 °C, the surface tension of reacting ABVR was determined for increasing heating times and the result obtained presented in Figure 6-9. It showed that there was no discernable trend in the values of surface tension with heating time for reacting ABVR at 466 °C. Surface tension was found to have an average value of 5.6 ± 1.8 mN/m (95 % confidence interval), which is lower than what was obtained at 400 °C and the prediction of Li et al. (2003). Likewise, surface tensions of reacting ABVR at 503 °C estimated with initial adhesive forces (Figure 6-3) are reported in Figure 6-10. The figure showed that surface tension maintained an average value of 5.5 ± 1.6 mN/m (95 % confidence interval), which is the same as the surface tension obtained at 466 °C. This same magnitude was obtained for surface tension of ABVR at 530 °C as shown in Figure 6-11. The peculiar trend in adhesive forces at 530 °C shown in Figure 6-4 did not have any dramatic effect on the surface tension of ABVR at 530 °C.

For reacting ABVR, surface tension showed no noticeable trend with heating time at 400 °C - 530 °C. This showed that surface tension is insensitive to composition, which is consistent with surface tension of organic liquids reported by Poling et al. (2000); since the reacting ABVR remained a hydrocarbon throughout its reaction. However, the values were found to be lower than values obtained for non-reacting ABVR, except at 400 °C. Surface tensions of reacting ABVR were found to be a factor of 2-3 times lower than the prediction of Li et al. (2003). Large error bars in the surface tension were due to the high uncertainties introduced by the noise in the data. Though the noise was filtered, yet some of its effects remaining in the data introduced some errors in the surface tension results.

6.2.3 DISCUSSION: VALIDATION OF RESULTS

To validate the measurements of surface tension of ABVR, it was necessary to compare the data to the measurements of Li et al. (2003) in which surface tension of non-reacting ABVR was measured (Figure 2-1). A comparison of these results is presented in Figure 6-12. The values reported in Figure 6-12 for the liquid bridge method are the surface tension at the earliest possible time after reaction began. The dynamic response in surface tension was reported to be very slow. The results from this study are compared to the equilibrium values reported by Li et al. (2003) as shown in Figure 6-12 because the extrapolation of initial and equilibrium values meet at 350 °C beyond which only the extrapolated equilibrium data gave reasonable values of surface tension with increasing temperature.

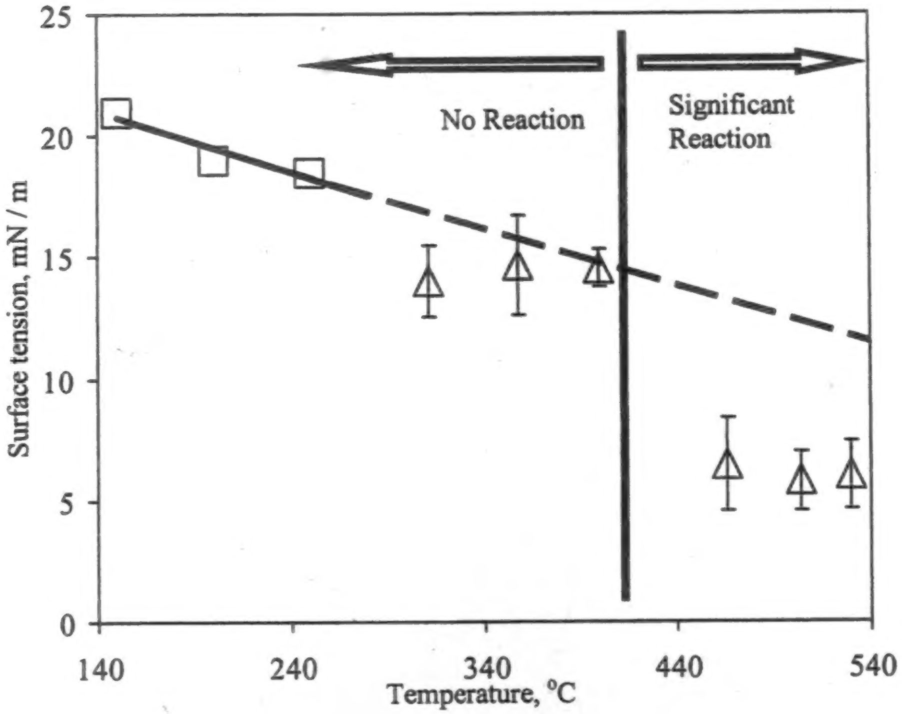

Figure 6-12. Surface tension of ABVR from pendant drop method (Li et al., 2003: equilibrium values □) and from liquid bridge method (Δ). The curves are from linear extrapolation of the data of Li et al., 2003

A constant surface tension was observed at temperatures of 358 °C and 400 °C within the margin of error of the liquid bridge method. A lower surface tension was obtained at 312 °C, which implied an incorrect trend of surface tension with temperature. The maximum surface tension obtained by the liquid bridge method at 312 °C was 15.7 mN/m compared to 16.7 mN/m predicted by Li et al. (2003). The errors introduced by the noise in the data used to determine the point of commencement of bridge elongation, which is crucial to surface tension determination, may account for the difference.

Figure 6-12 showed agreement to within a factor of 2 – 3 between average surface tensions obtained with the liquid bridge method and extrapolation of the data of Li et al. (2003) at higher temperatures (466 °C – 530 °C). It can be argued that the lower values of surface tension at 466 °C – 530 °C was a result of the significant reaction of the multi-component ABVR, leading to formation of solid coke particles in the liquid bridge at these temperatures, compared to no reaction at 312 °C – 400 °C where there were agreements with the predictions of Li et al. (2003). This difference might have also been caused by extrapolation of data of Li et al. (2003) over too wide a temperature range. Li et al. (2003) reported three data points for surface tension over a temperature range of 100 °C while these data points were extrapolated over a temperature range of 280 °C (250 °C – 530 °C). This huge extrapolation might have caused over-prediction of surface tension by the data of Li et al. (2003) at higher temperatures. Therefore, errors in the extrapolation of data points from Li et al. (2003) were critically investigated. Statistical analysis of the slope was employed in the investigation. The difference between the data estimated by the liquid bridge at 312 °C – 400 °C and those from the extrapolation of data from Li et al. (2003), was statistically insignificant at 95 % confidence. The difference between the data of Li et al. (2003) and the liquid bridge method was statistically significant (95 % confidence) for the range 466 °C – 530 °C. Table 6-2 gives the results obtained from the statistical analysis of the slope from data of both Li et al. (2003) and the liquid bridge method.

Table 6-2. Results from Statistical Analysis of Slopes

Temperature Range, °C	Data Source	Slope: $\left(\frac{d\gamma}{dT} \pm 95\%\ \text{CI}\right)$, $\frac{\text{mN}}{\text{m}-\text{K}}$
150 – 250	Li et al.	-0.024 ± 0.010
150 – 400	Li et al. & Liquid bridge	-0.028 ± 0.019
150 - 530	Li et al. & Liquid bridge	-0.043 ± 0.014

The statistical analysis suggested that the best estimates of surface tension from 150 °C – 530 °C would be obtained from a regression on all the data, as shown in Figure 6-13.

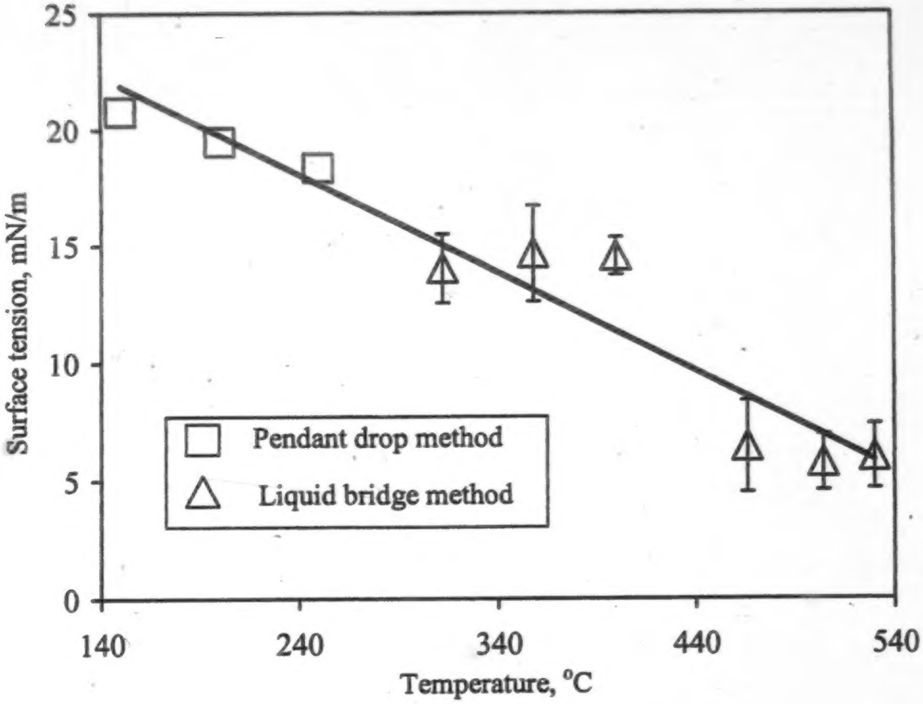

Figure 6-13. Trend in surface tension with temperature for pendant drop method (Li et al., 2002: equilibrium data□) and liquid bridge method (△)

Experimental data reported by Li et al. (2002) for the pendant drop method between 150 °C and 250 °C at equilibrium condition was used in Figure 6-13, instead of the mean values reported by Li et al. (2003). As illustrated in Figure 6-13, an expression can be written for the estimation of surface tension at any temperature between 150 °C and 530 °C.

$$\gamma = -0.0447T + 28.095; \qquad 150\,^{\circ}\mathrm{C} \leq T \leq 530\,^{\circ}\mathrm{C} \tag{6-2}$$

The liquid bridge method has given a good estimate of surface tension to within at least a factor of two. It has also shown good promise to more accurately determine surface tension if a means is found to completely eradicate the noise from the induction field.

6.3 VISCOSITY OF ABVR

In this section, the results of the measurements of viscosity of ABVR, for non-reacting temperatures using the Rheometric Mechanical Spectrometer (RMS 800, TA Instruments, Newcastle, Delaware, U.S.A.) and for reacting temperatures using the liquid bridge method, will be presented. Afterwards, the influence of dripping and the role of kinetics on the values of the estimated viscosity will be discussed. For reacting ABVR, results will show trends in viscosity with heating time at maximum elongation of bridge, $\mathbf{t_v}$, as defined in Section 5.1.

6.3.1 VISCOSITY OF NON REACTING ABVR

While the liquid bridge method was used to estimate surface tension at 312 °C and 358 °C, it could not be used to estimate viscosities at these temperatures due to the low adhesive forces. The forces at elongation of the bridge and at breakage of the bridge were identical, due to the low viscosity of the liquid. Instead, the Rheometric Mechanical Spectrometer (hereafter RMS) was used to measure the viscosity of ABVR at temperatures between 180 °C and 300 °C. The results obtained from those measurements are shown in Figure 6-14.

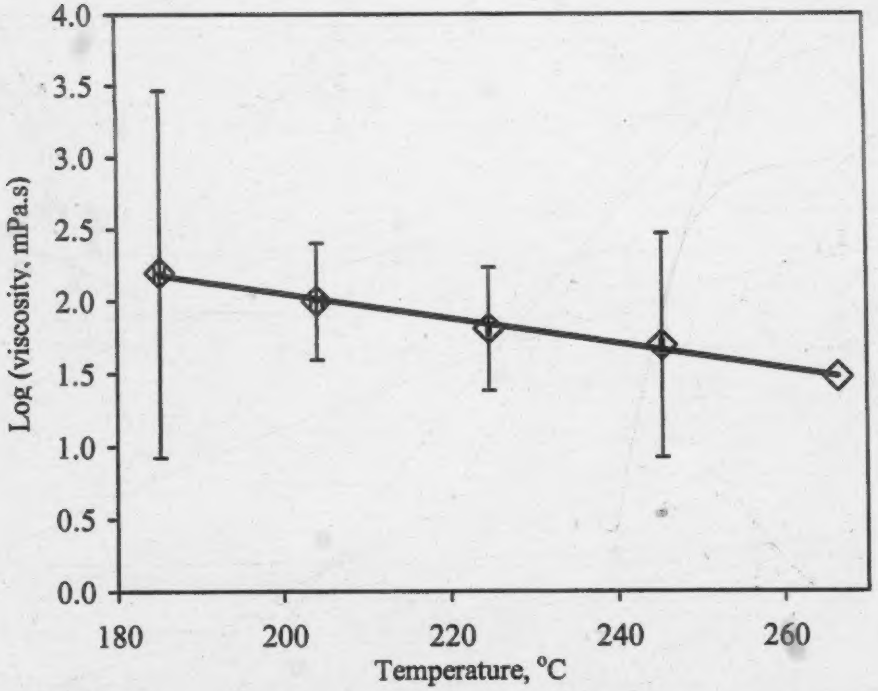

Figure 6-14. Logarithm of viscosity of non-reacting ABVR versus temperature (< 300 °C) using the RMS. Curve is correlation of data points

Figure 6-14 showed an exponential decrease in viscosity with temperature and a linear decrease in the logarithm of viscosity with temperature, which is similar to the observation of Svrcek and Mehrotra (1988) on Athabasca bitumen and in agreement with the ASTM D341 method for estimating viscosities of hydrocarbon with temperature. The data also produced an equally linear trend with an Arrhenius relationship between viscosity and temperature like that proposed by

Poling et al., 2000. However, to allow for easier presentation of the experimental data, the former correlation of log(viscosity) versus temperature was adopted.

When temperature becomes significantly higher, RMS could no longer be used because the signal transducer was not designed to be operated at a temperature > 350 °C. It was also not capable of rapid heating to a constant temperature, in order to get useful data on reacting fluids.

6.3.2 VISCOSITY OF REACTING ABVR

The results of measuring viscosity of ABVR at temperatures of 400 °C, 466 °C, 503 °C and 530 °C are presented in this section. Viscosity of ABVR at 400 °C is included in this section because there were some reactions at this temperature that had pronounced effects on the viscosity of ABVR. These reactions had no effect on the surface tension at 400 °C as it was shown in Figure 6-12 that surface tension at 400 °C did not differ significantly from that at 358 °C where there was no reaction. Viscosity results at 400 °C, 466 °C and 503 °C are shown in Figure 6-15, Figure 6-16 and Figure 6-17 respectively.

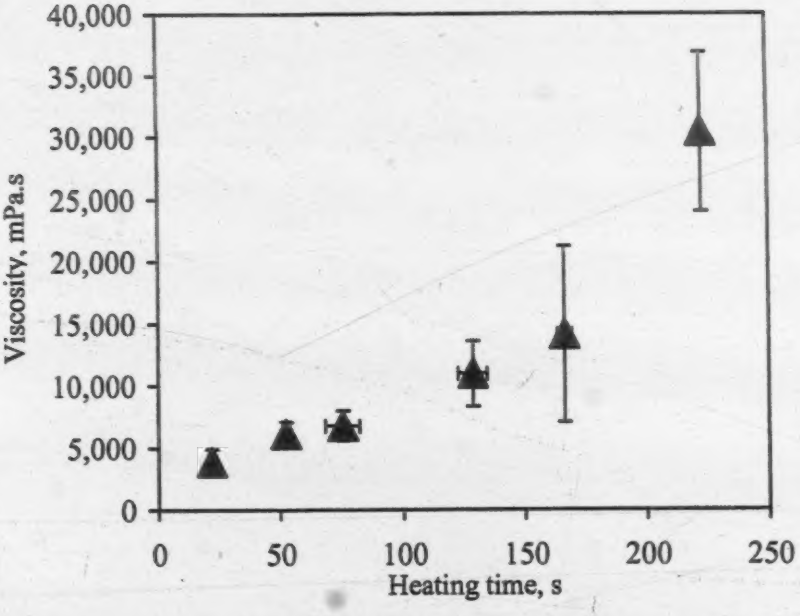

Figure 6-15. Viscosity of reacting ABVR versus heating time at 400 °C

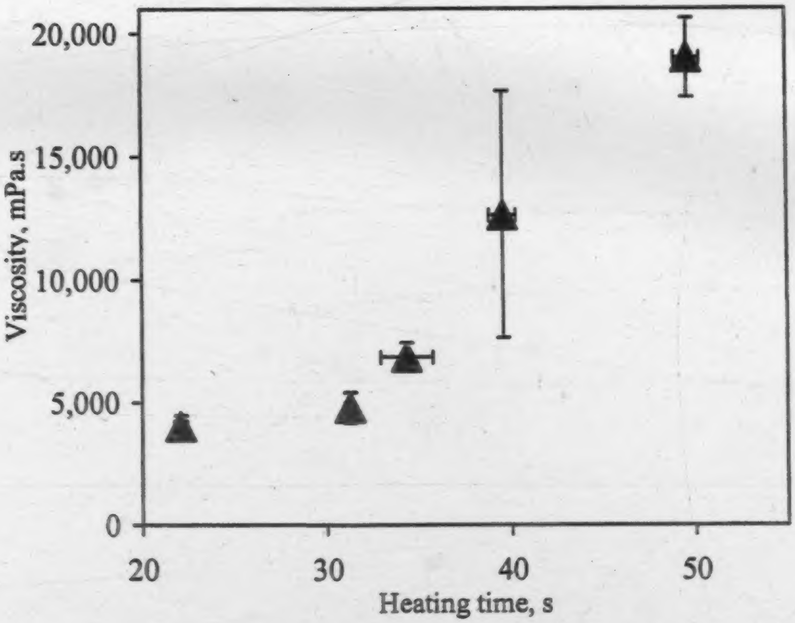

Figure 6-16. Viscosity of reacting ABVR versus heating time at 466 °C

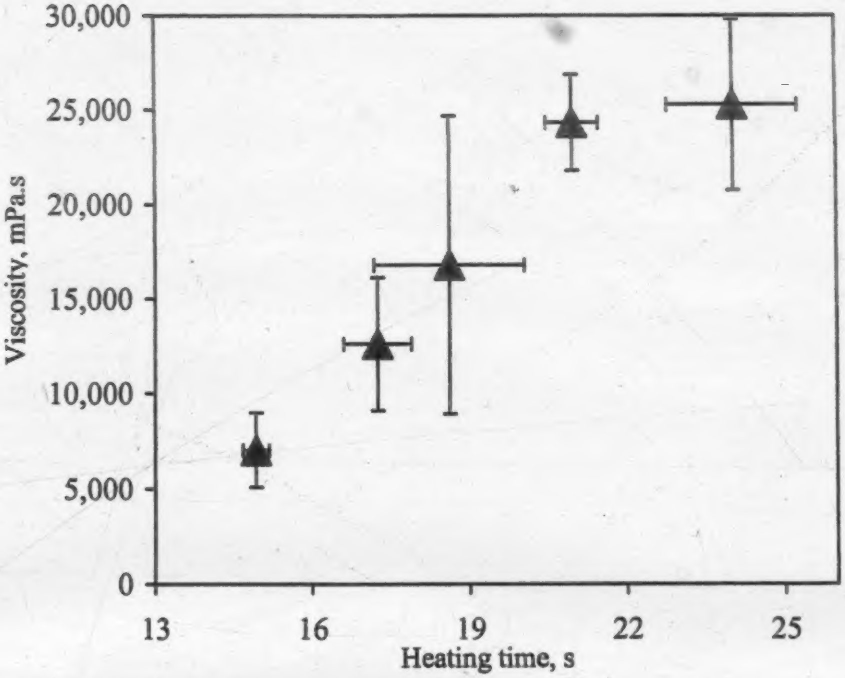

Figure 6-17. Viscosity of reacting ABVR versus heating time at 503 °C

Figure 6-15 showed an increase in viscosity of ABVR with heating time at 400 °C. Since kinetic data were not collected at 400 °C, the model developed by Gray et al. (2003) was extrapolated to obtain the data needed for the determination of the film thickness used in Equation 5-8. Viscosity of ABVR increased by four orders of magnitude in 240 seconds at 400 °C, increasing up to 35,000 mPa.s. This result is different from the trend noticed at temperatures less than 300 °C, where viscosity decreased with temperature. Therefore, Figure 6-15 showed that the reaction noticed at 400 °C, though not very vigorous, still had a significant effect on the viscosity of ABVR.

At 466 °C, similar results were obtained. Viscosity was found to increase by four orders of magnitude in 50 seconds, increasing up to 20,000 mPa.s. Compared to 400 °C, at which viscosity was only 5,000 mPa.s after 50 seconds, viscosity increase was more rapid at 466 °C. The viscosities obtained at 503 °C are shown in Figure 6-17. This figure showed increase of viscosity up to 26,000 mPa.s in 25 seconds. Compared with the results at 466 °C, which gave a viscosity of 7,000 mPa.s at 25 seconds heating time, viscosity response to reaction was more rapid at 503 °C than at 466 °C.

As discussed in Section 6.1.1, the liquid bridge at 530 °C solidified at some point during pull apart. Consequently, for the determination of viscosity at 530 °C, the liquid bridge method described in Section 5.1 was modified slightly to avoid regions of extreme stickiness and solidification. Instead of taking the force for viscosity measurement at the point of maximum elongation, the measurement was taken at a point between 1-2 seconds after commencement of bridge elongation. The results of measurement are presented in Figure 6-18 while the adhesive forces at the points of measurement are presented in Figure 6-19.

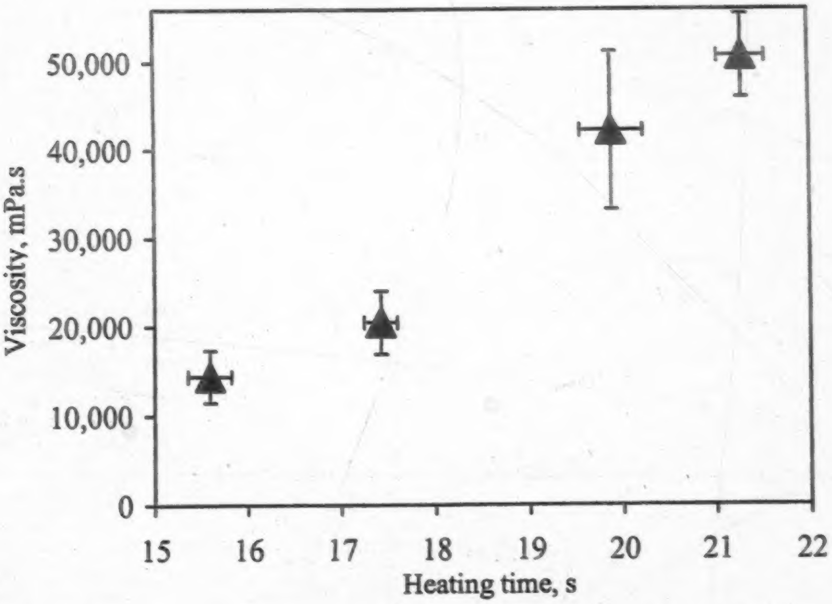

Figure 6-18. Viscosity of reacting ABVR versus heating time at 530 °C

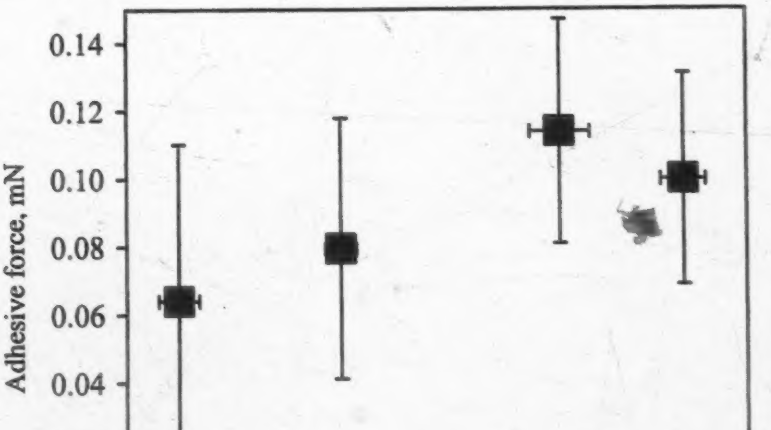

Figure 6-19. Selected Adhesive forces for measuring the viscosity of reacting ABVR at 530 °C

Reaction at 530 °C gave four orders of magnitude increase in viscosity in 22 seconds. Viscosity rose to 50,000 mPa.s, which made viscosity at 530 °C the most responsive to reaction. Also, when the data of Figure 6-19 are compared with Figure 6-4, it was observed that the range of forces in Figure 6-19 was consistent with those in Figure 6-4 at times to touch rods below 15 seconds. Also, the values in Figure 6-19 were within the same order of magnitude as the values in Figure 6-1, Figure 6-2 and Figure 6-3 for temperatures 400 °C, 466 °C and 503 °C respectively. These results showed that the modified method for measuring force at 530 °C was consistent with the results at lower temperatures. Also, the viscosity at 400 °C, 466 °C, 503 °C and 530 °C experienced a ~10^4 increase with changes in liquid composition, as reaction increased with heating time.

Increase in viscosity with heating time was extreme at these temperatures, in spite of the almost constant adhesive forces (Figure 6-1, Figure 6-2 and Figure 6-3). This result implied that changes in the other parameters in Equation 5-8 accounted for the considerable change in viscosity. Viscosity values were obtained with more certainty than the surface tension values, because the point of maximum elongation of the liquid bridge was not seriously impacted by the noise in the data. However, there is no independent method or standard with which the viscosity values can be checked to absolutely confirm this assertion.

6.3.3 INFLUENCE OF DRIPPING ON MEASURED VISCOSITY OF REACTING ABVR

The film thickness on the crossed rods is a critical parameter for viscosity measurement. At the reacting temperatures of 400 °C, 466 °C, 503 °C and 530 °C, it was noticed that the heating of the ABVR coating on the rods reduced the viscosity of ABVR considerably before the reaction commenced. During this period, the ABVR was found to drip. These drips, found to be minimal at 312 °C and 358 °C, had the unfortunate effect of reducing the actual film thickness on the rods, since some volume of the ABVR ended up in the drip. Consequently, extra care was taken to avoid contacting of the rods on the drips and the measurement was discarded whenever such contact occurred.

Since the viscosity estimation depends on the film thickness of the ABVR on the rods, as shown in Equation 5-8, it is important to estimate the effect the drip had on the viscosity estimation. The drip volume was estimated at the temperatures of interest using image analysis to determine the dimensions of each drip, which was assumed to be axially symmetric. Each drip was also assumed to have elliptical cross section at its base. While the major axis of the ellipse was measured by image analysis, the minor axis of the ellipse was assumed to be the known diameter of the rod, also used for scaling in image analysis for the worst case. The measured dimensions were used to estimate the volume of the drip by the method of cross sections (Edwards and Penney, 1982) implemented on Matlab 6.5.

Taking the drip into account, the actual remaining film thickness on the rods was estimated. The estimate of the actual film thickness was then used to evaluate a corrected viscosity. The data of Table 6-3 show the results of the evaluation and the comparison of viscosities obtained with those obtained without accounting for drip formation.

Table 6-3. Effect of Dripping on the Measured Viscosity of Reacting ABVR

Temperature, °C	Heating time, s	Viscosity, Pa.s	Viscosity corrected for Drip Volume, Pa.s
400	21.757	3.9 ± 1.0	4.9
	52.443	6.1 ± 0.9	7.7
	75.320	6.8 ± 1.2	8.5
	128.597	10.9 ± 2.6	13.7
	166.503	14.1 ± 7.1	17.7
	222.753	30.4 ± 6.4	38.2
466	22.067	4.0 ± 0.4	5.7
	31.225	4.8 ± 0.6	6.8
	34.315	6.9 ± 0.6	9.7
	39.570	12.6 ± 5.0	17.9
	49.630	19.0 ± 1.6	26.9
503	14.927	7.0 ± 2.0	11.0
	17.250	12.6 ± 3.5	19.8
	18.620	16.8 ± 7.9	26.4
	20.980	24.3 ± 2.5	38.1
	24.023	25.3 ± 4.5	39.6
530	15.593	14.4 ± 3.0	22.6
	17.423	20.4 ± 3.6	32.2
	19.890	42.2 ± 9.0	66.4
	21.287	50.7 ± 4.8	79.7

At 400 °C, the viscosities determined without allowing for dripping gave a result that agreed with the corrected viscosity within the margin of error of the liquid bridge method. Once again, this result confirmed that the dripping at lower temperature had negligible effects on the results. The observation was different at 466 °C, where the viscosity was underestimated by 23 % - 26 %. At 503 °C, difference in the viscosities was 33 % - 36 %. At 530 °C, viscosity was under-estimated by 33 % - 40 %. However, the viscosity reported as the best estimate was not corrected for dripping because the drip contained some vapor. Figure 6-7 shows a drip with longer life than those chosen for this analysis. The drips for correction were chosen as soon as they were formed with a view to minimizing the trapped vapor in the drip. The volume of the drip was over-estimated because of the vapor in the drips and the assumption that the minor axis at the base of the drip is equal to the diameter as the rod, which would also cause an over-estimation of the corrected viscosity. Consequently, Table 6-3 shows the maximum possible correction due to dripping. Due to the uncertainty in the volume of liquid in drips, the viscosities were not corrected for this effect. The data of Table 6-3 show a maximum bias of 30 %. Increased pressure would reduce the bias in viscosity estimates since the high pressure would reduce the vapor trapped in the drip.

6.3.4 ROLE OF KINETICS IN VISCOSITY OF REACTING ABVR

As mentioned in Section 5.3.3, the kinetic data were used to determine the depletion of the film thickness during reaction of ABVR. This film thickness allowed for the estimation of viscosity of reacting ABVR as shown in Equation 5-8. The reacting ABVR cracked in the process and was converted to gas, liquid and toluene insoluble solids. Based on the model developed by Gray et al. (2003), the experimental dry-out time (time to touch rods at dry out less time to reach 400 °C) at each of the temperatures was used to estimate the conversion of ABVR. The predicted conversion was shown in Figure 6-20 with increasing dry-out time, while Figure 6-5 gave the approximate experimental dry-out times. The model was extrapolated at 400 °C since no kinetic data was collected at that temperature.

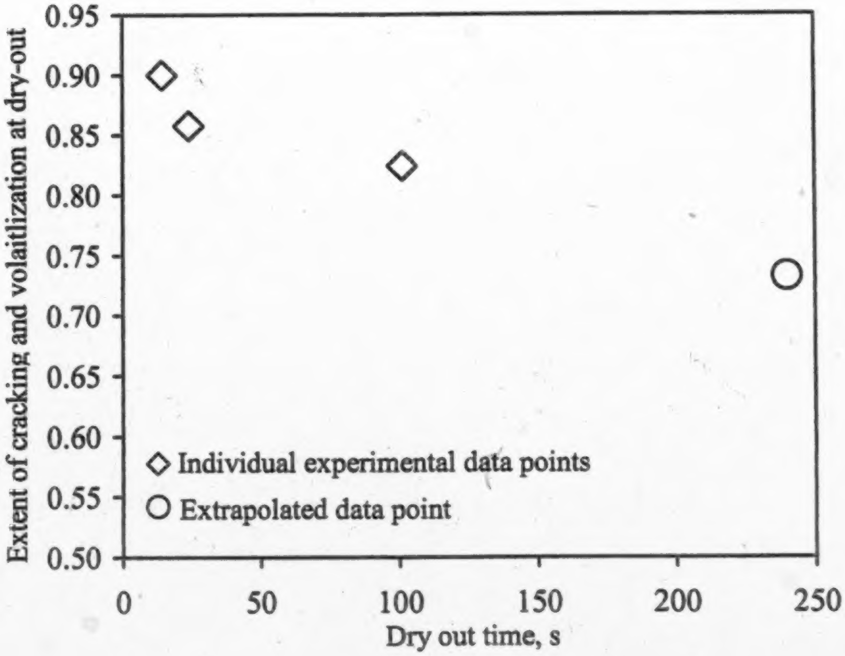

Figure 6-20. Predicted extent of cracking and volatilization of reacting ABVR at dry-out time (touch time at dry out less time to reach 400 °C). Times are from Figure 6-6

The estimate of the extent of cracking was found to have a gentle decrease with experimental dry-out time; therefore, dry-out time corresponds to a finite level of conversion that increased with temperature.

The trend in the predicted extent of cracking with dry out time led to further examination of the results to investigate the effects of kinetics on the results obtained for viscosity. To study this trend, the viscosity for reacting ABVR, at all the temperatures of interest, was plotted against the heating time in Figure 6-21. It was found that the slope of viscosity with reaction time increased as temperature increased. With reaction time (heating time less time to reach 400 °C) normalized with experimental dry-out time (touch time at dry out less time to reach 400 °C), a plot of logarithm of viscosity versus t/t_{dry} gave an almost linear trend, as illustrated in Figure 6-22.

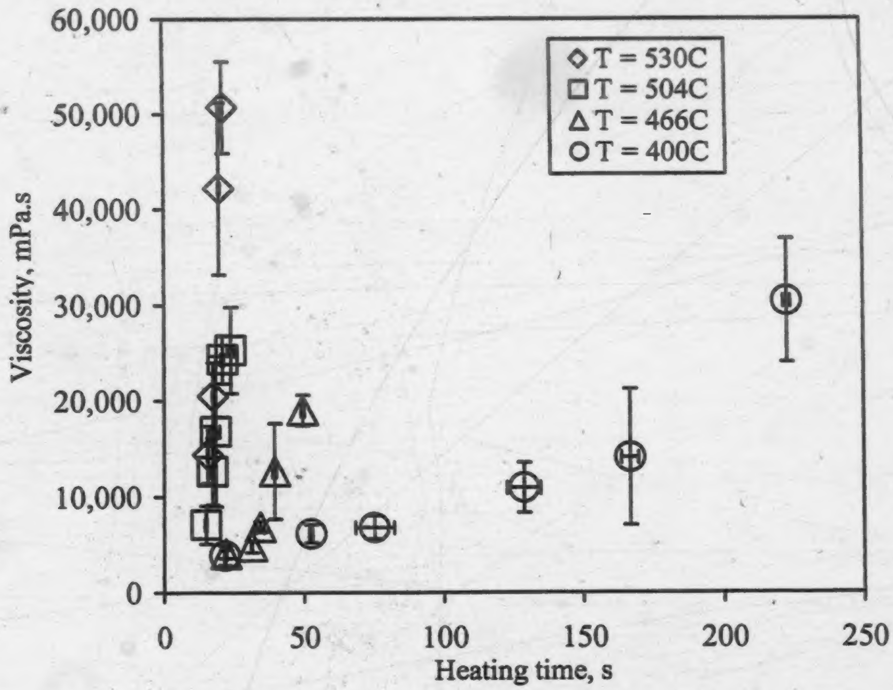

Figure 6-21. Trend in the viscosity of reacting ABVR with heating time

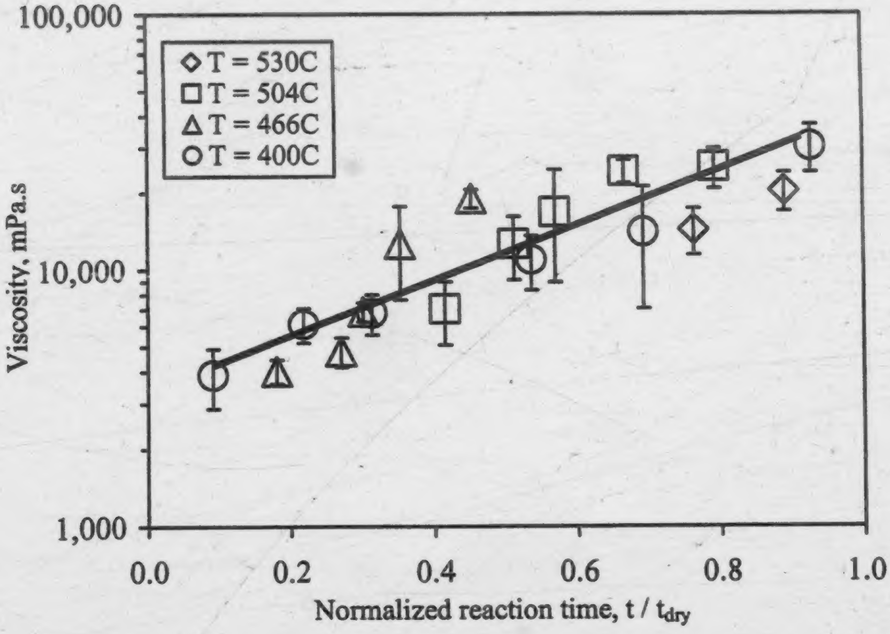

Figure 6-22. Semi-log plot showing viscosity versus normalized reaction time (heating time less time to reach 400 °C)

From the regression shown in Figure 6-22, an equation relating the viscosity to the reaction time and experimental dry-out time can be written as follows in Equation 6-3.

$$\ln(\eta) = 8.160 + 2.321\left(\frac{t}{t_{\text{dry-out}}}\right); \qquad 10\,\text{s} \le t \le t_{\text{dry-out}}(T) \quad \text{(6-3)}$$

where **t** is the reaction time and $\mathbf{t_{dry\text{-}out}}$ is the experimental dry-out time. If the correlation in Equation 6-1 is substituted for $\mathbf{t_{dry\text{-}out}}$, an expression can be written for viscosity in terms of reaction time and temperature.

$$\ln(\eta) = 8.160 + 2.321 * t * \exp\left(11.943 - \frac{11865}{T + 273.15}\right) \qquad (6\text{-}4)$$

$$\text{for } 400\,^{\circ}\mathrm{C} \le T \le 530\,^{\circ}\mathrm{C}; \quad 10\,\mathrm{s} \le t \le t_{dry-out}(T)$$

Where **T** is the temperature of reaction. The implication of Equation 6-4 is that, within the range of temperatures (400 °C –530 °C) considered in this study, a quick estimate of the viscosity of reacting ABVR can be obtained at any reaction temperature and reaction time. The use of Equation 6-4 in place of Equation 6-3 caused viscosity to be underestimated by 17.0 % at 400 °C and 504 °C, by 25 % at 530 °C. Viscosity was overestimated by 60 % at 466 °C because dry-out time at this temperature laid outside the correlation curve shown in Figure 6-5. Consequently, Equation 6-4 can estimate viscosity with only 25 % error compared to viscosity estimated using Equation 6-3.

6.4 DISCUSSION

Unlike the adhesive forces and surface tension of reacting ABVR that mostly remained within the same order of magnitude, the viscosity of reacting

ABVR increased by four orders of magnitude before dry-out was attained. Figure 6-22 gave the role of experimental dry-out time (touch time at dry out less time to reach 400 °C) and kinetics on the trends and values of viscosity with increasing reaction time. It is important to look at the trends in viscosity with temperature as done with surface tension in Figure 6-12. Consequently, Figure 6-23 shows the trends in viscosity with increasing temperature. The viscosity values presented for the liquid bridge method represent the values at the earliest possible reaction time after reaction began.

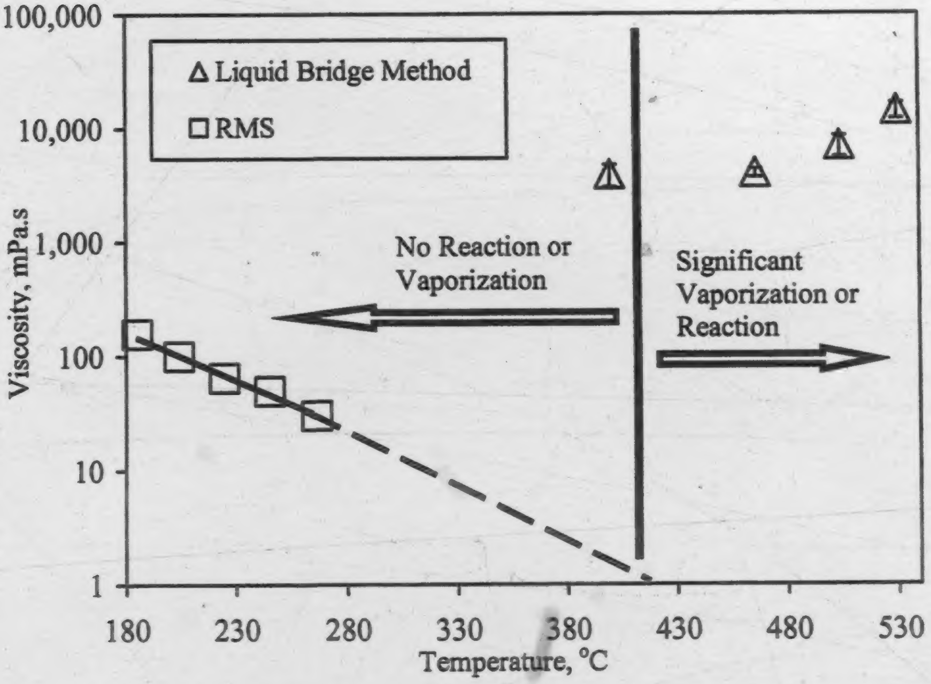

Figure 6-23. Semi-log plot showing viscosity of ABVR with increasing temperature from two different techniques. The curve is extrapolated from RMS data

Clearly, Figure 6-23 showed that the cracking reaction changed the liquid ABVR so much that the viscosity increased beyond the extrapolation of the data obtained from RMS. Although, 400 °C fell in the region described as having little reaction or vaporization, yet the limited reaction at that temperature was enough to increase the viscosity of ABVR considerably.

When Figure 6-12 was compared with Figure 6-23, it was noticed that the initial reaction did not affect the estimated value of the surface tension of ABVR throughout the entire range of 312 °C – 530 °C as temperature was the primary cause of the reduction in surface tension. However, at ≥ 400 °C, viscosity continually increased right from the moment reactions started till dry out was attained. The viscosity measured will be apparent viscosity because of the low sensitivity of the equipment. As reaction progresses, the ABVR continually approached non-Newtonian behavior because of gradual formation of solid coke products in the liquid bridge. The liquid bridge method was unable to detect this non-Newtonian behavior. An attempt made to increase the shear rate by doubling the pull-apart rate of rods produced the same viscosity values. The shear rate is not a controlled variable in this experiment as it depends on the properties of the liquid bridge and the free rod. So, doubling the pull-apart rate did not double the shear rate but only increased it by 20-30%. This shows that the liquid bridge method did not detect any non-Newtonian behavior since the increase in shear rate did not cause any change in viscosity

6.5 PROCESS IMPLICATIONS

Agglomeration, fouling and bogging are some of the unpleasant phenomena found in fluid cokers. Eliminating these phenomena will involve finding a means of evaluating stickiness forces between coke particles. These adhesive forces were suggested to be largely responsible for these phenomena (Gray et al., 2002). The findings of this study will aid in the estimation of adhesive forces between coke particles for any combination of particle size, film thickness and reaction. These forces could be estimated using Equation 5-7 for the static case and Equation 5-8 for the dynamic case. The surface tension term in Equation 5-7 will be evaluated using Equation 6-2 while the viscosity term in Equation 5-8 will be evaluated using Equation 6-4. However, a means will have to be found to determine the separation distance between coke particles and their rate of separation to be able to completely evaluate adhesive forces in the dynamic case.

The estimated adhesive forces can be combined with the existing reactor models for mixing and liquid reaction, and coupled with hydrodynamics to completely model the break up of aggregates formed by adherent particles. Such models will have to be tested at the pilot scale level to validate fouling and bogging predictions.

7. CONCLUSIONS & RECOMMENDATIONS

7.1 CONCLUSIONS

With the results obtained in this study, involving the measurement of the fluid properties of ABVR at coking process conditions, the following conclusions were reached.

1. The liquid bridge method was found to be a useful means of measuring the viscosity and surface tension of liquid forming a liquid bridge between two crossed cylinders in relative motion. The Liquid bridge method was capable of taking measurements of surface tension and viscosity in a single run. This method was successfully used to estimate the surface tension of ABVR and its viscosity at reacting temperatures.
2. At temperatures of 312 °C, 358 °C and 400 °C, at which the ABVR was found to undergo little or no reaction, the liquid bridge method was used to measure surface tension. The values obtained for surface tension were found to be 14.0 ± 1.5 mN/m and 14.7 ± 2.1 mN/m respectively for 312 °C and 358 °C. At 400 °C, the surface tension obtained at about 22 seconds after reaction started was 14.6 ± 0.8 mN/m. The values of surface tension at these three temperatures agreed with the prediction of Li et al. (2003) within an error of 2 mN/m.
3. Surface tension data for ABVR was obtained at 466 °C, 503 °C and 530 °C, in the presence of reaction and volatilization. Surface tensions

of ABVR were found to remain approximately constant with increasing reaction time at 400 °C, 466 °C, 503 °C and 530 °C. The surface tension at 466 °C after 22 seconds of reaction was found to be 6.4 ± 1.9 mN/m. At about 15 seconds after reaction started at 503 °C and 530 °C, the values of surface tension were found to be 5.8 ± 1.2 mN/m and 6.0 ± 1.4 mN/m respectively. Values of surface tension measured were within a factor of 2 of extrapolated values from Li et al. (2003) on the same material.

4. A predictive model was developed for the estimation of surface tension at any temperature between 150 °C and 530 °C for ABVR.

5. An estimate of viscosity was obtained from measurements. Viscosity was estimated at temperatures of 400 °C, 466 °C, 503 °C and 530 °C. For all the temperatures tested, viscosity was found to increase by four orders of magnitude before dry-out was attained. About 22 seconds after the reaction started, values of viscosity for reacting ABVR were found to be 3,800 ± 1000 mPas and 4,000 ± 400 mPas at 400 °C and 466 °C respectively. At about 15 seconds after reaction began, viscosity values were 7,000 ± 2,000 mPas and 14,000 ± 3,000 mPas at 503 °C and 530 °C respectively. Furthermore, viscosity at 400 °C was found to rise to 35,000 mPas in 240 seconds. At 466 °C, it was found to increase up to 20,000 mPas in 50 seconds while it rose to 26,000 mPas in 25 seconds at 503 °C. Finally, viscosity rose to 51,000 mPas in 22 seconds

at 530 °C. Viscosities measured had a maximum bias of 30 % due to dripping of liquid.

6. Kinetics were found to play a major role in the viscosity of reacting ABVR. With the experimental dry-out time from kinetics, reaction time was used to explain the trend in the extent of cracking and volatilization of the reacting ABVR. Furthermore, a normalized reaction time was used to better understand the trends in the viscosity of reacting ABVR. This ultimately allowed for the development of a predictive model useful for a first hand determination of viscosity within the temperature range of this study.

7.2 RECOMMENDATIONS

From the results obtained in this study, the following recommendations are proposed for advancement of this study.

1. Correlations were found for the estimation of surface tension and viscosity at any temperature and reaction time. It is necessary to develop a means of applying these correlations to estimate the adhesive forces between coke particles in fluid cokers for various combinations of particle diameter, film thickness and reaction time.
2. Viscosity measured at reaction conditions show that composition is important. Methods need to be developed to link the predicted compositions during reaction to the measured viscosities.

3. Means have to be found to completely eliminate the noise introduced by the radio frequency of the induction furnace. This way, much of the error introduced in the measurement by the incomplete removal of the noise could be eliminated.

4. Dripping was found to introduce bias in viscosity values and higher pressure might be able to reduce this bias by reducing the volume of volatile trapped in the drip. Higher-pressure experiments will have to be conducted to investigate the possibility of reducing the bias found in the viscosity of ABVR measured by this method.

REFERENCES

Andrade, E.N.da C., "The Viscosity of Liquid", *Nature*, **1930**, 125, 12-13

Anilkumar, G.G. and Neuman, R.D., "The Uncertainty in Absolute Values of Surface Tension of Water", *Colloids and Surfaces*, **1987**, 27, 1-14

Bird, R.B., Stewart, W.E. and Lightfoot, E.N., Transport Phenomena, John Wiley & Sons, Inc., New York **(2002)**

Bowman, C.W., "Molecular and Interfacial Properties of Athabasca Tar Sands", 7th World Petroleum Congress Proceedings, **1967**, 3, 583-613

Burdon, R.S., "Surface Tension And The Spreading of Liquids", *Cambridge Monographs on Physics*, Cambridge University Press, **(1949)**

Chen, P., "Understanding The Dynamic Surface Tension of Solutions Containing Volatile Organic Compounds (VOCs)", *Colloids and Surfaces A*, **2001**, 192, 195-204

Christensen, R.J., Lindberg, W.R. and Dorrence, S.M., "Viscous Characteristics of A Utah Tar Sand Bitumen", *Fuel*, **1984**, 63, 1312-1317

Darwish, E.I., Al-Sahhaf, T.A. and Fahim, M.A., "Prediction and Correlation of Surface Tension of Naphtha Reformate and Crude Oil", *Fuel*, **1995**, 74, 575-581

Dealy, J.M., "Rheological Properties of Oil Sand Bitumens", *Canadian Journal of Chemical Engineering*, **1979**, 57, 677-683

Dolbear, G.E., Tang, A., Moorehead, E.L., "Upgrading Studies with Californian, Mexican, and Middle Eastern crude oils", in Metal Complexes in Fossil Fuels, Filby, R.H.; Branthaver, J.F. eds., *ACS Symposium Series* 344, *American Chemical Society*, **1987**, Washington DC, 220-232.

Drelich, J. and Miller J.D., "Surface and Interfacial Tension of The Whiterocks Bitumen And Its Relationship To Bitumen Release from Tar Sands During Hot Water Processing", *Fuel*, **1994**, 73, 1504-1510

Drelich, J., Bukka, K., Miller, J.D. and Hanson, F.V., "Surface Tension of Toluene-Extracted Bitumens from Utah Oil Sands as Determined by Wilhelmy Plate and Contact Angle Techniques", *Energy & Fuels*, **1994**, 8, 700-704

Edwards, C.H. and Penney, D.E., *Calculus and Analytical Geometry*, Prentice-Hall Inc., New Jersey **(1982)**

Eggers, J. and Dupont, T.F., "Drop Formation in A One-Dimensional Approximation of The Navier-Stokes Equation", *Journal of Fluid Mechanics*, **1994**, 262, 205-221

Ennis, B.J., Li, J., Tardos, G.I. and Pfeffer, R., "The Influence of Viscosity on The Strength of An Axially Strained Pendular Liquid Bridge", *Chemical Engineering Science*, **1990**, 45, 3071-3088

Ennis, B.J., Tardos, G. and Pfeffer, R., "A Microlevel-based characterization of granulation phenomena", *Powder Technology*, **1991**, 65, 257-272

Eres, M.H., Weidner, D.E. and Schwartz, L.W., "Three-Dimensional Direct Numerical Simulation of Surface-Tension-Gradient Effects on The Leveling of An Evaporating Multi-component Fluid", *Langmuir*, **1999**, 15, 1859-1871

Evans, D.F. and Wennerstrom, H., "The Colloidal Domain: Where Physics, Chemistry, Biology, and Technology meet", VCH, New York **(1994)**

Fairbrother, R.J. and Simons, S.J.R., "Modeling of Binder-Induced Agglomeration", *Particle & Particle Systems Characterization*, **1998**, 15, 16-20

Fisher, L.R. and Israelachvili, J.N., "Experimental Studies on The Applicability of The Kelvin Equation to Highly Curved Concave Menisci", *Journal of Colloid and Interface Science*, **1981**, 80, 528-541

Frink, L.J.D. and Van Swol, F., "A Molecular Theory for Surface Forces Adhesion Measurements", *Journal of Chemical Physics*, **1997**, 106, 3782-3791

Gillette, R.D. and Dyson, D.C., "Stability of Fluid Interfaces of Revolution between Equal Solid Circular Plates", *Chemical Engineering Journal*, **1971**, 2, 44-54

Gray, M.R., Jokuty, P., Yeniova, H., Nazarewycz, L., Wanke, S.E., Achia, U., Krzywicki, A., Sanford, E.C., Sy, O.K.Y., "The Relationship Between Chemical Structure And Reactivity of Alberta Bitumen", *Canadian Journal of Chemical Engineering*, **1991**, 69, 833-843

Gray, M.R., *Upgrading of Petroleum Residues and Heavy Oils*, Marcel Dekker Inc., New York (1994)

Gray, M.R., Le, T., McCaffrey, W.C., Berruti, F., Soundararajan, S., Chan, E., Huq, I. and Thorne, C., "Coupling of Mass Transfer and Reaction in Coking of

Thin Films of an Athabasca Vacuum Residue", *Industrial and Engineering Chemistry Research*, **2001**, 40, 3317-3324

Gray, M.R., Zhang, Z., McCaffrey, W.C., Huq, I., Boddez, L., Xu, Z. and Elliott, J.A.W, "Measurement of Adhesive Forces During Coking of Athabasca Vacuum Residue", *Industrial and Engineering Chemistry Research*, **2002**, submitted

Gray, M.R., McCaffrey, W.C., Huq, I., Le, T., "Kinetics of Cracking and Devolatilization During Coking of Athabasca Residues", *Industrial and Engineering Chemistry Research*, **2003**, submitted

Hatschek, E., *The Viscosity of Liquids*, G. Bell And Sons, LTD, England **(1928)**

Haumesser, P., Bancillon, J. and Daniel, M., "High Temperature Contactless Viscosity Measurements by The Gas-Film Levitation Technique: Application to Oxide And Metallic Glasses", *Review of Scientific Instruments*, **2002**, 73, 3275-3285

Horozov, T.S., Dushkin, C.D., Danov, K.D., Arnaudov, L.N., Velev, O.D., Mehreteab, A. and Broge, G., "Effect of the Surface Expansion And Wettability of The Capillary on The Dynamic Surface Tension Measured by The Maximum Bubble Pressure Method", *Colloids and Surfaces A*, **1996**, 113, 117-126

Huang, C. and Kono, H.O., "A Mathematical Coalescence in the Batch Fluidized Bed Granulator", *Powder Technology*, **1988**, 55, 35-49

Isaacs, E.E. and Smolek, K.F., "Interfacial Tension Behavior of Athabasca Bitumen/Aqeous Surfactant Systems", *Canadian Journal of Chemical Engineering*, **1983**, 61, 233-240

Jacobs, F.A., Donnelly, J.K., Stanislav, J. and Svrcek, W.Y., "Viscosity of Gas Saturated Bitumen", *Journal of Canadian Petroleum Technology*, **1980**, 19, 46-50

Khan, M.A.B., Mehrotra, A.K. and Svrcek, W.Y., "Viscosity Models for Gas-free Athabasca Bitumen", *Journal of Canadian Petroleum Technology*, **1984**, 23, 47-53

Li, X., Elliott, J.A.W. and McCaffrey, W.C., "Dynamic Interfacial Tensions and Contact Angle of Materials Involved in Fluidized Coking", *Report on Syncrude/NSERC CRD*, **2002**

Li, X., Elliott, J.A.W., McCaffrey, W.C., Yan, D., Li, D. and Famulak, D., "Dynamic Surface Tensions of Athabasca Bitumen Vacuum Residue", *Industrial and Engineering Chemistry Research*, **2003**, submitted

Lielmezs, J. and Herrick, T.A., "New Surface Tension Correlation for Liquids", *Chemical Engineering Journal*, **1986**, 32, 165-169

Malyshenko, S.P. and Dunikov, D.O., "On The Surface Tension Corrections in Non uniform And Non equilibrium Liquid-Gas Systems", *International Journal of Heat and Mass Transfer*, **2002**, 45, 5201-5208

Man, K.F., "Surface Tension Measurements of Liquid Metals by The Quasi-containerless Pendant Drop Method", *International Journal of Thermophysics*, **2000**, 21, 793-804

Matsumoto, T., Nakano, T., Fujii, H., Kamai, M. and Nogi, K., "Precise Measurement of Liquid Viscosity And Surface Tension with An Improved Oscillation Drop Method", *Physical Review E*, **2002**, 65, 1-3

Mazzone, D.N., Tardos, G.I. and Pfeffer, R., "The Behavior of Liquid Bridges Between Two Relatively Moving Particles", *Powder Technology*, **1987**, 51, 71-83

McCaffrey, W.C., Cameron, R.A. and Gray, M.R., "Physical Behavior of Bitumen under Rapid Heating", *Preprint of American Chemical Society, Division of Petroleum Chemistry*, **1998**, 43, 616-618

Mehrotra, A.K., Yee, C.T. and Svrcek, W.Y., "Prediction of Surface Tension of Athabasca Bitumen", *Canadian Journal of Chemical Engineering*, **1985**, 63, 340-343

Meseguer, J., "The Breaking of Axisymmetric Slender Liquid Bridges", *Journal of Fluid Mechanics*, **1983**, 130, 123-151

Moriarty, J.A., Schwartz, L.W. and Tuck E.O., "Unsteady Spreading of Thin Liquid Films With Small Surface Tension", *Physics of Fluids A*, **1991**, 3, 733-742

Okada, M., Ohtake, T., Hattori, M. and Watanabe, K., "Measurement of the surface tension for n-Hexane and n-Octane", *Nippon-Kikai-Gakkai-Ronbunshu, B-Hen Transactions of The Japan Society of Mechanical Engineers Part B*, **1989**, 52, 1649-1652

Peregrine, D.H., Shoker, G. and Symon, A., "The Bifurcation of Liquid Bridges", *Journal of Fluid Mechanics*, **1990**, 212, 25-39

Pismen, L.M., "Interaction of Reaction-Diffusion Fronts and Marangoni Flow on The Interface of A Deep Fluid", *Physical Review Letters*, **1997**, 78, 382-385

Pitois, O., Moucheront, P. and Chateau, X., "Liquid Bridge between Two Moving Spheres: An Experimental Study of Viscosity Effects", *Journal of Colloid and Interface Science*, **2000**, 231, 26-31

Pitois, O., Moucheront, P. and Chateau, X., "Rupture Energy of A Pendular Liquid Bridge", *European Physical Journal B*, **2001**, 23, 79-86

Plateau, J.A.F., "Experimental And Theoretical Researches on The Figures of Equilibrium of A Liquid Mass Withdrawn from The Action of Gravity", translated in *Annual Reports of The Smithsonian Institution*, **1863-1866**, 206 – 435

Poling, B.E, Prausnitz, J.M. and O'Connell, J.P., *The Properties of Gases and Liquids*, 5th ed., McGraw-Hill, New York **(2000)**

Puttagunta, V.R., Singh, B. and Miadonye, A., "Correlation of Bitumen Viscosity with Temperature and Pressure", *Canadian Journal of Chemical Engineering*, **1993**, 71, 447-450

Ricci, E. and Passerone, A., "Review: Surface Tension and Its Relations with Adsorption, Vaporization and Surface Reactivity of Liquid Metals", *Material Science and Engineering*, **1993**, A161, 31-40

Rolo, L.I., Caço, A.I., Queimada, A.J., Marrucho, I.M. and Coutinho, J.A.P., "Surface Tension of Heptane, Decane, Hexadecane, Eicosane, and Some of Their Binary Mixtures", *Journal of Chemical Engineering Data*, **2002**, 47, 1442-1445

Sanford E.C. and Chung, K.H., "The Mechanism of Pitch Conversion During Coking, Hydrocracking and Catalytic Hydrocracking of Athabasca Bitumen", *AOSTRA Journal of Research*, **1991**, 7, 37-45

Sangiorgi, R., Caracciolo, G. and Passerone, A., "Factors Limiting the Accuracy of Measurements of Surface Tension by The Sessile Drop Method", *Journal of Materials Science*, **1982**, 2895-2901

Schramm, L.L. and Kwak, J.C.T., "The Rheological Properties of an Athabasca Bitumen and Some Bituminous Mixtures and Dispersions", *Journal of Canadian Petroleum Technology*, **1988**, 26-35

Shu, W.R., "A Viscosity Correlation for Mixtures of Heavy Oil, Bitumen, and Petroleum Fractions", *Society of Petroleum Engineers Journal*, **1984**, 24, 277-282

Slobozhanin, L.A., Alexander, J.I.D. and Patel, V.D., "The Stability Margin for Stable Weightless Liquid Bridges", *Physics of Fluids*, **2002**, 14, 209-224

Soundararajan, S., "Determination of Thermal Cracking Kinetics of Athabasca Bitumen vacuum residue", M.Sc. Thesis, University of Saskatchewan, **2001**

Svrcek, W.Y. and Mehrotra, A.K., "Gas Solubility, Viscosity And Density Measurements for Athabasca Bitumen", *Journal of Canadian Petroleum Technology*, **1982**, 21, 31-38

Svrcek, W.Y. and Mehrotra, A.K., "One Parameter Correlation for Bitumen Viscosity", Chemical Engineering Research and Design, **1988**, 66, 323-327

Tabor, D., "Surface Forces and Surface Interactions", *Journal of Colloid and Interface Science*, **1977**, 58, 2-13

Tester, W.J. and Modell, M., Thermodynamics and Its Applications, Prentice Hall PTR, New Jersey, U.S.A **(1996)**

Tripathi, A. and Mathur, V.K., "Estimation of Surface Tension of Hydrocarbon Mixtures", *Indian Journal of Technology*, **1977**, 15, 277-280

Van Wazer, J.R., Lyons, J.W., Kim, K.Y. and Colwell, R.E., "Viscosity and Flow Measurement: A Laboratory Handbook of Rheology", John Wiley & Sons, New York, **(1963)** Ward, C.A. and Stanga, D., "Interfacial Conditions During Evaporation or Condensation of Water", *Physical Review E*, **2001**, 64, 1-9

Ward, S.H. and Clark, K.A., "Determination of The Viscosities And Specific Gravities of The Oils in Samples of Athabaska Bituminous Sand", *Research Council of Alberta*, **1950**, Rept.(57)

Willet, C.D., Adams, M.J., Johnson, S.A. and Seville J.P.K., "Capillary Bridges between Two Spherical Bodies", *Langmuir*, **2000**, 16, 9396-9405

Wilson, S.D.R., "The Slow Dripping of A Viscous Fluid", *Journal of Fluid Mechanics.*, **1988**, 190, 561-570

APPENDIX A

PROOFS AND EXPERIMENTAL DATA

A1. PROOF OF CAPILLARY FORCE FORMULAE

First, a review of steps leading to the expression proposed by Frink et al. (1997).

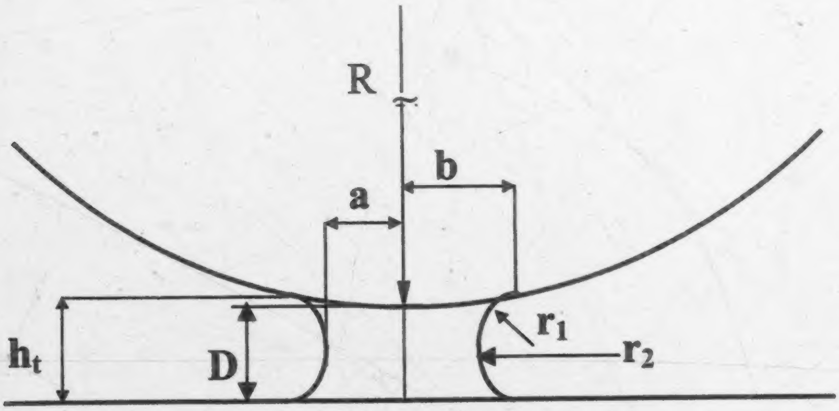

Assuming a capillary condensed liquid where liquid-vapor interface forms part of a sphere and also using Derjaquin approximation for flat plate and a sphere as shown below.

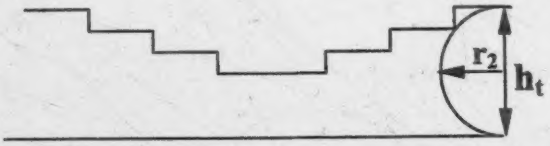

$$r_2 = \frac{h_t}{2\cos\theta} \tag{1}$$

And from the Laplace equation

$$P^L - P^V = \gamma\left(\frac{1}{b} + \frac{1}{r_2}\right) \qquad (2)$$

For a case when D << b, $b \longrightarrow \infty$ and substituting this fact and Equation 1 into Equation 2.

$$P^L - P^V = \gamma\frac{2\cos\theta}{h_t} \cong f_s \qquad (3)$$

Where **P^L**, **P^V** and **f_s** are respectively pressure in liquid, pressure in gas/air and solvation force per unit area. Once again, recall the Derjaquin approximation.

$$F_{cap} = \int_{h=D}^{\infty} f(h)2\pi x\,dx \qquad (4)$$

Where **F_{cap}** is the total capillary forces between two bodies and for two spheres of radii **R_1** and **R_2**:

$$h = D + \frac{x^2}{2}\left(\frac{1}{R_1} + \frac{1}{R_2}\right) \qquad (5)$$

And for the special case of a sphere and a flat plate with $R_1 = R$ and $R_2 = \infty$, this reduces to the following.

$$h = D + \frac{x^2}{2R} \tag{6}$$

$$x = \sqrt{(h - D)2R} \tag{7}$$

$$\frac{dx}{dh} = \frac{1}{2}\left[(h - D)2R\right]^{-\frac{1}{2}} . 2R \tag{8}$$

To find the total force between sphere and plate, substitute Equations 3, 7 and 8 into Equation 4.

$$F_{cap} = \int_{h=D}^{\infty} \gamma \frac{2\cos\theta}{h_t} 2\,\pi\,R\,dh \tag{9}$$

$$F_{cap} = \frac{4\gamma\pi R\cos\theta}{h_t} . \, h\Big|_{D}^{h_t} \tag{10}$$

$$F_{cap} = \frac{4\gamma\pi R\cos\theta}{h_t} . \left(h_t - D\right) \tag{11}$$

Equation 11 is the same equation obtained by Frink et al. (1997). Now, what is left is the application to the specific problem at hand. Once again, the following can be written from the Laplace equation when the liquid-vapor interface does not necessarily form part of a sphere.

$$\frac{1}{a}+\frac{1}{r_2} = \frac{1}{b}+\frac{1}{r_1} \tag{12}$$

Measurements of **r₂**, **a** and **b** can be used to obtain **r₁**. Then solvation force per unit area and the total force using Equation 4 can be found as follows.

$$f_s = P^L - P^V = \gamma\left(\frac{1}{b}+\frac{1}{r_1}\right) \tag{13}$$

$$F_{cap} = 2\gamma\pi R\left(\frac{1}{b}+\frac{1}{r_1}\right)(h_t - D) \tag{14}$$

It should be noted that $\mathbf{h_t}$ could be found as follows.

$$h_t = D + \frac{b^2}{2R} \tag{15}$$

Substituting Equation 15 in Equation 14 and simplifying for the total capillary force in the bridge between sphere and plate.

$$F_{cap} = F_s = \pi\gamma b\left(1 + \frac{b}{r_1}\right) \qquad (16)$$

This is the same equation used as Equation 3-2 in the theory section.

A2. STATISTICAL METHOD FOR FINDING POINT OF COMMENCEMENT OF BRIDGE ELONGATION

To allow for this determination, the slope for all the data points was found for both rods. The displacement plot was analyzed for each of the data points starting with the absolute distance of the top rod, **d_t**, at a point when the rods were certainly known to be moving together. At each of the N previous sample points, the following were determined:

1. **$t_{0.025,N}$**, t-statistics corresponding to a 95 % confidence interval with last N data points from the slopes of the two rods.
2. **Sd_b**, the standard deviation in the data from the lower rod controlled by the stepper motor for the previous N data points.

The absolute error in the separation between the rods could then be determined as follows.

$$\mathrm{Err}_N = \frac{t_{0.025,N} - sd_b}{2\sqrt{N}} \tag{17}$$

Err represents the error inherent in the system when the two rods were moving together. The confidence interval for the point when the rods certainly start moving apart will be known using the following.

$$d_t = d_b \pm Err_N \tag{17}$$

To determine the point of commencement of bridge elongation, each of the data points is tested for the condition in Equation 17 until a point is reached when the condition fails. The time at the first point where the condition fails is the time when the elongation of bridge begins. The idea behind this is simply to find the first point when the difference in the absolute distance between the rods is greater than the error in the slope of the rods in the region when the two rods were moving together.

A3. PARAMETRIC ESTIMATION DATA

k_1	k_2	k_3
0.6771	0.75215	400

Frames	D	2a	2b	$2r_2$	time (secs)	ampl. diff (volts)	Force (mN)	dD/dt (mm/s)	r_1 (contact) (mm)	Fcap (N)	Fcalc (mN)	Fdiff (N/m)	Fdiff	Diff in F	Sq. Resd.	
3	0.058	0.211	0.211	N/A	51.556	0.933	**0.593**	1.247		3.890E-04	**0.575**	0.012	0.389	0.041	0.002	**N2000 - 7m**
4	0.078	0.136	0.170	0.179	51.573	0.935	**0.595**	3.626	0.071	1.863E-05	**0.508**	0.047	1.493	0.071	0.005	
5	0.179	0.090	0.151	0.216	51.590	0.934	**0.594**	6.474	0.055	1.789E-05	**0.688**	0.108	3.402	-0.065	0.004	
6	0.295	0.058	0.146	0.295	51.607	0.936	**0.595**	7.682	0.036	2.203E-05	**0.698**	0.177	5.581	-0.072	0.005	
7	0.435	0.021	0.136	inf	51.623	0.936	**0.595**	8.419	0.013	4.336E-05	**0.697**	0.251	7.937	-0.073	0.005	
3	0.093	0.426	0.464	0.093	46.100	0.696	**0.443**	3.169	0.046	1.390E-04	**0.350**	0.030	0.941	0.158	0.025	**N1000 - 10m**
4	0.146	0.352	0.428	0.146	46.117	0.696	**0.443**	3.673	0.068	8.759E-05	**0.299**	0.054	1.726	0.225	0.051	
5	0.216	0.274	0.387	0.216	46.134	0.695	**0.442**	4.910	0.088	6.133E-05	**0.310**	0.086	2.734	0.184	0.034	
6	0.310	0.193	0.376	0.310	46.151	0.694	**0.441**	4.922	0.087	5.884E-05	**0.281**	0.124	3.947	0.236	0.056	
7	0.380	0.165	0.356	0.380	46.167	0.687	**0.437**	5.186	0.085	5.426E-05	**0.273**	0.152	4.841	0.242	0.059	
8	0.483	0.068	0.339	0.483	46.184	0.686	**0.436**	6.171	0.036	9.489E-05	**0.336**	0.173	5.490	0.151	0.023	
2	0.084	0.396	0.438	0.084	79.517	0.606	**0.385**	3.757	0.041	1.421E-04	**0.395**	0.021	0.656	-0.017	0.000	**N600 - 9m**
3	0.147	0.354	0.409	0.147	79.533	0.605	**0.385**	5.434	0.069	8.250E-05	**0.388**	0.046	1.423	-0.005	0.000	
4	0.265	0.208	0.409	0.265	79.550	0.605	**0.385**	4.809	0.081	7.345E-05	**0.297**	0.086	2.651	0.144	0.021	
5	0.307	0.208	0.357	0.307	79.567	0.601	**0.382**	4.023	0.095	5.286E-05	**0.231**	0.106	3.246	0.266	0.071	
6	0.400	0.129	0.349	0.400	79.584	0.597	**0.380**	5.539	0.068	6.408E-05	**0.290**	0.132	4.047	0.146	0.021	
3	0.052	0.184	0.217	0.069	53.147	0.734	**0.467**	1.370	0.033	4.518E-05	**0.372**	0.023	0.752	0.111	0.012	**N4000 - 7m**
4	0.078	0.121	0.161	0.147	53.163	0.735	**0.467**	2.491	0.056	1.893E-05	**0.540**	0.037	1.200	-0.065	0.004	
5	0.135	0.090	0.151	0.285	53.180	0.735	**0.467**	4.431	0.062	1.609E-05	**0.794**	0.063	2.070	-0.237	0.056	
6	0.229	0.060	0.129	0.341	53.197	0.733	**0.466**	6.388	0.042	1.569E-05	**0.961**	0.108	3.519	-0.322	0.104	
7	0.345	0.044	0.104	Inf	53.213	0.730	**0.464**	7.266	0.202	6.318E-06	**0.948**	0.165	5.392	-0.313	0.098	
2	0.090	0.507	0.588	0.090	45.890	1.275	**0.811**	0.666	0.044	2.330E-04	**0.688**	0.054	1.660	0.104	0.011	**N8000 - 13m**
3	0.090	0.444	0.486	0.090	45.910	1.278	**0.813**	0.554	0.044	1.622E-04	**0.541**	0.061	1.869	0.235	0.055	
4	0.106	0.374	0.444	0.106	45.920	1.277	**0.812**	1.549	0.051	1.220E-04	**1.124**	0.077	2.350	-0.162	0.026	
5	0.136	0.295	0.336	0.136	45.940	1.279	**0.813**	2.764	0.064	6.236E-05	**1.713**	0.107	3.275	-0.342	0.117	
6	0.217	0.220	0.307	0.271	45.960	1.281	**0.815**	6.662	0.100	3.992E-05	**3.464**	0.176	5.380	-0.645	0.416	

Sum of square residuals 1.281

A4. VISCOSITY AND SURFACE TENSION OF STANDARD OIL

A.4.1. Trend in Surface tension of standard oils with film thickness

Oil Type	Film Thickness (microns)	Surface Tension, by Liquid bridge method (N/mm)	Surface Tension by Pendant drop method (N/mm)
N600	3.658	33.589	32.610
	10.974	32.192	32.610
	14.633	31.260	32.610
N1000	3.844	29.086	31.432
	9.611	31.467	31.432
	15.378	31.829	31.432
	15.378	30.535	31.432
N2000	3.719	27.430	31.655
	7.438	28.983	31.655
	11.156	34.158	31.655
	14.875	29.759	31.655
N8000	1.833	29.035	32.667
	5.500	31.829	32.667
	7.344	32.399	32.667

A.4.2. Viscosity of standard oils

Oil Type	Viscosity (mPas)			
	Calc.	Calc. Error	Actual.	Actual. Err.
N600	3766.3	813.0	2621.0	259.0
N1000	4015.1	1266.5	2576.0	573.0
N2000	6066.3	1389.1	5995.0	803.3
N4000	6597.1	2948.6	9323.3	1086.7
N8000	22010.3	12171.9	21034.0	1131.0

A5. PROPERTIES OF ABVR

A.5.1 Adhesive Forces of ABVR

Reaction time, sec	Forces, mN			Average Force, mN	Error in Force, mN
	Series 1	Series 2	Series 3		
T = 400 °C					
20	0.060	0.052	0.055	0.056	0.004
50	0.041	0.068	0.044	0.051	0.015
70	0.065	0.044	0.055	0.055	0.011
130	0.048	0.056	0.051	0.052	0.004
160	0.085	0.062	0.066	0.071	0.012
220	0.058	0.085	0.068	0.070	0.014
240	0.000	0.000	0.000	0.000	0.000
T = 466 °C[*]					
19	0.131	0.134	0.071	0.112	0.035
26	0.122	0.139	0.124	0.129	0.009
40	0.130	0.141		0.135	0.008
55	0.148	0.134		0.141	0.010
63	0.083	0.143		0.113	0.042
75	0.087	0.178	0.195	0.153	0.058
85	0.089	0.141	0.152	0.127	0.034
95	0.000	0.074	0.000	0.025	0.000
105	0.000	0.000	0.000	0.000	0.000
T = 503 °C[*]					
11	0.124	0.133	0.133	0.130	0.005
13	0.118	0.128	0.127	0.124	0.005
15	0.119	0.129	0.121	0.123	0.005
17	0.145	0.150	0.145	0.147	0.003
19	0.137	0.136	0.134	0.136	0.002
21	0.109	0.124	0.131	0.121	0.011
23	0.120	0.115	0.123	0.120	0.004
25	0.054	0.098	0.099	0.084	0.026
27	0.060	0.046	0.068	0.058	0.011
29	0.014	0.014	0.014	0.014	0.000
T = 530 °C					
12.50	0.057	0.061	0.051	0.056	0.005
13.75	0.064	0.190	0.139	0.131	0.063
15.00	0.106	0.200	0.123	0.143	0.050
16.25	1.650	1.406	0.412	1.156	0.656
17.50	0.899	0.136	0.027	0.518	0.475
18.75	0.000	0.000		0.000	0.000

---

[*] Data collected by L. Boddez

A.5.2 Selected Adhesive Forces for Viscosity Measurement at 530 °C

Average time, sec	**Forces, mN**			**Average Force, mN**	**Error in Force, mN**
	Series 1	**Series 2**	**Series 3**		
15.593	0.139	0.057	0.061	0.056	0.004
17.423	0.064	0.051	0.123	0.051	0.015
19.890	0.130	0.076	0.136	0.055	0.011
21.287	0.071	0.095	0.133	0.052	0.004

A.5.3 Dry out times of reacting ABVR from adhesive force measurements

Temperature, °C	Time to touch Rods at Dry-out, s	Heating time to reach 400 °C, s	Experimental Dry out time, s	Predicted Extent of Reaction and Volatilization
400	240 ± 10	[∅]	240	0.7325
466	105 ± 10[♠]	3.83	101.17	0.8241
503	29 ± 2[♠]	4.92	24.08	0.8579
530	19 ± 1	4.58	14.42	0.8997

[∅] Not corrected for heat up time because of the high time to touch rods

[♠] Values from data collected by L. Boddez (Figure 6-2 and Figure 6-3)

A.5.4 Viscosity of non -reacting ABVR (Measurement with RMS)

Series 1		Series 2		Average Values					
Temp., °C	**Viscosity, mpa.s**	**Temp., °C**	**Viscosity, mPa.s**	**Average temp., °C**	**Temp. error, °C**	**Av. Viscosity (A), mPa.s**	**Error in Av. Viscosity (B), mPa.s**	**Log(A)**	**Log(B)**
185.60	169.90	184.70	143.50	185.15	0.64	156.70	18.67	2.20	1.27
204.60	97.82	203.60	101.40	204.10	0.71	99.61	2.53	2.00	0.40
224.80	66.25	224.50	62.49	224.65	0.21	64.37	2.66	1.81	0.42
245.20	53.58	245.50	45.21	245.35	0.21	49.40	5.92	1.69	0.77
266.50		266.50	29.97	266.50		29.97		1.48	

A.5.5 Viscosity of reacting ABVR at Varying Heating time

Series 1		Series 2		Series 3		Average Values				
Time, sec	Viscosity, mPa.s	Time, sec	Viscosity, mPa.s	Time, sec	Viscosity, mPa.s	Time, sec	Time error, sec	Normalized time	Viscosity, mPa.s	Viscosity error, mPa.s
T = 400 °C										
21.47	2,874	22.13	4,888	21.67	3,884	21.76	0.34	0.091	3,882	1,007
51.97	5,110	52.82	6,325	52.54	6,970	52.44	0.43	0.219	6,135	945
83.20	5,628	72.73	6,675	70.03	8,039	75.32	6.96	0.314	6,781	1,209
131.01	13,397	121.81	8,195	132.97	11,221	128.60	5.96	0.536	10,937	2,612
167.76	13,662	168.65	21,376	163.10	7,247	166.50	2.98	0.694	14,095	7,074
223.96	33,431	222.77	34,779	221.53	23,013	222.75	1.22	0.928	30,408	6,439
T = 466 °C										
22.43	4,343	21.77	4,192	22.00	3,528	22.07	0.34	0.210	4,021	434
31.06	5,239	31.04	8,267	31.41	4,350	31.23	0.26	0.297	4,794	629
35.33	7,269	33.30	6,440		0	34.32	1.44	0.327	6,854	586
40.32	18,424	38.85	9,636	39.49	5,057	39.57	0.74	0.377	12,645	5,006
50.28	17,424	48.93	20,633	48.59	7,387	49.63	0.68	0.473	19,009	1,605
T = 503 °C										
14.64	5,051	15.09	8,974	15.05	7,073	14.93	0.25	0.515	7,033	1,962
16.63	9,122	17.20	12,608	17.92	16,127	17.25	0.65	0.595	12,619	3,503
17.01	14,600	19.07	25,533	19.78	10,275	18.62	1.44	0.642	16,803	7,864
21.17	26,869	21.35	24,285	20.42	21,798	20.98	0.49	0.723	24,317	2,536
25.38	20,094	23.73	28,480	22.96	27,260	24.02	1.24	0.828	25,278	4,531
T = 530 °C										
15.49	13,489	15.43	11,955	15.86	17,668	15.59	0.23	0.821	14,371	2,957
17.42	22,195	17.25	16,354	17.60	22,791	17.42	0.18	0.917	20,447	3,557
20.06	38,500	19.50	35,615	20.11	52,435	19.89	0.34	⊗	42,183	8,995
21.34	45,525	21.51	55,027	21.01	51,457	21.29	0.25	⊗	50,670	4,800

⊗ Omitted because viscosities were evaluate at times greater than the dry-out time

A.5.6 Surface Tension of ABVR at Varying Heating time

Series 1		Series 2		Series 3		Average Values			
Time, sec	Surface tension, mN/m	Time, sec	Surface Tension, mN/m	Time, sec	Surface Tension, mN/m	Time, sec	Time error, sec	Surface tension, mN/m	Surface tension error, mN/m
T = 312 °C									
20.85	12.83	21.60	13.80	21.36	15.66	21.27	0.38	14.02	1.46
T = 358 °C									
22.45	16.88	21.66	14.22	21.20	12.86	21.77	0.63	14.66	2.05
T = 400 °C									
21.47	15.47	22.13	13.97	21.67	14.21	21.76	0.34	14.55	0.80
51.97	10.60	52.82	17.53	52.54	11.21	52.44	0.43	13.11	3.83
83.2	16.74	72.73	11.31	70.03	14.08	75.32	6.96	14.04	2.72
131.01	12.43	121.81	14.28	132.97	13.12	128.60	5.96	13.28	0.93
168.47	11.63	167.76	17.00	163.1	15.86	166.44	2.92	14.83	2.83
223.96	14.83	222.98	19.13	221.53	17.36	222.82	1.22	17.11	2.16
T = 466 °C									
21.29	4.28	21.95	7.04	21.53	8.00	21.59	0.33	6.44	1.93
30.67	6.31	30.21	5.05	33.06	8.83	31.31	1.53	6.73	1.92
38.81	5.48	39.69	6.28	38.81	4.01	39.10	0.51	5.26	1.15
49.88	9.74	49.41	9.74	48.46	6.19	49.25	0.72	8.55	2.05
T = 503 °C									
14.42	5.05	14.51	7.12	14.91	5.10	14.61	0.26	5.76	1.18
16.13	6.19	16.75	3.65	17.53	6.54	16.80	0.70	5.46	1.57
16.72	6.91	18.68	4.17	19.50	5.78	18.30	1.43	5.62	1.38
20.30	5.41	21.21	8.15	22.53	3.90	21.35	1.12	5.82	2.15
T = 530 °C									
15.16	7.02	15.43	4.45	15.19	6.57	15.26	0.15	6.01	1.37
15.86	4.73	17.29	3.99			16.58	1.01	4.36	0.53
19.54	5.01	19.07	7.74	19.68	5.62	19.43	0.32	6.12	1.43
20.72	3.68	20.70	3.43	20.51	5.12	20.64	0.12	4.08	0.91

A.5.7 Equilibrium Surface Tension data (Li et al., 2002)

Temp., °C	Surface tension, mN/m	
	Series 1	Series 2
150	20.83	20.72
200	19.22	19.68
250	18.34	18.33

A.5.8 Viscosity at lowest heating time and Normalized Reaction time

Temp (°C)	Heating Time, s	Reaction time, s	Normalized Time	Viscosity (mPas)	Visc. Error (mPa.s)
400	21.757	21.757	0.091	3,882	1,007
	52.443	52.443	0.219	6,135	945
	75.320	75.320	0.314	6,781	1,209
	128.597	128.597	0.536	10,937	2,612
	166.503	166.503	0.694	14,095	7,074
	222.753	222.753	0.928	30,408	6,439
466	22.067	18.237	0.180	4,021	434
	31.225	27.395	0.271	4,794	629
	34.315	30.485	0.301	6,854	586
	39.570	35.740	0.353	12,645	5,006
	49.630	45.800	0.453	19,009	1,605
503	14.927	10.007	0.416	7,033	1,962
	17.250	12.330	0.512	12,619	3,503
	18.620	13.700	0.569	16,803	7,864
	20.980	16.060	0.667	24,317	2,536
	24.023	19.103	0.793	25,278	4,531
530	15.593	11.013	0.764	14,371	2,957
	17.423	12.843	0.891	20,447	3,557

APPENDIX B

PROGRAM CODES

B1. FILTRATION DRIVER CODE (MATLAB 6.5)

```
%CODE FOR FILTERING DISPLACEMENT DATA FROM THE 2 RODS

[x,a]=xlsread('J14T53026mf.xls');

b=x(2378:3401,2);

d=x(2378:3401,3);

tt=x(2378:3401,1);

bm=wavetimefreq(b,4,1)

dm=wavetimefreq(d,5,1)

bf=bm.tf(1,:);

df=dm.tf(1,:);

z=[tt df' bf'];

figure

plot(tt,bf',tt,df')

figure

plot(tt,bf',tt,b)

save J14T53026mfout z -ascii


%CODE FOR FILTERING VOLTAGE DATA FROM THE PIVOTED ROD

[x,a]=xlsread('trialv.xls');

f=x(2378:3401,2);

tt=x(2378:3401,1);

fm=wavetimefreq(f,4,1)
```

```
ff=fm.tf(1,:);

z=[tt ff'];

figure

plot(tt,ff')

figure

plot(tt,ff',tt,f)

save trialvout z -ascii
```

B2. DIFFERENTIAL EQUATION SOLVER FOR HIGH TEMPERATURE LIQUID FILM MODEL (MATLAB 6.5)

```
%GENERAL CODE FOR THE SOLUTION BY PARAMETRIC
 %  ESTIMATION

% Entering the Experimental data

cx=[8.4946, 7.3813, 6.8874, 5.7442, 5.5148, 5.2112, 4.9499];

t=[30, 60, 90, 240, 280, 340, 400];

k=[0.5, 1.0];  %Initial values of the unknown.

[kfinal, v]=fminsearch(@EulerNV,k)

xfinal= EulerNV2(kfinal)

sum1=0; sum2=0; N=length(t);

for i=1:N

   sum1=sum1+cx(i)^2; sum2=sum2+cx(i);

end

%Computing the correlation coefficient
```

```
R=sqrt(1-(N-1)*v/(sum1-(sum2^2)/N))

plot(t,xfinal,'-b',t,cx,'-m')

title('Film Thickness versus t at 400C')

legend('xopt','xexpt')

xlabel('t(secs)')

ylabel('Film Thickness (microns)')


function v = EulerNV(k1)

cxi=[8.4946, 7.3813, 6.8874, 5.7442, 5.5148, 5.2112, 4.9499];

ti=[30, 60, 90, 240, 280, 340, 400];

%Specifying the initial guess for the specific problem

xi=0; yi=20.44;

%Now writing the main program

h=0.1; xout=0.1; N=length(ti); sum=0;

j=1; x=xi; xp(j)=xi; yp(j)=yi; y=yi;

for i=1:N

   xf(i)=ti(i);

   while x(j)<xf(i)

      xe=x(j)+xout;

      if (xe>xf(i))

         xe=xf(i);

      end
```

```
    h1=h;
    [x(j+1), y(j+1)]=eulereqNV(k1,xp(j),yp(j),h1,xe);
    j=j+1;
    xp(j)=x(j);
    yp(j)=y(j);
    if (x(j)>=xf)
      break
    end
  end
  ct(i)=yp(j);
  sum=sum+(cxi(i)-ct(i))^2;
end
v=sum/(N-1)
```

```
function ct = EulerNV2(k1)
cxi=[8.4946, 7.3813, 6.8874, 5.7442, 5.5148, 5.2112, 4.9499];
ti=[30, 60, 90, 240, 280, 340, 400];
%Specifying the initial guess for the specific problem
xi=0; yi=20.44;
%Now writing the main program
h=0.1; xout=0.1; N=length(ti);
j=1; x=xi; xp(j)=xi; yp(j)=yi; y=yi;
```

```
for i=1:N
  xf(i)=ti(i);
  while x(j)<xf(i)
    xe=x(j)+xout;
    if (xe>xf(i))
      xe=xf(i);
    end
    h1=h;
    [x(j+1), y(j+1)]=eulereqNV(k1,xp(j),yp(j),h1,xe);
    j=j+1;
    xp(j)=x(j);
    yp(j)=y(j);
    if (x(j)>=xf)
      break
    end
  end
  ct(i)=yp(j);
end

function [x, y]=eulereqNV(k1,x,y,h,xend)
x=x+h;
if (x>xend)
```

```
  h=h+xend-x;
  x=xend;
end
f1 = fcv2VTB(k1,x,y);
y=y+f1*h;
if (x>=xend)
  break
end

function f2 = fcv2VTB(k2,x,y)
f2=-k2(1)*(y)^k2(2);
```

APPENDIX C

DETAILED EXPERIMENTAL PROCEDURE

C1. FABRICATION OF RODS

1. Each of the Curie-point rods was bent to a 45° shape as shown in Figure 4-2 (The unbent portion was reduced by half for Curie-point rods at 300 °C, 358 °C and 400 °C to prevent them from bending during pull apart because those rods are very soft)
2. The bent rods were taken to the glass blower where a glass rod of diameter 3.9 mm and length 110 mm was firmly pressed to the longer unbent portion of the rod
3. The glass portion of the rod was then marked for identification

C2. COATING OF RODS

1. The marked glass rod was weighed
2. The unbent portion of the rods were taped while exposing only the mid section of the Curie-point rod
3. A 2 % solution by weight of the liquid (standard oil during calibration or ABVR for high temperature) was prepared with methylene chloride
4. The 2 % solution was then sprayed on the mid section of the Curie-point rods.
5. After spraying, the glass portion of the rod was cleaned with paper towel soaked in methylene chloride to ensure that only the desired portion was coated
6. The coated alloy was left for two days to evaporate the solvent

7. After two days, the coated rod assembly was weighed to determine the mass of liquid film on the rod
8. The film thickness on the rod was calculated based on Equation 4-2
9. Taping, weighing and spraying steps were repeated with drying out in between until the desired film thickness of 25 μm – 28 μm was obtained

C3. CONDUCTING A RUN

1. Two coated rods of desired film thickness were loaded on the equipment as shown in Figure 4-1
2. The balance was adjusted such that the free rod (upper rod) was positioned within the range of the two LVDTs and with enough room to move down 90,000 steps
3. LabView program was started for the control of the stepper motor that moved the controlled rod
4. From LabView, the predesigned program "LesC.vi" was opened in an inactive mode
5. To make the program active, the "start" button was clicked followed by the "on/off" button and finally the "run" button, which is a white arrow symbol on the menu of the program and "save file" window appears to save the data from the run
6. The file "temp/test" was resaved and made the program active giving the graphical display of the responses from the two LVDTs and the

program allowed the stepper motor to have the controlled rod (lower rod) moved up till it just touched the free rod

7. The step rate was set to 100, which corresponds to 4148 steps/second or 0.4086 mm/s
8. From the touch point, the controlled rod was moved down a predetermined number of steps depending on the reaction time desired. (For example for reaction time of 20 seconds, the lower rod was moved down 80,000 steps while using minimum step rate of 100, which implied a rate of approximately 4000 steps per second)
9. The LabView program was closed
10. After all the glass fittings were properly sealed, the front side of the equipment was connected to the nitrogen purge line through the flow meter and the rear side was connected to the nitrogen supply line
11. The nitrogen cylinder was opened fully to allow for flow of nitrogen
12. The test-utility program was opened (via start/programs/Advantech Driver for 95 and 98/Test Utility) to control the opening of the valve on the nitrogen line
13. The pre-designed file "PCL-7330-I/O = 300H" was opened and started to open the valve on the nitrogen line and begin the flow of nitrogen
14. The flow of nitrogen was monitored on the flow meter with the stopwatch while the valve on the nitrogen line was adjusted till a flow-rate of 9-12 dm^3/min was obtained

15. When this flow-rate was attained, the test-utility program was closed

16. The glass housing portion of Figure 4-1 was then inserted into the induction coil of the furnace

17. The lighting was set to the appropriate position to provide illumination for the enhancement of the video recordings

18. The rods were brought into the view of the camera such that the experiments could be recorded into a videotape and afterwards the lighting was turned off

19. The front end of the equipment was removed from the flow meter and connected directly to the nitrogen purge line while every other setting remained the same

20. The GeniDAQ runtime program was opened (via Start/programs/Advantech GeniDAQ/GeniDAQ runtime) to control the operation of the valve on the nitrogen line and that of the induction furnace

21. The pre-designed file "p20-300s.gni" was opened to reopen the nitrogen line and purge the equipment with nitrogen for 20 minutes, and immediately afterwards, to turn on the furnace for 300 seconds

22. The program was started and purging of the equipment with nitrogen began. The stop watch was started to synchronized the time of the equipment to allow for the necessary moving around for the experiment

23. 16 minutes into the purging, the power supply for the furnace was switched on, thought the induction furnace was still off till the GeniDAQ runtime turned it on at the end of purging time of 20 minutes

24. 16.5 minutes into the purging, the circulation fan was switched-on to ensure the circulation of the nitrogen

25. 17 minutes into the purging, LabView program was restarted as explained in steps 5 and 6

26. This time, a different name was given to the file into which the data from the experiment would be saved

27. 18 minutes into the purging, the nitrogen was turned low to reduce the oscillation of the free rod

28. 19.5 minutes into the purging, the lights were turned on

29. The nudge amount was set, on the LabView program interface, depending on the desired press together. (For the example of 80,000 steps, the nudge amount was 85,105 steps including 5,105 steps for press together)

30. To obtain the desired nudge action on LabView, the "set parameter" button was clicked, the "move absolute" position set to zero and the "set" button clicked

31. At exactly 20 minutes after purging started, the induction furnace automatically came on and heating of the rod and ABVR started

32. The "run/stop" button in the "take-measurement" was clicked as desired to start the nudge action of the rods (for the example given in step 7, the button must be clicked immediately after the furnace came on to get a reaction time of 5 seconds. If 15 seconds reaction time is desired, the "run/stop" button must be clicked 5 seconds after the furnace came on, as timed by the stopwatch)

33. Clicking the "run/stop" button initiated the nudge, press together and pull apart of the rod and the green color of the button indicated the execution of the nudge command

34. After the nudge, pull apart, bridge formation and elongation were completed, the stepper motor stopped to indicate the end of the experiment

35. At the end of the experiment, the lights were switched off, the LabView program stopped by clicking the "stop", "exit" and "on/off" buttons in that order

36. Pressing the red button stopped the furnace and the GeniDAQ program stopped by clicking the stop button. The furnace power was switched off and the nitrogen cylinder closed

37. The experiment was completed by saving the data file in a removable disk for further processing on another computer

38. The rods were cleaned with abrasive and reused for experiments. Rods were typically used for a maximum of 3 times before they regain their magnetism. So, each rod is rechecked for magnetism before every reuse